Compressive Sampling for Wireless Communications

Ph.D. Thesis

Shahzad Gishkori

Compressive Sampling for Wireless Communications

Proefschrift

ter verkrijging van de graad van doctor
aan de Technische Universiteit Delft,
op gezag van de Rector Magnificus Prof. ir. K.Ch.A.M. Luyben,
voorzitter van het College van Promoties,
in het openbaar te verdedigen op donderdag 19 juni 2014 om 15.00 uur

door

Shahzad Sarwar GISHKORI
elektrotechnisch ingenieur (ir)

geboren te Dera Ghazi Khan, Pakistan.

Dit proefschrift is goedgekeurd door de promotor:
Prof. dr. ir. G.J.T. Leus

Samenstelling promotiecommissie:

Rector Magnificus	voorzitter
Prof. dr. ir. G.J.T. Leus	Technische Universiteit Delft, promotor
Prof. dr. K.L.M. Bertels	Technische Universiteit Delft
Prof. dr. ing. F. Le Chevalier	Technische Universiteit Delft
Prof. dr. ing. V. Lottici	Universitá di Pisa, Italia
Prof. Dr.-Ing. R. Fischer	Universität Ulm, Deutschland
Dr. Y. Vanderperren	European Patent Office, Rijswijk
Dr. Y. Zhang	IMEC-NL, Eindhoven
Prof. dr. ir. A.-J. van der Veen	Technische Universiteit Delft (reserve lid)

ISBN # 978-94-6186-329-4

Thesis Cover was designed by Gull Gishkori.

To the kind memories of my mother.

And He (your Lord) has subjected to you whatever is in the heavens and whatever is in the earth. Verily, in it are signs for a people who ponder. [Al-Qur'an, 45:13]

Summary

Wireless communications is undergoing massive development in all forms of its manifestations. In the field of short-range communications, technologies like ultra-wideband (UWB) systems are promising very high data rates, fine timing resolution and coexistence with other physical layer standards. Along with these benefits, the promise of low-cost and low-complexity devices makes UWB systems a highly sought-after option. The main reason for these benefits is the utilization of a very large bandwidth. However, these benefits come at a price, that is the high sampling rate required to receive such signals. According to the Nyquist sampling theorem, a signal can be fully determined if sampled at twice its maximum frequency. This means that the UWB signals may require a sampling rate in the order of Giga samples per second. At the receiver, the sampling is carried out by an analog-to-digital converter (ADC). The power consumption of an ADC is proportional to its sampling rate. A very high sampling rate means stressing the ADC in terms of power consumption. This can put the whole idea of low-cost and low-complexity UWB systems in jeopardy. Therefore, using subsampling methods is indispensable. In this regard, we propose the utilization of compressive sampling (CS) for UWB systems. CS promises a reasonable reconstruction performance of the complete signal from very few compressed samples, given the sparsity of the signal. In this thesis, we concentrate on impulse-radio (IR) UWB systems. IR-UWB signals are known to be sparse, meaning, a large part of the received signal has zero or insignificant components. We exploit this time-domain sparsity and reduce the sampling rate much below the Nyquist rate but still develop efficient detectors.

We propose CS-based energy detectors for IR-UWB pulse position modulation (PPM) systems in multipath fading environments. We use the principles of generalized maximum likelihood to propose detectors which require the reconstruction of

the original signal from compressed samples and detectors which skip this reconstruction step and carry out detection on the compressed samples directly, thereby further reducing the complexity. We provide exact theoretical expressions for the bit error probability (BEP) to assess the performance of our proposed detectors. These expressions are further verified by numerical simulations.

We also propose CS-based differential detectors for IR-UWB signals. These detectors work on consecutive symbols. We develop detectors with separate reconstruction and detection stages as well as detectors that perform these steps jointly. We further present detectors which do not need reconstruction at all and can work directly on the compressed samples. However, this can put some limitations on the overall flexibility of the detector in terms of the measurement process. To assess the performance of all these detectors, we also provide maximum a posteriori (MAP) based detectors. We provide numerical simulations to display the detection results.

We extend the CS-based classical differential detectors to the case of multiple symbol differential detectors. To keep the implementation complexity at its minimum, we work only with compressed samples directly. We use the principles of the generalized likelihood ratio test (GLRT) to eliminate the limitations on such detectors, in terms of the measurement process. Apart from focusing on compressed detectors which contain full timing information, we also propose detectors which need such information at symbol level only. This effectively results in low-cost and low-complexity detectors.

Finally, we present some work on the theoretical aspects of CS. We develop algorithms which exploit the block sparse structure of the signal. This block sparsity is combined with varying block sizes and signal coefficients having smooth transitions. Such signals are often encountered in a wide range of engineering and biological fields.

Contents

List of Figures

List of Tables

Part I: Preamble

Chapter 1

Introduction

This thesis is concerned with the application of compressive sampling to wireless communications, especially the ultra-wideband systems. Reducing the sampling rate is a fundamental challenge in receiving signals with very large bandwidth. Compressive sampling can be of substantial help in this regard. We start this chapter by elaborating upon the overall motivation of the thesis. We then provide an outline of the presented work along with highlighting our major contributions.

1.1 Motivation

Digital communications has become an integral part of our everyday life. Rapid inclusion of new devices and applications is redefining human interactions. This evolution has rendered wired communications essentially obsolete and given way to wireless communications into taking a pivotal role. In this regard, short-range communications is attracting accelerated interest due to its ubiquitous nature. Ultra-wideband (UWB) communications is at the forefront of short-range communications, primarily because of the benefits associated with very large bandwidth. However, this very large bandwidth gives rise to further challenges. One of the key challenges is the excessive sampling rate required to receive the UWB signals, since according to the classical Shannon-Nyquist-Whittaker-Kotelnikov sampling theorem [3], [4], a band limited signal $x(t)$, i.e., $X(\omega) = 0, |\omega| > \omega_{\max}$ (rad/sec) can be fully determined from its samples $x(iT)$ if $T \leq \pi/\omega_{\max}$. In simple words, the sampling rate should be twice the maximum frequency. For the multiple GHz bandwidth of UWB signals, the classical sampling theorem implies exorbitant sampling

rates which can heavily stress the analog-to-digital converters (ADCs) in terms of power consumption. To make UWB systems practically viable, the power consumption must be reduced which in turn means reducing the sampling rates. Given the sparse nature of particular UWB signals [3], one can turn to compressive sampling (CS) [5, 6] which offers reasonable performance at reduced sampling rates. This thesis basically explores the application of CS for UWB signals, addressing the challenges and highlighting principal gains.

1.2 Ultra-Wideband Systems

The history of UWB communications dates back to the early twentieth century marked by the famous spark-gap experiment of Marconi. However, the present thrust came after the federal communications commission (FCC) [7] ruling, allowing the use of UWB for data communications within a band of 7.5 GHz, thus paving the way for extremely high rate data transmissions. Naturally, the utilization of such a large bandwidth is only possible with minimal power transmission so as to reduce interference with several other pre-allocated bands. Thus, UWB systems offer high data rates but at a short range. In this perspective, UWB can be used in numerous scenarios. Figure 1.1 shows the scenarios with a potential UWB application as envisaged by the European Union project PULSERS [1]. Major categories are wireless personal area networks (WPANs), sensor networks, peer-to-peer networks and wireless local area networks (WLANs).

According to the FCC, UWB signals are defined as signals having a fractional bandwidth greater than 20% or signals having an absolute bandwidth greater than 0.5 GHz. There are two general mechanisms to generate a UWB signal. One is termed as carrier based, which uses spreading techniques, e.g., direct sequence[1], frequency hopping or orthogonal frequency division. In general, the transceiver architecture of carrier based techniques is complex due to the presence of mixers and related circuitry. The other is termed as carrierless and is known as impulse-radio (IR), which basically uses the transmission of a short pulse in the time-domain and thus occupies the complete frequency band[2]. The transceiver architecture of IR is relatively simpler. Further, the transmit power in IR-UWB can be decreased by exploiting spreading as well, which basically means that the same information is

[1] Such a spreading is possible in theory but requires extremely high chip rate which may limit its practical implementation.

[2] In order to satisfy spectral requirements, the pulse can be generated as different derivatives of the Gaussian pulse or by modulating a Gaussian pulse.

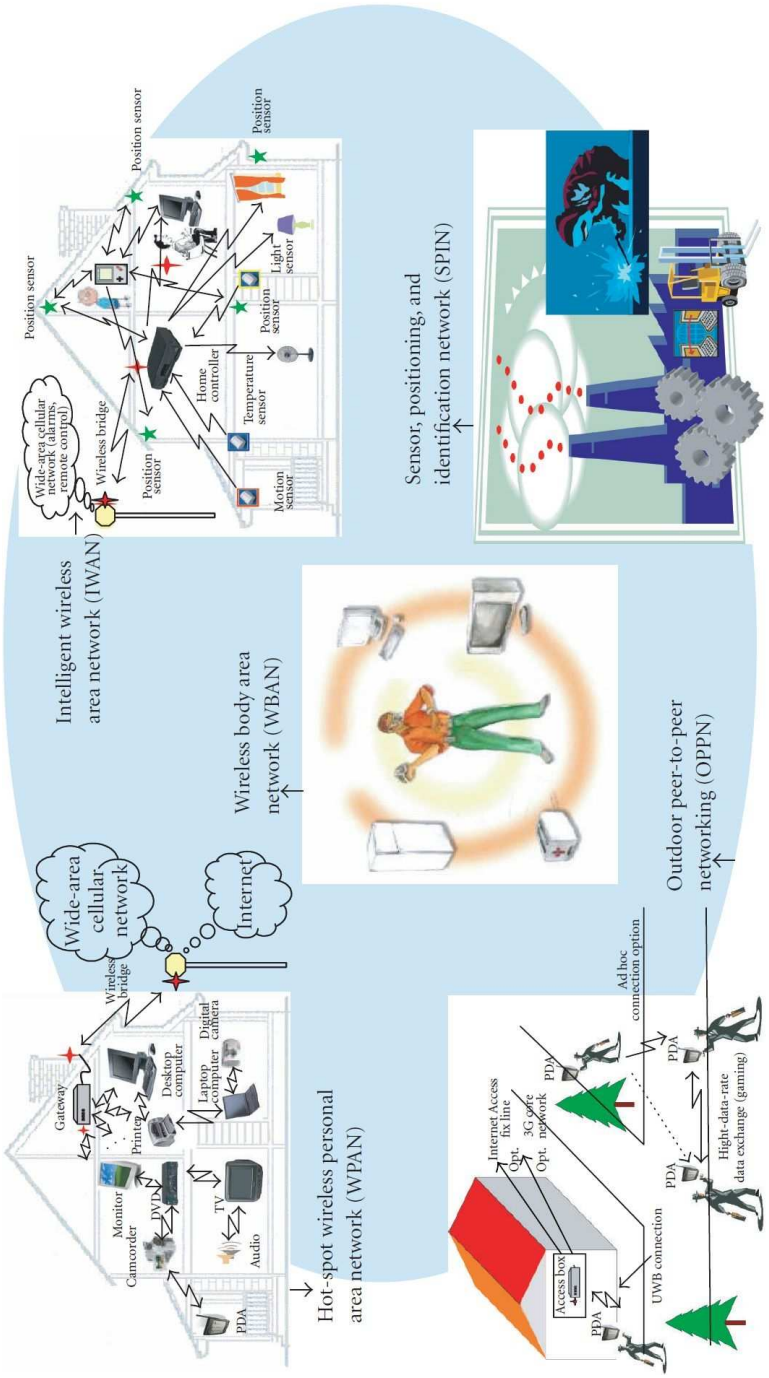

Figure 1.1: UWB applications scenarios [1]

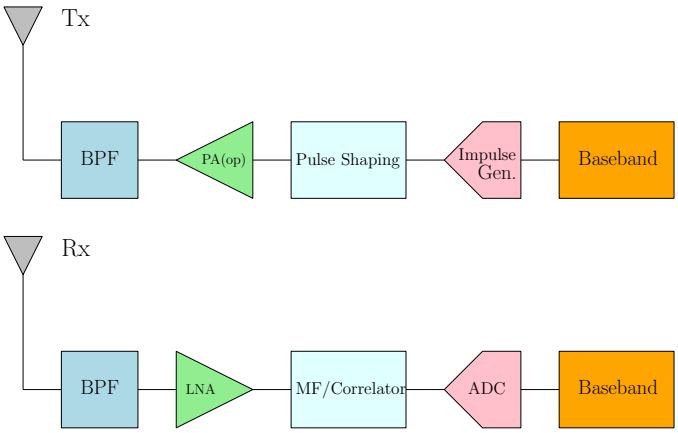

Figure 1.2: UWB architecture

transmitted over multiple frames, with each frame transmitting at a very low power. In this thesis, we concentrate on IR-UWB due to its simplicity of implementation.

IR-UWB is a baseband technique. A bandlimited impulse is transmitted directly without the need for upconversion to radio frequency (RF). Consequently, the receiver does not need an RF to intermediate frequency (IF) step which means, local oscillators and phase locked loop (PLL) units are not required. This particular aspect of the IR-UWB architecture saves a lot of power and makes the UWB systems low-cost and low-complexity systems. Figure 1.2 shows a general transmit and receive architecture of UWB systems [8, 9]. However as we shall see in the next section, the ADC block still remains a power hungry unit, an aspect that is addressed in this thesis.

One unique characteristic of IR-UWB signals is the exploitation of the rich multipath environment. Each transmitted pulse is received in the form of hundreds of separable echoes. In narrowband signals the different paths are not separable and thus can be problematic. However in UWB, multiple paths can be exploited to collect most of the received energy. The separability of the paths is because of the high bandwidth of the signal. Thus, the received signal comprises insignificant or zero values between the paths. This can potentially give a sparse character to the received UWB signal. IR-UWB signaling commonly employs simple modulation schemes, e.g., pulse position modulation (PPM) and pulse amplitude modulation (PAM). These modulation schemes combined with the very low duty-cycle nature of transmitted symbols, can further promote sparsity in the received signal. The sparsity in IR-UWB signals is an important aspect which we shall dwell on, in most

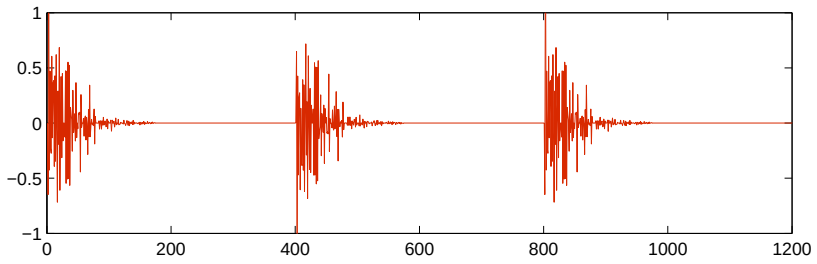

Figure 1.3: IR-UWB received signal

of the thesis. Here, we elaborate on it by giving a simple example. Figure 1.3 shows a typical, UWB PAM received signal in its Nyquist rate sampled form, highlighting the sparse nature of the received signal.

1.3 ADC Power Consumption

The ADC is one of the most power hungry units in the receiver. Therefore, it is important to elaborate upon the factors which can affect the amount of power consumed in ADCs. The two major factors having a direct bearing on the amount of power consumed in the ADCs are the sampling rate (f_s) and the resolution, i.e., the effective number of bits (ENOB). The widely used figures of merit relating f_s and ENOB are P and F, defined in [2] as

$$P = 2^{\mathrm{ENOB}} f_s \tag{1.1}$$

$$F = \frac{2^{\mathrm{ENOB}} f_s}{P_{\mathrm{diss}}} \tag{1.2}$$

where P_{diss} denotes power dissipation. From (1.1)-(1.2), we can see that P evaluates the collective performance of ENOB and f_s, whereas, F brings power efficiency into the comparison as well. Performance trends of different ADCs, w.r.t. P and F, can be found in [2, 10], where ADCs are basically grouped in terms of their architecture. From (1.2), we can see that the ADC performance is inversely proportional to the power dissipation and the relationship between the sampling rate and the power dissipation is almost linear. A derivation of the exact relationship between the two is given in [11] with a couple of assumptions: *i)* The power is consumed only at the sample-and-hold block of the ADC, *ii)* The input signal supplies

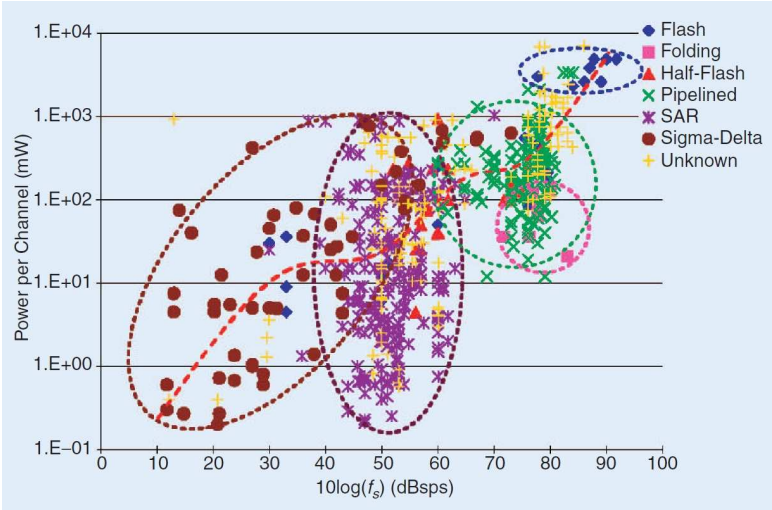

Figure 1.4: ADC, Power versus sampling rate [2]

the power to charge the sample-and-hold capacitance. This relationship can then be written as

$$P_{\min} = k\,T\,f_s\,10^{(6N+1.76)/10}\ [\mathrm{W}] \tag{1.3}$$

where $P_{\min}$ is the minimal power, N denotes the stated number of resolution bits, k describes Boltzmann's constant and T is the temperature (in Kelvin). From (1.3), we can see an exact linear relationship between the sampling rate and the power dissipation. This relationship was confirmed by practical experiments in [2] and the result is shown in Figure 1.4. For different architectures of ADCs, a general trend of linearity between the sampling rate and the power consumption can be seen. Flash ADCs provide the highest sampling rates, on the order of Giga samples per second, but at the same time, they consume the maximum power due to their parallel structure. Thus, reducing the sampling rates can have a drastic effect on the ADC efficiency. The issue of reducing the sampling rate is extensively addressed in this thesis.

Apart from the sampling rates, we can see from (1.3) that the resolution bits have an enormous influence on the power consumption as well. Moreover, there is an interesting relationship between ADC resolution and the sampling rate. Figure 1.5 shows this relationship for different ADC architectures. We can see that although Flash ADCs offer the highest sampling rates, their performance over resolution is quite poor. In contrast, Sigma-Delta ADCs can offer a better resolution

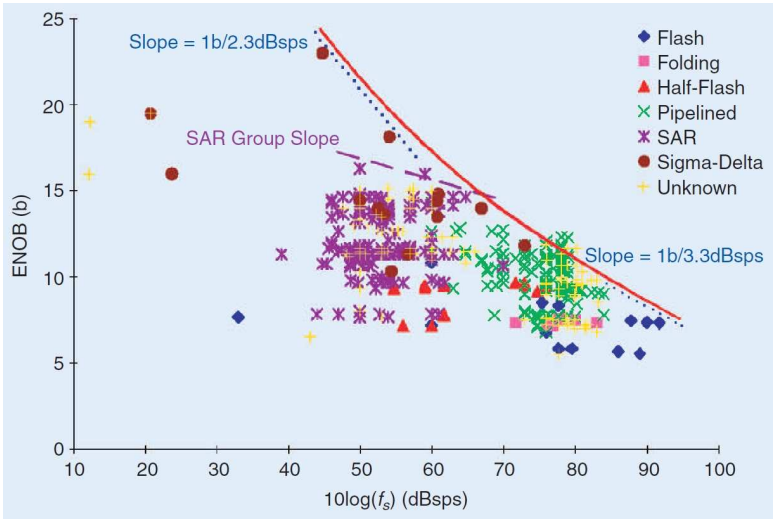

Figure 1.5: ADC, ENOB versus sampling rate [2]

performance but suffer from lower sampling rates. This gives another motivation to reduce the ADC sampling rates. By reducing the sampling rates, we can use those architectures of ADCs which offer low sampling rates but provide room for improving the resolution, which can be critical in some applications.

1.4 Outline and Contributions

In this thesis, our primary focus is on the application of CS for IR-UWB systems. We develop novel strategies for UWB energy detectors and UWB differential detectors, operating at low sampling rates. We show that CS can reduce the sampling rates much below the Nyquist rate and still offer reasonable performance. We propose detectors which may need reconstruction of the received signal from its low rate samples, as a first step and then carry out detection on the reconstructed samples, as a second step. We also propose detectors which skip the reconstruction step altogether and carry out detection directly on the low rate samples. The latter can further reduce the implementation complexity of a UWB receiver. To assess the performance of our proposed CS-based detectors, we also derive theoretical expressions for the bit error probability (BEP), which can easily be extended to their Nyquist rate counterpart. We also provide simulation results to establish the validity of these theoretical expressions.

Chapter 2:

In this chapter, we provide a comprehensive overview of CS. We give a description regarding its evolution in its present form. This description provides substantial insight in the subject in order to pursue further research.

Chapter 3:

In this chapter, we develop CS-based energy detectors for UWB pulse position modulation. We present detectors which require reconstruction of the original signal as well as detectors which work directly on the compressed samples. We also provide theoretical BEP expressions as performance benchmarks. The contributions of this chapter are enlisted below.

- We first present a CS framework to reduce the receiver sampling rate for IR-UWB PPM signals much below the Nyquist rate. For the sake of theoretical performance evaluations of the detection algorithms, our sensing mechanism works under two general assumptions. In the first assumption, the measurement matrix consists of random elements such that the resulting rows are approximately orthogonal to each other. In the second assumption, the orthogonality of the rows of the measurement matrix is assumed to be exact.

- Using the principles of GML, we develop CS-based energy detectors for the signal reconstructed from its compressed samples. In this regard, signal reconstruction is carried out by using approximate message passing algorithm (AMP). We also propose energy detectors which operate on the compressed signal directly and do not need reconstruction.

- We show that the performance of our proposed energy detectors is independent of the spreading factor. This is in contrast to the traditional approach, where performance worsens by increasing the number of frames per transmitted symbol.

- We provide bit error probability (BEP) expressions for the proposed compressed detectors for a deterministic channel as well as a Gaussian distributed channel. We show that these expressions can be easily modified for the energy detectors based on Nyquist-rate sampling.

The chapter has been published as

- S. Gishkori and G. Leus, "Compressive Sampling Based Energy Detection of Ultra-Wideband Pulse Position Modulation", *IEEE Transactions on Signal Processing*, vol. 61, no. 15, pp. 3866–3879, Aug. 2013

Chapter 4:

In this chapter, we apply CS to classical differential detectors for UWB systems. We develop detectors which carry out detection by first doing the reconstruction step separately and detectors which do both steps of reconstruction and detection jointly. A theoretical performance comparison is given against maximum a posteriori (MAP) based detectors. The contributions of this chapter are enlisted below.

- The proposed CS-based differential detectors are noncoherent and therefore, do not require any channel estimation.
- A direct detection method working directly on the compressed samples is proposed, which avoids signal reconstruction. However, its performance is limited by the fact that the measurement process must be the same for consecutive symbols.
- We propose a differential detector based on a two-step approach. In the first step, the sparse regularized least squares error is minimized to reconstruct the transmitted symbol waveforms from the compressed samples, and then, the recovered symbol waveforms are used to perform conventional differential detection.
- We also propose a differential detector with a joint formulation of the cost function, as the composition of the sparse regularized least squares error for two compressed-rate consecutive received signal waveforms and the squared DD error, which is minimized using an iterative efficient method derived form the elastic net optimization framework. Thus, reconstruction of the compressed signal samples and detection of encoded information is performed in a joint approach.
- Finally, a compressed-rate maximum a posteriori (MAP) based detector is derived as performance benchmark for the proposed detectors, assuming a Laplacian distributed channel response (i.e., the channel taps are Laplacian distributed).

The chapter has been published as

- S. Gishkori, G. Leus and V. Lottici, “Compressive Sampling Based Differential Detection of UWB Impulse Radio Signals”, *Elsevier Physical Communication*, vol. 5, no. 2, pp. 185–195, Jun. 2012

Chapter 5:

In this chapter, we present CS-based differential detectors for multiple symbols. The detectors work directly on the compressed samples and do not require reconstruction. We present detectors which are fully synchronized in terms of timing information and detectors which require the timing information at symbol level only. The contributions of this chapter are enlisted below.

- The proposed CS-based schemes consider multiple symbols for differential detection and are derived by avoiding the reconstruction step, i.e., they work directly on the compressed signal samples. This results in reducing the sampling rate as well as the implementation complexity related to the evaluation of the correlation coefficients needed by the objective function.
- To alleviate the limitations as experienced by the CS-based noncoherent receivers working directly on the compressed symbols, the measurement process can be either the same or different from symbol to symbol, thus offering an additional degree of freedom that can help the receiver better adapt to various scenarios.
- We also propose detectors which require symbol level synchronization (SLS) only, thus the robustness to timing errors of the proposed CS-based schemes is brought from pulse or frame level to symbol level. This feature relaxes the performance of the timing synchronizer, so further lowering the overall receiver complexity.
- A particular effort is put on cutting back the complexity required to optimize the objective function over each data block for both the ideally-synchronized CMSDD and the SLS-CMSDD, which grows exponentially in the block size. To this end, a modified sphere decoding (SD) algorithm is derived enabling the joint detection of blocks of tens of symbols at polynomial complexity.

The chapter is accepted for publication as

- S. Gishkori, V. Lottici and G. Leus, “Compressive Sampling Based Multiple Symbol Differential Detection for UWB Communications”, *IEEE Transactions on Wireless Communications - To appear*

Chapter 6:

In this chapter, we present some work on the theoretical aspects of CS. We develop algorithms which exploit the block sparse structure of the signal. This block sparsity is combined with varying block sizes and signal coefficients having smooth transitions. The contributions of this chapter are enlisted below.

- We propose new LASSO formulations to handle block sparse smooth signals.
- We propose to combine group sparsity with element-wise sparsity, along with sparsity in the difference of consecutive elements. This results in variable group sizes with smooth reconstructed signal transitions.
- We also propose to use the concept of overlapping groups along with element-wise fusion to reconstruct block sparse smooth signals of varying block sizes.
- Finally, we propose iterative solvers in the form of alternating direction ... method of multipliers for our proposed problem formulations.

This chapter is accepted for publication as

- S. Gishkori and G. Leus, "Compressed Sensing for Block-Sparse Smooth Signals", *IEEE ICASSP*, Florence, Italy, May 2014

Chapter 7:

In this chapter, we provide the conclusions, highlighting major results and observations from the thesis. We also provide future directions for research into this exciting field.

Chapter 2

Compressive Sampling

Compressive sampling or compressed sensing (CS) is primarily related to solving a certain system of linear equations. Although the field of linear algebra provides well established methods to solve a general system of linear equations, it has a subclass, namely the category of solving underdetermined systems, which has only recently been getting substantial attention. CS relates to this subclass, especially when the objective function exhibits sparsity. In this chapter, we describe the fundamental concepts relating to CS. More details can be found in [12, 13, 14].

2.1 Underdetermined Systems of Linear Equations

Let us consider a general system of equations

$$\mathbf{y} = \mathbf{\Phi x} \tag{2.1}$$

where $\mathbf{x}$ is an $N \times 1$ vector of optimization variables, $\mathbf{\Phi}$ is an $M \times N$ matrix of measurement functionals and $\mathbf{y}$ is an $M \times 1$ vector of measurements. We can see that (2.1) depicts a measurement system. Each element of $\mathbf{y}$ represents a measurement of $\mathbf{x}$, obtained through the respective row of $\mathbf{\Phi}$. Here, $\mathbf{x}$ represents the unknowns and the problem is to find $\mathbf{x}$ from $\mathbf{y}$ given $\mathbf{\Phi}$. If $\mathbf{\Phi}$ is full column-rank, i.e., $M \geq N$ (that is to say, the number of measurements is equal or more than the number of unknowns), the solution to (2.1) is quite elementary.

Now, consider the case in (2.1) where $\mathbf{\Phi}$ is full rank but $M < N$. This is an instance of the set of underdetermined systems of linear equations (USLEs), i.e., the number of unknowns is larger than the number of measurements. This system

does not have a unique solution. Depending upon the different combinations of columns of $\mathbf{\Phi}$, $\mathbf{x}$ can have an infinite number of representations [15] from $\mathbf{y}$. One way to circumvent the problem of uniqueness is to introduce the objective function as an argument of a convex function and to formulate the optimization problem as the minimization of this convex function subject to the equality constraints of (2.1). A popular choice for such a convex function is the squared ℓ_2-norm. The optimization problem can now be written as

$$\begin{aligned} \mathrm{P}_2: \qquad & \arg\min_{\mathbf{x}} \quad \|\mathbf{x}\|_2^2 \\ & \text{s.t.} \quad \mathbf{y} = \mathbf{\Phi}\mathbf{x}. \end{aligned} \tag{2.2}$$

The unique solution to the optimization problem P_2 can be easily obtained as what is known as the minimum norm solution.

Although the squared ℓ_2-norm helps to achieve a unique solution to the underdetermined system P_2, it basically measures the total energy of the objective function $\mathbf{x}$ rather than targeting the individual elements. Therefore, if $\mathbf{x}$ is sparse, i.e., it has a few nonzero elements and many exactly zero elements, P_2 fails to reproduce them in $\hat{\mathbf{x}}$. In order to measure sparsity, i.e., the number of nonzero elements of $\mathbf{x}$, one may replace the squared ℓ_2-norm with an ℓ_0-norm[1], which basically optimizes the count of nonzero elements. Then (2.2) can be replaced by

$$\begin{aligned} \mathrm{P}_0: \qquad & \arg\min_{\mathbf{x}} \quad \|\mathbf{x}\|_0 \\ & \text{s.t.} \quad \mathbf{y} = \mathbf{\Phi}\mathbf{x}. \end{aligned} \tag{2.3}$$

A sparse solution is made available by using P_0 instead of P_2, but answers to whether it is unique and globally optimal, are not as straightforward as in the case of P_2, due to the nonconvex nature of the ℓ_0-norm. Apart from the issues of uniqueness and optimality of the solution, even solving P_0 is very challenging. It is in essence an exhaustive search problem, where every combination of K columns of $\mathbf{\Phi}$ (assuming $\mathbf{x}$ has K nonzero elements, i.e., K is the order of sparsity: $\|\mathbf{x}\|_0 = K$) is tried for a possible solution. The complexity of the problem increases exponentially in N and it has been established that P_0 is NP-hard in general.

Naturally, the aforementioned challenges motivate finding efficient solvers for P_0 and/or approximations of P_0. One suitable option in terms of approximating

[1]Note that the ℓ_0-norm is the limit as $p \to 0$ of ℓ_p-norm, i.e., $\|\mathbf{x}\|_0 = \lim_{p\to 0} \|\mathbf{x}\|_p^p = \lim_{p\to 0} \sum_{i=0}^{N-1} |[\mathbf{x}]_i|^p$.

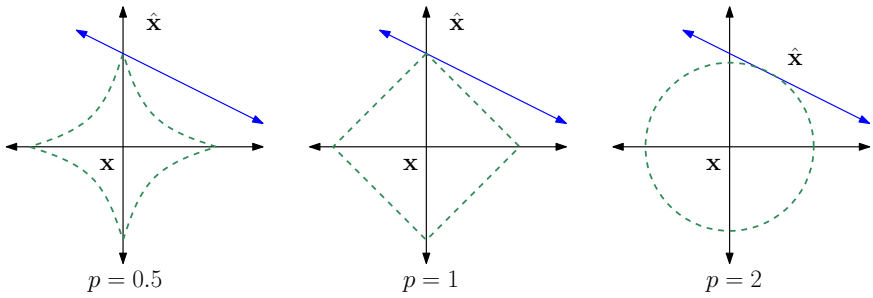

Figure 2.1: Comparison of possible estimates by using an ℓ_p-norm for different values of p

P_0, is to replace the ℓ_0-norm by an ℓ_1-norm, which also provides sparse solutions. The new optimization problem can then be written as

$$\begin{aligned} \mathrm{P}_1 : \qquad & \arg\min_{\mathbf{x}} \quad \|\mathbf{x}\|_1^1 \\ & \text{s.t.} \quad \mathbf{y} = \mathbf{\Phi}\mathbf{x}. \end{aligned} \tag{2.4}$$

In contrast to P_0, P_1 is a convex optimization problem and can be easily solved by being cast as a linear program (LP). P_1 is also known as basis pursuit (BP) [15]. In a way, P_1 offers a compromise between the two extremes of P_0 and P_2. It is closer to P_0 in terms of offering sparsity and it is closer to P_2 in terms of being convex. Nonetheless, it needs to be established under what conditions P_1 produces its best solution and when it is equivalent to P_0.

In general, the comparison between the above mentioned optimization problems is in fact a comparison between different ℓ_p-norms. A generic formulation of the optimization problem based on an ℓ_p-norm can be written as

$$\begin{aligned} \mathrm{P}_p : \qquad & \arg\min_{\mathbf{x}} \quad \|\mathbf{x}\|_p^p \\ & \text{s.t.} \quad \mathbf{y} = \mathbf{\Phi}\mathbf{x}. \end{aligned} \tag{2.5}$$

For the sake of developing a general intuition into solving P_p with different values of p, we present here a simple example. Let $\mathbf{x} \in \mathbb{R}^2$ with an order of sparsity $K = 1$, so $N = 2$ and $\mathbf{x}$ has one zero and one nonzero element. Let only one measurement be available, so $M = 1$. Now a possible solution can be obtained by blowing an ℓ_p-ball centered at the origin of $\mathbf{x}$, till it intersects with the feasible set defined by the equality constraint in (2.5). Figure 2.1 provides a comparison of such estimates for different values of p. We can see that for $p = 2$, a nonsparse

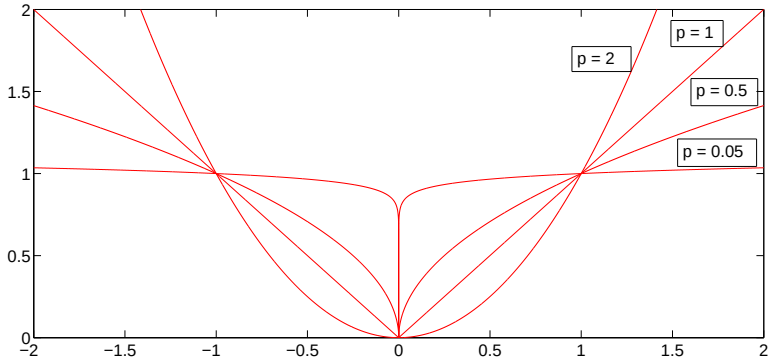

Figure 2.2: Plot of $|x|^p$ for different values of p

solution is obtained, whereas for $p \leq 1$, there is a high probability of obtaining a sparse estimate. Note that in the extreme case, an ℓ_0-norm is obtained as $p \to 0$. Although, $p \leq 1$ generates parsimonious estimates, but if $0 < p < 1$ the problem becomes nonconvex. This can be seen by simply plotting the ℓ_p-norms for different values of the argument. In Figure 2.2, we plot the ℓ_p-norms with a scalar argument x, i.e., $|x|^p$ for different values of p. We can see that for $0 < p < 1$, the ℓ_p-norm becomes nonconvex. Only in the case when $p = 1$, both sparsity and convexity can be combined.

2.2 Requisites for the Sparse Solution of a USLE

A USLE is basically an ill-posed problem. We saw in the previous section, different formulations which can offer a sparse solution for such systems. However, there are certain questions which should be answered in order to obtain a sparse solution of a USLE.

- Starting with P_0, what conditions must be satisfied to guarantee the uniqueness and optimality of the sparse solution?
- Can a unique solution be guaranteed for the approximate problem formulation, i.e., P_1?
- If the measurements are contaminated with noise, can the estimation errors be bounded?

Before we move on to answer the above mentioned questions, we first describe some key concepts which play an important role in specifying conditions for sparse solutions of a USLE.

Spark

Spark is one of the central properties of a matrix which should be investigated in order to guarantee a successful sparse recovery. This term was first introduced in [16] and defined as

Definition 2.2.1 (Spark)**.** *Given a matrix* $\mathbf{\Phi}$*,* $\mathrm{spark}(\mathbf{\Phi})$ *is the cardinality of the smallest subset of linearly dependent columns of* $\mathbf{\Phi}$*.*

Note the difference between spark of a matrix as defined above and the commonly known rank of a matrix. The $\mathrm{rank}(\mathbf{\Phi})$ indicates the largest number of columns of $\mathbf{\Phi}$ that are linearly independent, whereas $\mathrm{spark}(\mathbf{\Phi})$ indicates the smallest subset of columns of $\mathbf{\Phi}$ with linearly dependent columns. The rank of a matrix can be easily determined by various algebraic methods whereas, despite some superficial resemblance, the spark of a matrix can only be determined through a combinatorial search over all subsets of its columns, since it finds a bound on the null space of a matrix. In some literature, $\mathrm{spark}(\mathbf{\Phi}) - 1$ has also been termed as 'Kruskal rank' [17].

Mutual Coherence

The mutual coherence is an easily verifiable property of a matrix in order to establish its performance in sparse recovery. It was proposed in [16, 18] and can be defined as

Definition 2.2.2 (Mutual Coherence)**.** *The mutual coherence of a matrix* $\mathbf{\Phi}$*,* $\mu(\mathbf{\Phi})$*, is the maximum absolute inner product of different columns of* $\mathbf{\Phi}$*. It is denoted as*

$$\mu(\mathbf{\Phi}) = \max_{1 \leq i,j \leq N, i \neq j} \frac{|[\mathbf{\Phi}]_{:,i}^T \, [\mathbf{\Phi}]_{:,j}|}{\|[\mathbf{\Phi}]_{:,i}\|_2 \, \|[\mathbf{\Phi}]_{:,j}\|_2}. \tag{2.6}$$

Mutual coherence basically provides the interdependence of different columns of the matrix. If the matrix comprises of orthogonal columns, then the mutual coherence would be very low.

In case of random orthogonal matrices[2], it was empirically observed in [18] that the upper bound on the mutual coherence can be related to the maximum absolute value of the matrix which is proportional to $\sqrt{\log(NM)/M}$ with $M \to \infty$. This 'generic' [18] aspect of mutual coherence leads to another definition of the mutual coherence which was given in [19] as

Definition 2.2.3 (Mutual Coherence - Generic)**.** *The mutual coherence of an orthonormalized $M \times N$ matrix[3] $\mathbf{\Theta}$, $\mu_g(\mathbf{\Theta})$, is the largest absolute entry of $\mathbf{\Theta}$. It is given as*

$$\mu_g(\mathbf{\Theta}) = \sqrt{N}. \max_{i,j} |[\mathbf{\Theta}]_{i,j}|. \tag{2.7}$$

It basically indicates how concentrated the rows of a matrix are. Its value ranges as $1 \leq \mu_g(\mathbf{\Theta}) \leq \sqrt{N}$. This modified definition of mutual coherence generates further insights in providing guarantees for the sparse solution. In case the signal is sparse only when represented in some basis, i.e.,

$$\mathbf{x} = \mathbf{\Psi s} \tag{2.8}$$

where $\mathbf{\Psi}$ is the $N \times N$ orthonormal basis matrix (e.g., a Wavelet or Fourier matrix) and $\mathbf{s}$ is an $N \times 1$ vector of coefficients with an order of sparsity $\|\mathbf{s}\|_0 = K$, the measurement process can be written as

$$\mathbf{y} = \mathbf{\Phi x} = \mathbf{\Theta s} \tag{2.9}$$

where $\mathbf{\Theta} = \mathbf{\Phi\Psi}$. In such scenarios, mutual coherence basically highlights the correlation between the measurement matrix $\mathbf{\Phi}$ and the signal representation basis $\mathbf{\Psi}$. As we shall see in the subsequent sections, the mutual coherence between these two matrices can have drastic impact on sparse solutions. Note that if $\mathbf{\Psi} = \mathbf{I}_N$, then $\mathbf{x} = \mathbf{s}$, $\mathbf{\Theta} = \mathbf{\Phi}$ and (2.9) reverts to (2.1).

Restricted Isometry Property

The restricted isometry property (RIP) [20] is a strong property of the measurement matrices which can provide guarantees even when the measurements are contaminated with noise. It can be defined as

[2]Here it is implied that the resulting $M \times N$ matrix $\mathbf{\Phi}$ is a concatenation of $M \times M$ random orthogonal matrices, and N is a multiple of M.

[3]Note that the orthonormalization is in terms of rows of the matrix $\mathbf{\Theta}$.

Definition 2.2.4 (RIP)**.** *A matrix $\mathbf{\Phi}$ with unit ℓ_2-norm columns satisfies RIP of order K given $\delta_K \in (0,1)$ if*

$$(1-\delta_K)\|\mathbf{x}\|_2^2 \leq \|\mathbf{\Phi x}\|_2^2 \leq (1+\delta_K)\|\mathbf{x}\|_2^2 \tag{2.10}$$

holds for all $\mathbf{x}$ with maximum order of sparsity K.

The definition of the RIP implies that if a matrix $\mathbf{\Phi}$ obeys an RIP of order K (if δ_K is not too close to unity), then it approximately preserves the Euclidean length of K-sparse vectors, which basically means that a K-sparse vector cannot be in the null space of $\mathbf{\Phi}$ and every submatrix of $\mathbf{\Phi}$ with less than K columns behaves like an orthonormal matrix.

2.2.1 Conditions for a Unique Solution of P_0

A key condition for a unique solution of P_0 can be given using the spark of a matrix. Since the spark of a matrix puts a bound on its null space, it can be said that if $\mathbf{\Phi z} = \mathbf{0}$ (i.e., $\mathbf{z}$ lies in the null space of $\mathbf{\Phi}$), then it must be true that $\|\mathbf{z}\|_0 \geq \mathrm{spark}(\mathbf{\Phi})$. From Definition 2.2.1, the following theorem, as given in [16], can then be obtained.

Theorem 2.2.1. *A USLE, $\mathbf{y} = \mathbf{\Phi x}$, has a necessarily sparsest possible solution $\mathbf{x}$, if it obeys, $\|\mathbf{x}\|_0 < \mathrm{spark}(\mathbf{\Phi})/2$.*

Proof. Assume, apart from $\mathbf{x}$, there is an alternative solution $\mathbf{z}$ satisfying the same USLE, i.e., $\mathbf{y} = \mathbf{\Phi z}$. This means, $\mathbf{\Phi x} - \mathbf{\Phi z} = \mathbf{0}$, implying that $\mathbf{x} - \mathbf{z}$ lies in the null space of $\mathbf{\Phi}$. From the definition of spark, we can say, $\|\mathbf{x} - \mathbf{z}\|_0 \geq \mathrm{spark}(\mathbf{\Phi})$. But we know that the order of sparsity of the difference cannot be greater than the sum of the order of sparsity, i.e., $\|\mathbf{x} - \mathbf{z}\|_0 \leq \|\mathbf{x}\|_0 + \|\mathbf{z}\|_0$. Now, since our solution obeys, $\|\mathbf{x}\|_0 < \mathrm{spark}(\mathbf{\Phi})/2$, any alternative solution must have the order of sparsity $\|\mathbf{z}\|_0 > \mathrm{spark}(\mathbf{\Phi})/2$. □

Since the relation $\|\mathbf{x}\|_0 < \mathrm{spark}(\mathbf{\Phi})/2$ means that every submatrix of $\mathbf{\Phi}$ with $2K$ columns is full column-rank, Theorem 2.2.1 leads to following corollary.

Corollary 2.2.1.1. *Given that $\mathrm{spark}(\mathbf{\Phi}) > 2K$, a unique sparse solution can be guaranteed for $M \geq 2K$.*

So, it can be said that better results can be obtained for higher values of the spark. Generally, the spark ranges as $1 \leq \mathrm{spark}(\mathbf{\Phi}) \leq M+1$. Thus if the elements of $\mathbf{\Phi}$ are drawn from a Gaussian distribution, $\mathrm{spark}(\mathbf{\Phi}) = M+1$, then a

unique solution can be guaranteed for $K < M/2$ since every submatrix of $\mathbf{\Phi}$ with M columns is full-rank.

The spark of a matrix provides elegant guarantees for a sparse solution. However, determining its exact value for general matrices is quite hard. Nonetheless, a lower bound on the value of the spark can be obtained easily. In this regard, [16] gave the following relationship

$$\text{spark}(\mathbf{\Phi}) \geq 1 + \frac{1}{\mu(\mathbf{\Phi})} \tag{2.11}$$

where $\mu(\mathbf{\Phi})$ is the mutual coherence (see Definition 2.2.2). From (2.11), the following theorem for a unique solution can then be given as in [16]

Theorem 2.2.2. *A USLE,* $\mathbf{y} = \mathbf{\Phi x}$*, has a necessarily sparsest possible solution* $\mathbf{x}$*, if it obeys,* $\|\mathbf{x}\|_0 < 0.5(1 + 1/\mu(\mathbf{\Phi}))$.

Note from (2.6) that the minimum value of $\mu(\mathbf{\Phi})$ is $\mu(\mathbf{\Phi}) = 1/\sqrt{M}$. Therefore, Theorem 2.2.2 guarantees a sparse solution for $K < \sqrt{M}/2$ which is less than the order of sparsity guaranteed by Theorem 2.2.1, i.e., $K < M/2$.

2.2.2 Conditions for a Unique Solution of P_1

Since solving P_0 is NP-hard, the other suitable choice as mentioned earlier is to solve P_1 (also known as BP) instead. However, it needs to be established what conditions are required for the unique solution of P_1 and/or its equivalence with P_0. In this regard, [16] claimed the following

Theorem 2.2.3. *A USLE,* $\mathbf{y} = \mathbf{\Phi x}$*, has a necessarily sparsest possible solution* $\mathbf{x}$ *of* P_1 *and equivalent of* P_0*, if it obeys,* $\|\mathbf{x}\|_0 < 0.5(1 + 1/\mu(\mathbf{\Phi}))$.

Thus, the conditions for solving P_1 are same as that of solving P_0. Therefore, the bound on the maximum order of sparsity is also quite restricting, i.e., $K < \sqrt{M}/2$. In this regard, [6] proved that the bound on the order of sparsity can be relaxed and an equivalence between P_1 and P_0 holds for $K \approx \mathcal{O}(M/\log(N))$. To make the results more concrete, [19] utilized the generic definition of mutual coherence (Definition 2.2.3) and gave the following theorem

Theorem 2.2.4. *For* $\mathbf{x}$*, sparse in basis* $\mathbf{\Psi}$*, form a USLE* $\mathbf{y} = \mathbf{\Phi\Psi s}$ *by selecting uniformly random* M *measurement vectors in* $\mathbf{\Phi}$*. Then if*

$$M \geq C\mu_g^2(\mathbf{\Phi\Psi})K \log N \tag{2.12}$$

for $C > 0$, P_1 gives a sparse solution with overwhelming probability. The probability of success can be higher than $1 - \delta$, provided that

$$M \geq C\mu_g^2(\mathbf{\Phi}\mathbf{\Psi})K \log N/\delta. \tag{2.13}$$

It was because of these important results that CS started to achieve widespread recognition. To put the results of Theorem 2.2.4 in proper perspective, some remarks are in order.

- The mutual coherence plays a critical role. In order to decrease the number of measurements, coherence between the measurement matrix $\mathbf{\Phi}$ and basis matrix $\mathbf{\Psi}$ should be as small as possible. An example of such an incoherent pair can be when $\mathbf{\Phi}$ consists of spikes, i.e., comprises of the rows of an identity matrix, while $\mathbf{\Psi}$ is the Fourier matrix. This model corresponds to the classic sampling-in-time scenario. For such a time-frequency pair, the incoherence is maximum as the spikes and complex exponentials have minimum coherence [13]. Further, instead of a Fourier basis, sparsity can occur in other bases as well, e.g., wavelet bases. Since spikes are incoherent with wavelet bases [13], such a pair of measurement and representation bases can be very useful especially for sensing images. In terms of the measurement matrices, random matrices are incoherent with most of the fixed basis matrices [13]. Examples of such matrices are, Gaussian matrices or Bernoulli matrices, etc.

- One unique characteristic of Theorem 2.2.4 is that any set of random measurements can guarantee a unique solution. So without specifying any specific set of measurements, information loss can still be avoided even with fewer measurements. Also, given the incoherence of $\mathbf{\Phi}$ and $\mathbf{\Psi}$, M of the order of $K \log N$ can be sufficient.

- Finally, $\mathbf{s}$ (and eventually $\mathbf{x}$) can be exactly reconstructed from compressed measurements by simply minimizing a convex function. For this, one does not need to know the exact number of nonzero entries of $\mathbf{s}$, or their location or even their magnitude, for that matter.

From the above, one can visualize a general sensing mechanism. Sensing is done through a random (nonadaptive), i.e., incoherent measurement procedure and then reconstruction follows through a possible linear programming stage. Lastly, we would also like to mention a general rule of thumb for sparse recovery, as noticed by [6]. One can expect exact recovery, if for every nonzero element of $\mathbf{x}$, at least four incoherent measurements are available. This is also known as the de facto four-to-one rule.

2.2.3 Conditions for the Sparse Solution with Noisy Measurements

Till now, we considered an ideal scenario regarding the measurements $\mathbf{y}$, without noise or perturbations. However, in most practical situations, the measurement process is contaminated with noise. In this section, we look at the robustness of a sparse solution in the presence of nonidealities. In such situations, it is hard to give conditions of uniqueness or equivalence. Instead, the notion of a stable solution is used to give conditions or bounds on sparse recovery.

Let $\mathbf{v}$ represent an $M \times 1$ vector of bounded noise, i.e., $\|\mathbf{v}\|_2 \leq \epsilon$, then the USLE with contaminated measurements can be written as

$$\mathbf{y} = \mathbf{\Phi}\mathbf{x} + \mathbf{v} \tag{2.14}$$

and P_0 takes the shape

$$\begin{aligned} \mathrm{P}_0^{\epsilon}: \qquad & \arg\min_{\mathbf{x}} \quad \|\mathbf{x}\|_0 \\ & \text{s.t.} \quad \|\mathbf{y} - \mathbf{\Phi}\mathbf{x}\|_2 \leq \epsilon. \end{aligned} \tag{2.15}$$

For a stable sparse solution of P_0^{ϵ}, [21] proposed the following theorem

Theorem 2.2.5. *Consider a USLE,* $\mathbf{y} = \mathbf{\Phi}\mathbf{x} + \mathbf{v}$. *If* $\mathbf{x}$ *satisfies* $\|\mathbf{x}\|_0 < 0.5(1 + 1/\mu(\mathbf{\Phi}))$ *and can represent* $\mathbf{y}$ *within a tolerance* ϵ*, i.e.,* $\|\mathbf{y} - \mathbf{\Phi}\mathbf{x}\|_2 \leq \epsilon$*, then* P_0^{ϵ} *has a solution* $\hat{\mathbf{x}}$*, such that*

$$\|\hat{\mathbf{x}} - \mathbf{x}\|_2^2 \leq \frac{4\epsilon^2}{1 - \mu(\mathbf{\Phi})(2K - 1)}. \tag{2.16}$$

Now by relaxing the ℓ_0-norm by an ℓ_1-norm in the context of (2.14), P_1 can be rewritten as

$$\begin{aligned} \mathrm{P}_1^{\epsilon}: \qquad & \arg\min_{\mathbf{x}} \quad \|\mathbf{x}\|_1 \\ & \text{s.t.} \quad \|\mathbf{y} - \mathbf{\Phi}\mathbf{x}\|_2 \leq \epsilon \end{aligned} \tag{2.17}$$

which is also known as basis pursuit denoising (BPDN) [15], although originally proposed in [22]. For the stable sparse solution of P_1^{ϵ}, some very nice results have been proposed using the RIP (Definition 2.2.4). In this regard, [23] proposed the following

Theorem 2.2.6. *Consider a USLE,* $\mathbf{y} = \mathbf{\Phi}\mathbf{x} + \mathbf{v}$. *If RIP holds for* K *such that,* $\delta_{3K} + 3\delta_{4K} < 2$ *(or* $\delta_{2K} < \sqrt{2} - 1$*), then* P_1^{ϵ} *has a solution* $\hat{\mathbf{x}}$ *that satisfies*

$$\|\hat{\mathbf{x}} - \mathbf{x}\|_2 \leq C_v \epsilon \tag{2.18}$$

where C_v *is a positive constant.*

It is also possible that it is not only the measurements $\mathbf{y}$ that are corrupted by noise, but the optimization vector $\mathbf{x}$ is also not exactly sparse, i.e., it has a few nonzero elements and many more with negligibly small values. Let $\mathbf{x}_K$ be an $N \times 1$ vector that contains the K largest nonzero elements of $\mathbf{x}$ and the rest set to exactly zero. In such a scenario, [23] proposed the following modified theorem

Theorem 2.2.7. *Consider a USLE,* $\mathbf{y} = \mathbf{\Phi x} + \mathbf{v}$. *If RIP holds for* K *such that,* $\delta_{3K} + 3\delta_{4K} < 2$ *(or* $\delta_{2K} < \sqrt{2} - 1$*), then* P_1^{ϵ} *has a solution* $\hat{\mathbf{x}}$ *that satisfies*

$$\|\hat{\mathbf{x}} - \mathbf{x}\|_2 \leq (C_k/\sqrt{K})\|\mathbf{x} - \mathbf{x}_K\|_1 + C_v\epsilon \tag{2.19}$$

where C_k *and* C_v *are positive constants.*

The results of Theorem 2.2.7 are quite strong. In case $\mathbf{x}$ is exactly K-sparse, then it guarantees stable recovery. Even if $\mathbf{x}$ is not exactly K-sparse, the solution is as good as the one obtained by pre-selecting the K most significant nonzero elements of $\mathbf{x}$.

2.3 Measurement Matrices

We have seen in the previous section that most of the conditions for sparse recovery relate to the properties of measurement matrices. The question is how to design such matrices. Since RIP is a very generalized property which guarantees sparse recovery in different scenarios, one is tempted to find matrices which satisfy this property, i.e., their different subsets of columns are nearly orthogonal. This is the point where randomness comes into play and assumes a critical role. In the following we present some of the most widely used measurement matrices which satisfy RIP for substantially large values of K, i.e., the order of sparsity.

- **Gaussian Matrices**: An $M \times N$ Gaussian measurement matrix $\mathbf{\Phi}$ can be designed by taking independent identically distributed elements from a zero-mean normal distribution with variance $1/M$, i.e., $[\mathbf{\Phi}]_{i,j} \sim \mathcal{N}(0, 1/M)$. If

  $$M \geq C\, K \log(N/K) \tag{2.20}$$

  where C is a positive constant, then $\mathbf{\Phi}$ satisfies RIP with high probability.

- **Bernoulli Matrices**: An $M \times N$ Bernoulli measurement matrix $\mathbf{\Phi}$ comprises of independent, equiprobable elements with values $\pm 1/\sqrt{M}$. Similar to Gaussian matrices, if $\mathbf{\Phi}$ obeys (2.20), then RIP is satisfied with high probability.

- **Fourier Matrices**: An $M \times N$ Fourier measurement matrix $\mathbf{\Phi}$ can be designed by selecting M rows, uniformly at random, from an $N \times N$ Fourier matrix. The columns of the resulting matrix are further normalized to unit ℓ_2-norm. It was proved in [24] that RIP is held with overwhelming probability if

$$M \geq C\, K (\log N)^6 \tag{2.21}$$

which was further improved by [25] to

$$M \geq C\, K (\log N)^4. \tag{2.22}$$

However, satisfying (2.20) can also guarantee promising results.

2.4 Sparse Recovery Algorithms

Over the past few years, a plethora of algorithms has emerged in order to recover sparse signals from compressed measurements. Here, we briefly describe some of the major categories because elaborating upon a particular algorithm can be too specific. However, in subsequent chapters we provide a detailed discussion on some of the algorithms.

2.4.1 Greedy Algorithms

Greedy algorithms attempt to provide an approximate solution of P_0. We know that P_0 calls for an exhaustive search, in general. Greedy algorithms abandon this approach in favor of the one-at-a-time strategy. The algorithms proceed in a sequential manner. In each step, a suitable column is selected, which basically reduces a residual error, and made part of a candidate set. Limits can be put either on the magnitude of the residual error or the number of columns in the candidate set. Clearly, this strategy is more feasible than an exhaustive search. However, the performance can vary with different situations. Since these algorithms are myopic in nature, finding a global optimum can be challenging. A large number of variants are available which basically improve the complexity and/or performance, e.g., matching pursuit (MP) [26, 27], orthogonal matching pursuit (OMP) [28, 29, 30], flexible tree search based OMP (FT-OMP) [31], compressive sampling MP (CoSaMP) [32], etc.

2.4.2 Algorithms Based on Convex Relaxations

Algorithms based on convex relaxations basically solve P_1 or P_1^ϵ, also known as BP and BPDN, respectively. These algorithms have a major difference from the greedy approaches, in that their optimization approach is mostly global in nature. There is a vast variety of such algorithms. After casting the problem as an LP, solutions can be provided by interior-point methods [15], especially for large scale systems. Further, a number of iterative thresholding algorithms (ITH) can also be used [33, 34, 35, 36], again especially for large scale systems. Various solvers of the least absolute shrinkage and selection operator (LASSO) [37] problem can also be used, e.g., least angle regression (LARS) [38] and coordinate descent methods [39]. Similarly, some Bayesian approaches, e.g., Bayesian compressive sampling [40] can also be utilized.

2.4.3 Algorithms Based on Different Priors

Most of the CS literature has focused on solving P_1 or P_1^ϵ, where the basic aim is purely to recover a sparse signal. Therefore, only one prior, i.e., an ℓ_1-norm over the optimization vector, has been under investigation for a large part. However, most of the signals are not just sparse, they also offer some special structure in the sparsity as well. Thus, sparsity problems with priors of different types have recently been proposed in the literature. For example, in case of block sparsity there are algorithms like group LASSO [41], sparse group LASSO [42], etc. In order to tackle correlations in sparse elements, algorithms like elastic net [43] have been proposed. Similarly, smoothness in sparsity has been addressed in fused LASSO [44].

Part II: Papers Included

Chapter 3

Compressive Sampling Based Energy Detection of UWB Pulse Position Modulation

Shahzad Gishkori and Geert Leus

Abstract

Compressive sampling (CS) based energy detectors are developed for ultra-wideband (UWB) pulse position modulation (PPM), in multipath fading environments so as to reduce the sampling complexity at the receiver side. Due to sub-Nyquist rate sampling, the CS process outputs a compressed version of the received signal such that the original signal can be recovered from this low dimensional representation. Using the principles of generalized maximum likelihood (GML), we propose two types of energy detectors for such signals. The first type of detectors involves the reconstruction of the received signal followed by a detection stage. Statistical properties of the reconstruction error have been used for the realization of such kind of detectors. The second type of detectors does not rely on reconstruction and carries out the detection operation directly on the compressed signal, thereby offering a further reduction in the implementation complexity. The performance of the proposed detectors is independent of the spreading factor. We analyze the bit error performance of the proposed energy detectors for two scenarios of the propagation channel: when the channel is deterministic, and when it is Gaussian distributed. We provide exact bit error probability (BEP) expressions of the CS-based energy detectors for each scenario of the channel. The BEP expressions obtained for the detectors working on the compressed signal directly, can naturally be extended to BEP expressions for the related energy detectors working on the Nyquist-rate sampled signal. Simulation results validate the accuracy of these BEP expressions.

3.1 Introduction

Digital communications is witnessing a phenomenal growth in applications which involve signals of very high bandwidth. Impulse-radio (IR) ultra-wideband (UWB) signals are attractive because they offer high user capacity, fine time resolution as well as low probability of interception and detection [45, 8]. A big hurdle in the implementation of IR-UWB systems is the efficiency of the analog-to-digital converters (ADCs). According to the classical Shannon-Nyquist-Whittaker-Kotelnikov sampling theorem [3, 4], a band-limited signal $x(t)$ (i.e., $X(\omega) = 0, |\omega| > \omega_m$) can be determined completely from its samples $x(nT_s)$ if $T_s \leq \pi/\omega_m$. So the sampling rate should be at least twice the highest frequency. Therefore, if the bandwidth of the signal is too high, ADCs can be heavily stressed causing an increase in the power consumption [2, 10]. It could take decades before the ADC technology is fast, precise and low-cost enough for the present-day high-bandwidth applications

[46]. On the other hand, it has been described in [3] that most of the signals with large bandwidths have a small rate of information. This property of wideband signals makes them sparse in information which has led to sampling methods based on the amount of information (or the rate of innovation). The combination of sparsity with finite rate of innovation has been described in [47], primarily for the non-discrete domain. Compressive sampling (CS) [5, 6] offers more flexible options to deal with sparse signals in terms of the location of the information and the non-uniformity of the measurements as we shall elaborate upon in subsequent sections. In this paper, we use CS to capitalize on the time-domain sparsity of the IR-UWB signals to reduce the sampling rate as well as the implementation complexity of energy detectors.

Relation to prior work. We consider UWB pulse position modulation (PPM) signals. PPM is advantageous because of its simplicity and the ease of controlling delays [45] but the disadvantage, in the context of UWB signals, is the relatively large bandwidth associated with it, which causes a large number of visible propagation paths [48]. In this paper, we concentrate on noncoherent PPM receiver design through energy detection [49, 50, 51] and adopt CS for reduced system complexity as well as power consumption. The resulting detection procedure resembles a generalized maximum likelihood (GML) detector. The symbol decision is determined by the pulse position that contains most of the energy. Note that different works on CS in combination with UWB signals have appeared recently, e.g., in [52] for coherent receivers, in [53] for symbol-rate sampling but requiring pre-identification of the channel which was then extended to [54] for channel and timing estimation, in [55] for a GLRT-based detector which was then extended to [56] with an effective measurement matrix design but both requiring the transmission of pilot symbols, in [57] for joint time of arrival estimation and data decoding which requires channel estimation, in [58] and [59] to account for narrow-band interference, in [60] and [61] for UWB channel estimation, in [62] for time-delay estimation and in [63] for differential detection of UWB signals. In contrast to previous methods, we present noncoherent UWB detectors. We neither require pre-identification of the channel, nor the transmission of pilot symbols. Most of the previous methods also require signal reconstruction whereas, we present a method which skips this step altogether. Note that previous examples of detection with compressed symbols can be found in [63] and [64].

Our Contributions.

- We utilize the CS framework to reduce the receiver sampling rate for IR-UWB PPM signals much below the Nyquist rate.

- Using the principles of GML, we develop CS-based energy detectors for the signal reconstructed from its compressed samples. We also propose energy detectors which operate on the compressed signal directly and do not need reconstruction.

- We show that the performance of our proposed energy detectors is independent of the spreading factor.

- We provide bit error probability (BEP) expressions for the proposed compressed detectors for a deterministic channel as well as a Gaussian distributed channel. We show that these expressions can be easily modified for the energy detectors based on Nyquist-rate sampling.

Organization. The paper is organized as follows. Section 3.2 presents the system model. Section 3.3 provides the CS-based energy detectors using the GML criteria for the reconstructed signal as well as for the compressed signal without reconstruction. Section 3.4 provides the theoretical BEP expressions for the CS-based energy detectors when the channel is considered deterministic. Section 3.5 provides the theoretical BEP expressions when the channel is considered to be Gaussian distributed. Finally, Section 5.6 presents the simulations and the concluding remarks are given in Section 3.7.

3.2 System Model

To transmit the kth information symbol, consider an $\mathcal{M}$-ary PPM signal $s_k(t)$ of length T. Every symbol consists of N_f frames, each with frame duration T_f, so that the symbol time is given by $T = N_f T_f$. The motivation for a multiple-frame transmission has been attributed to the federal communications commission (FCC) limits on the signal power spectral density [7]. Repeating a pulse N_f times, reduces the energy of an individual pulse for a constant symbol energy. In PPM, the signal is modulated by delaying the transmitted pulse within a frame. The ease of implementing these delays also reflects the simplicity of PPM. Let the base pulse delay be defined as, $T_{\mathcal{M}} \triangleq T_f/\mathcal{M}$, then the transmitted signal for the kth information symbol $a_k \in \{0, 1, \ldots, \mathcal{M}-1\}$ can be written as $s_k(t) = \sum_{j=0}^{N_f-1} q(t - (j + kN_f)T_f - a_k T_{\mathcal{M}})$, where $q(t)$ is the unit-energy pulse waveform of duration T_q such that $T_q \ll T_{\mathcal{M}}$. If $g(t)$ represents the impulse response of the physical communication channel, then the received signal corre-

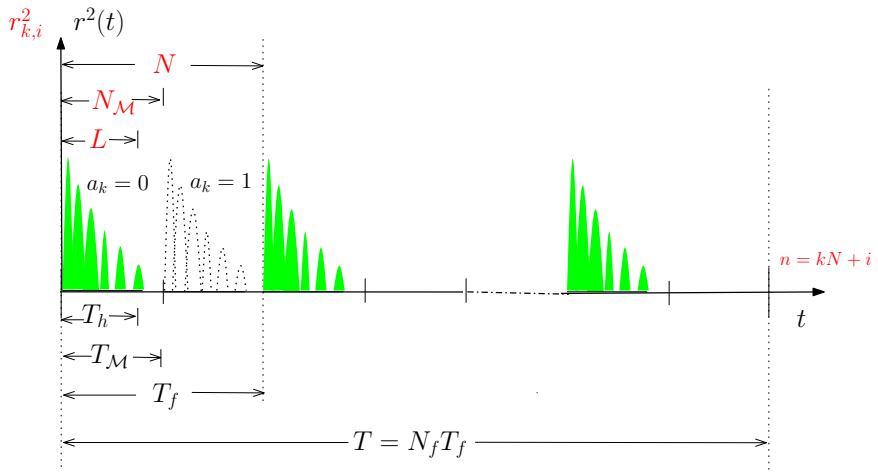

Figure 3.1: The squared received signal without noise for $\mathcal{M} = 2$. Labels below the time axis show the usual time-based parameters, while the labels above the time axis show values for the squared Nyquist-rate sampled version of $r(t)$, i.e., $r^2_{k,i}$

sponding to the kth information symbol is given by

$$\begin{aligned} r_k(t) &= s_k(t) \star g(t) + v_k(t) \\ &= \sum_{j=0}^{N_f-1} h(t - jT_f - kT - a_k T_{\mathcal{M}}) + v_k(t). \end{aligned}$$

where $v_k(t)$ is the additive noise corresponding to the kth information symbol and $h(t) \triangleq q(t) \star g(t)$ is the received pulse waveform of duration T_h. We can represent $r_k(t)$ by its Nyquist-rate sampled version. We take N samples per frame period T_f such that N/T_f is equivalent to the Nyquist rate. Let $N_{\mathcal{M}} \triangleq N/\mathcal{M}$ be the integer number of Nyquist-rate samples in each slot, then the sampled received signal corresponding to the kth information symbol in the jth frame is given by

$$r^{(j)}_{k,i} \triangleq r_k(jT_f + iT_f/N) = h_{i-jN-kNN_f-a_k N_{\mathcal{M}}} + v^{(j)}_{k,i}, \tag{3.1}$$

for $i = 0, 1, \ldots, N-1$, where $h_i \triangleq h(iT_f/N)$ and $v^{(j)}_{k,i} \triangleq v_k(jT_f + iT_f/N)$. We assume that the elements $v^{(j)}_{k,i}$ are independent identically distributed (i.i.d.) zero-mean Gaussian with variance σ^2. The support of h_i is given by $[0, L-1]$, where $L \triangleq \lceil NT_h/T_f \rceil$ (see Figure 3.1). Since we want to make the detection process separable in the different frames/symbols, we do not want the received pulses to

overlap and thus we require $T_h \leq T_{\mathcal{M}}$ or $L \leq N_{\mathcal{M}}$. We can also write (3.1) in the following vector form

$$\mathbf{r}_k^{(j)} = \mathbf{u}^{(j)}(a_k, \mathbf{h}) + \mathbf{v}_k^{(j)} \tag{3.2}$$

where $\mathbf{r}_k^{(j)} \triangleq [r_{k,0}^{(j)}, r_{k,1}^{(j)}, \ldots, r_{k,N-1}^{(j)}]^T$, $\mathbf{v}_k^{(j)} \triangleq [v_{k,0}^{(j)}, v_{k,1}^{(j)}, \ldots, v_{k,N-1}^{(j)}]^T$ and $\mathbf{h} \triangleq [h_0, h_1, \ldots, h_{L-1}]^T$. Since we assume that the channel does not vary within a symbol period, $\mathbf{u}^{(j)}(a_k, \mathbf{h})$ is the same for every frame, i.e., $\mathbf{u}^{(0)}(a_k, \mathbf{h}) = \mathbf{u}^{(1)}(a_k, \mathbf{h}) = \cdots = \mathbf{u}^{(N_f-1)}(a_k, \mathbf{h}) = \mathbf{u}(a_k, \mathbf{h})$. The $N \times 1$ vector $\mathbf{u}(a_k, \mathbf{h})$ consists of $\mathcal{M} - 1$ blocks of zero values and only one block with L nonzero values provided by $\mathbf{h}$. Let $\tilde{\mathbf{h}} \triangleq [\mathbf{h}^T, \mathbf{0}_{(N_{\mathcal{M}}-L)\times 1}^T]^T$, then the structure of $\mathbf{u}(a_k, \mathbf{h})$ can be represented as

$$\mathbf{u}(a_k, \mathbf{h}) \triangleq \left[\mathbf{0}_{a_k N_{\mathcal{M}} \times 1}^T, \tilde{\mathbf{h}}^T, \mathbf{0}_{(\mathcal{M}-a_k-1)N_{\mathcal{M}}\times 1}^T\right]^T$$

which reflects the enormous amount of sparsity present in UWB PPM signals (e.g., the subsequent sparsity pattern of $r_k(t)$ can be seen as in Figure 3.1). The covariance matrix of $\mathbf{v}_k^{(j)}$ can be written as $\mathrm{E}\left\{\mathbf{v}_k^{(j)}\mathbf{v}_k^{(j)T}\right\} = \sigma^2\mathbf{I}_N$. We can finally convert (3.2) in the following symbol level compact form

$$\mathbf{r}_k = \left[\mathbf{1}_{N_f\times 1} \otimes \mathbf{u}(a_k, \mathbf{h})\right] + \mathbf{v}_k \tag{3.3}$$

where $\mathbf{r}_k \triangleq [\mathbf{r}_k^{(0)T}, \mathbf{r}_k^{(1)T}, \ldots, \mathbf{r}_k^{(N_f-1)T}]^T$, $\mathbf{v}_k \triangleq [\mathbf{v}_k^{(0)T}, \mathbf{v}_k^{(1)T}, \ldots, \mathbf{v}_k^{(N_f-1)T}]^T$ and $\mathbf{1}_{N_f\times 1}$ is a vector of ones of length N_f.

The CS theory implies that the sparse received signal (comprising K basis functions) is operated upon by a certain transform operator which generates M linear measurements of the received signal such that $M \ll N$, where N represents the number of Nyquist-rate samples of the received signal. This process is carried out in the analog domain [46, 65, 66]. Here, we represent this transform operator as an $M \times N$ measurement matrix $\mathbf{\Phi}\colon \mathbb{R}^N \longrightarrow \mathbb{R}^M$, with M linear functionals as its rows. Each measurement provides a compressed sample of the received signal which eventually leads to a lower M-dimensional representation of the N-dimensional signal. The ratio between M and N is called the undersampling ratio $\mu \triangleq M/N$. The measurement matrix plays an important role in recovering the signal from its compressed samples. For this, it has to satisfy the restricted isometry property (RIP) [6]. A large number of random matrices, e.g., Gaussian and Bernoulli matrices, as well as structured matrices (with randomly selected rows), e.g., Fourier (for signals with time-domain spasity), satisfy this property.

At this point, we would like to elucidate the structure of the measurement matrix used in the context of our work. To this end, we present the following assumptions.

Assumption 1. The entries of the measurement matrix $\mathbf{\Phi}$ are zero-mean i.i.d. with variance $1/M$. As a result, its covariance matrix can be written as $\mathrm{E}\{\mathbf{\Phi}\mathbf{\Phi}^T\} = \frac{1}{\mu}\mathbf{I}_M$. Now, as $N \longrightarrow \infty$, it can be stated that the rows of the measurement matrix $\mathbf{\Phi}$ are approximately orthogonal to each other, i.e.,

$$\mathbf{\Phi}\mathbf{\Phi}^T \approx \frac{1}{\mu}\mathbf{I}_M. \tag{3.4}$$

Assumption 2. Considering a $\mathbf{\Phi}$ matrix for which the approximation (3.4) in Assumption 1 is exact, i.e.,

$$\mathbf{\Phi}\mathbf{\Phi}^T = \frac{1}{\mu}\mathbf{I}_M. \tag{3.5}$$

In other words, the rows of the measurement matrix are orthogonal and its columns have unit ℓ_2-norm.

Assumption 3. Given a $M_{\mathcal{M}} \times N_{\mathcal{M}}$ matrix $\tilde{\mathbf{\Phi}}$ where $M_{\mathcal{M}} \triangleq M/\mathcal{M}$, in order to treat each of the $\mathcal{M}$ slots separately, the measurement matrix can be designed as $\mathbf{\Phi} = \mathbf{I}_{\mathcal{M}} \otimes \tilde{\mathbf{\Phi}}$.

Note that Assumption 3 can be used along with either Assumption 1 or 2. In the former case, the entries of the matrix $\tilde{\mathbf{\Phi}}$ will be zero-mean i.i.d. with variance $1/M_{\mathcal{M}}$, and in the latter case, the rows of the matrix $\tilde{\mathbf{\Phi}}$ will be orthogonal with unit ℓ_2-norm columns. Assumptions 1 and 2 play an important role in the performance analysis of the proposed detectors. We will explain this in the related sections.

Now, applying CS to (3.2) we can write its compressed version as

$$\mathbf{y}_k^{(j)} \triangleq \mathbf{\Phi}\mathbf{r}_k^{(j)} = \mathbf{\Phi}\mathbf{u}(a_k, \mathbf{h}) + \boldsymbol{\xi}_k^{(j)} \tag{3.6}$$

where $\mathbf{y}_k^{(j)}$ is the $M \times 1$ measurement vector for the jth frame and $\boldsymbol{\xi}_k^{(j)} \triangleq \mathbf{\Phi}\mathbf{v}_k^{(j)}$ is the $M \times 1$ noise vector. The noise $\boldsymbol{\xi}_k^{(j)}$ is also zero-mean Gaussian with covariance matrix

$$\mathrm{E}\left\{\boldsymbol{\xi}_k^{(j)}\boldsymbol{\xi}_k^{(j)T}\right\} = \mathbf{\Phi}\mathrm{E}\left\{\mathbf{v}_k^{(j)}\mathbf{v}_k^{(j)T}\right\}\mathbf{\Phi}^T \cong \frac{\sigma^2}{\mu}\mathbf{I}_M \tag{3.7}$$

depending upon Assumption 1 or 2. Note that unlike the commonly used signal models for CS, the noise in our case is also compressed. Thus the choice of the measurement matrix becomes relevant to determine whether the resulting compressed noise is i.i.d. or not. The symbol level joint model can be written as

$$\mathbf{y}_k = \left[\mathbf{I}_{N_f} \otimes \mathbf{\Phi}\right]\mathbf{r}_k = \left[\mathbf{1}_{N_f \times 1} \otimes \mathbf{\Phi}\mathbf{u}(a_k, \mathbf{h})\right] + \boldsymbol{\xi}_k \tag{3.8}$$

where $\mathbf{y}_k \triangleq [\mathbf{y}_k^{(0)T}, \mathbf{y}_k^{(1)T}, \ldots, \mathbf{y}_k^{(N_f-1)T}]^T$ and $\boldsymbol{\xi}_k \triangleq [\boldsymbol{\xi}_k^{(0)T}, \boldsymbol{\xi}_k^{(1)T}, \ldots, \boldsymbol{\xi}_k^{(N_f-1)T}]^T$ are the $N_f M \times 1$ joint compressed measurement and noise vectors for the kth symbol, respectively.

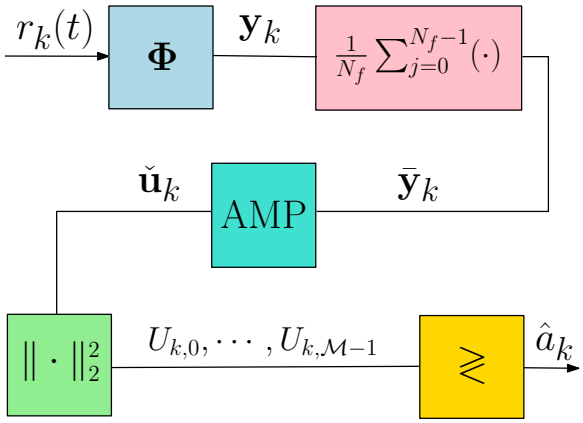

Figure 3.2: Block diagram for the CS-based ED with reconstructed signals.

3.3 CS Based Detection

For low system complexity and power consumption, we focus on the noncoherent reception of UWB PPM signals [49], which is akin to GML detection. The received signal is sampled at a compressed rate according to (3.6). A straightforward receiver then would require the reconstruction of the actual received signal to carry out the detection process. The other approach may be the detection from the compressed samples directly without reconstructing the received signal. We shall explore both approaches, i.e., the detection after reconstruction and the detection without reconstruction of the compressed received signal (see Figures 3.2 and 3.3 for the block diagrams of the two respective proposed approaches). Either way, we have to handle each frame individually, and we want to find an optimal way to handle multiple frames.

3.3.1 Reconstruction Based Detectors

Signal reconstruction and error statistics

The reconstruction of a sparse signal calls for the solution of an ℓ_0-norm optimization problem. Since the related problem is NP-hard, its ℓ_1-norm equivalent optimization problem, i.e., the convex relaxation of the ℓ_0-norm, has been suggested in the literature [15]. One way to reconstruct the received signal from its compressed samples consists of solving the following optimization problem, (from (3.8) for

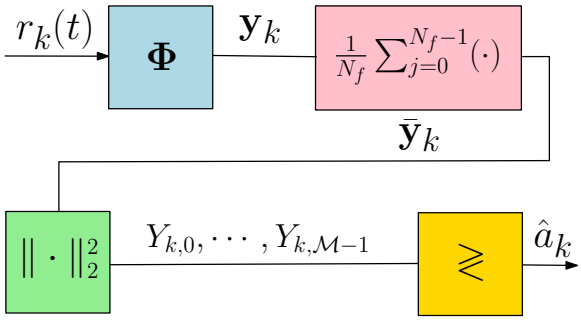

Figure 3.3: Block diagram for the CS-based ED with compressed signals.

$N_f = 1$)

$$\hat{\mathbf{u}}_k = \arg\min_{\mathbf{u}_k} \|\mathbf{u}_k\|_1^1 \quad \text{s.t.} \quad \|\mathbf{y}_k - \mathbf{\Phi}\mathbf{u}_k\|_2^2 \leq \epsilon \tag{3.9}$$

where $\mathbf{u}_k$ corresponds to $\mathbf{u}(a_k, \mathbf{h})$ and ϵ is a constant. The ℓ_1-norm minimization problem (3.9), also known as basis pursuit (BP), can recover the sparse signal from its compressed samples but the bottleneck is the size of the signal model. With $N \longrightarrow \infty$, this method becomes computationally expensive (as the worst-case complexity can be of $\mathcal{O}(M^2N^{1.5})$ for interior point algorithms). Alternatively, matching pursuit algorithms can also be used, e.g., orthogonal matching pursuit (OMP) [29, 30] (with a complexity of $\mathcal{O}(KMN)$). These methods are based on iteratively selecting the columns of the measurement matrix, one by one, that are most correlated with the observation vector and its subsequent residual vectors. Variants of matching pursuit algorithms include other greedy algorithms that, in contrast, select more than one column of the measurement matrix through correlations. A case in point is the compressive sampling matching pursuit (CoSaMP) [32] (with a complexity of $\mathcal{O}(MN)$), which also has elaborate performance bounds. In CoSaMP, the signal is estimated by solving a least-squares problem on the candidate components in every step, which involves matrix inversion. This inversion step remains a bottleneck in reducing the computational complexity. The iterative thresholding (ITH) algorithms [67] (with a complexity of $\mathcal{O}(N \log N)$), on the other hand, do not have to invert a matrix, and reconstruct a sparse signal from its

compressed samples through the following simple iterations

$$\hat{\mathbf{u}}_k^{[n+1]} = \mathcal{S}\left(\hat{\mathbf{u}}_k^{[n]} + \mathbf{\Phi}^T \mathbf{z}_k^{[n]}, \lambda^{[n]}\right) \tag{3.10}$$

$$\mathbf{z}_k^{[n]} = \mathbf{y}_k - \mathbf{\Phi}\hat{\mathbf{u}}_k^{[n]} \tag{3.11}$$

where n is the iteration index and $\mathcal{S}(x, \lambda)$ is the thresholding operator. Variants of ITH are generated depending upon the thresholding to be hard, i.e., $\mathcal{S}(x, \lambda) \triangleq x\mathbb{I}_{\{|x|>\lambda\}}$ (where $\mathbb{I}$ is the indicator function) or soft $\mathcal{S}(x, \lambda) \triangleq \text{sign}(x)(|x|-\lambda)_+$. In general, we will use $\mathcal{S}(x, \lambda)$ to denote a soft thresholding operator. To compare the performance of different ITH algorithms with other approaches e.g., BP or OMP, a performance measure depicting the transitions between success and failure phases of an algorithm, named the sparsity-undersampling (SU) measure, was proposed in [67]. The sparsity $\rho \triangleq \frac{K}{M}$ is the ratio between the number of non-zero components in the sparse signal vector and the number of compressed measurements, whereas the undersampling ratio μ is the ratio between the number of compressed measurements and the total number of elements in the signal vector. Through exhaustive simulations, it was observed in [67] that although ITH is fast and has a low complexity, it unfortunately performs poorly on the SU measure. To retain the fast speed of an iterative algorithm but surpass the performance barrier on the SU measure, the following iterative algorithm, named the approximate message passing (AMP) algorithm, was proposed in [34, 35, 36]. It can be summarized as

$$\hat{\mathbf{u}}_k^{[n+1]} = \mathcal{S}\left(\hat{\mathbf{u}}_k^{[n]} + \mathbf{\Phi}^T \mathbf{z}_k^{[n]}, \lambda^{[n]}\right) \tag{3.12}$$

$$\begin{aligned}\mathbf{z}_k^{[n]} &= \mathbf{y}_k - \mathbf{\Phi}\hat{\mathbf{u}}_k^{[n]} \\ &\quad + \frac{1}{\mu}\mathbf{z}_k^{[n-1]}\left\langle \mathcal{S}'\left(\hat{\mathbf{u}}_k^{[n-1]} + \mathbf{\Phi}^T \mathbf{z}_k^{[n-1]}, \lambda^{[n-1]}\right)\right\rangle\end{aligned} \tag{3.13}$$

where $\mathcal{S}'(\mathbf{x}, \lambda)$ is the derivative of the soft thresholding operator $\mathcal{S}(\mathbf{x}, \lambda)$ (it generates a 1 for every nonzero element of $\mathbf{x}$) and $\langle \mathbf{x} \rangle$ gives the average value of the elements of $\mathbf{x}$, thus $\langle \mathcal{S}'(\mathbf{x}, \lambda) \rangle = \frac{1}{N}\|\mathcal{S}(\mathbf{x}, \lambda)\|_0$ where N is the number of elements in $\mathbf{x}$. The key difference between ITH and AMP is the additional term in (3.13), i.e., $\frac{1}{\mu}\mathbf{z}_k^{[n-1]}\left\langle \mathcal{S}'\left(\hat{\mathbf{u}}_k^{[n-1]} + \mathbf{\Phi}^T \mathbf{z}_k^{[n-1]}, \lambda^{[n-1]}\right)\right\rangle$, altering the residual. In statistical physics, such a term is known as the "Onsager reaction term". For our context and reference we name it as the correction term (CT).

AMP has been derived from the message passing (MP) algorithm which is used in graphical inference models [68]. It was used in [40] for compressed sensing through belief propagation over factor graphs [69]. The problem with the message

passing algorithm is that instead of updating only N nodes at each iteration, it updates MN nodes, causing an increase in the computational complexity. If the number of nodes to be updated is restricted to the N variable nodes then message passing reduces to ITH. AMP provides the middle way. By neglecting the weakly dependent updates in the MP algorithm, it updates only N nodes, but what is lost by not updating the M measurement nodes is gained by the addition of the CT. See [35] for a complete derivation of this approximation leading to AMP.

AMP assumes the measurement matrix $\mathbf{\Phi}$ to be a random measurement matrix whose elements are zero-mean i.i.d. with variance $1/M$. In our context, Assumption 1 then becomes relevant. Note, AMP is valid under $N \longrightarrow \infty$. Our Assumption 1 also requires this tendency of N so that (3.4) can hold. Now, the most important feature of AMP is the statistical characterization of the reconstruction error at every iteration. This can be understood by developing certain heuristics for the iterative approaches. From (3.11), the correlation of the measurement matrix with the residual vector at the nth iteration can be expanded as

$$\mathbf{\Phi}^T \mathbf{z}_k^{[n]} = (\mathbf{u}_k - \hat{\mathbf{u}}_k^{[n]}) + \mathbf{H}(\mathbf{u}_k - \hat{\mathbf{u}}_k^{[n]}) + \mathbf{\Phi}^T \boldsymbol{\xi}_k \tag{3.14}$$

where $\mathbf{H} \triangleq (\mathbf{\Phi}^T\mathbf{\Phi} - \mathbf{I}_N)$. Now, as described in [34], if it is assumed that $\mathbf{H}$ does not correlate with the vector $\hat{\mathbf{u}}_k^{[n]}$ then $\mathbf{H}(\mathbf{u}_k - \hat{\mathbf{u}}_k^{[n]})$ can be viewed as a vector of i.i.d. Gaussian random variables and the variance of each variable can be given as $\frac{1}{M}\|\mathbf{u}_k - \hat{\mathbf{u}}_k^{[n]}\|_2^2$. Let the noisy estimate of the received signal be defined as

$$\check{\mathbf{u}}_k^{[n]} \triangleq \hat{\mathbf{u}}_k^{[n]} + \mathbf{\Phi}^T \mathbf{z}_k^{[n]} \tag{3.15}$$

and the error in estimating the true signal from this estimate be defined as

$$\mathbf{w}_k^{[n]} \triangleq \check{\mathbf{u}}_k^{[n]} - \mathbf{u}_k \tag{3.16}$$

with $\sigma_w^{[n]2}$ denoting the variance of each of its elements. If the above mentioned heuristics are true, then the variance of the elements of the error vector $\mathbf{w}_k$ can be tracked by the following state evolution (SE) method for every iteration

$$\sigma_w^{[n+1]2} = \Psi\left(\sigma_w^{[n]2}\right) \tag{3.17}$$

where the function $\Psi(\sigma_w^{[n]2})$ is defined as

$$\Psi\left(\sigma_w^{[n]2}\right) \triangleq \frac{1}{\mu}\left(\sigma^2 + \mathrm{E}\left\{\left\|\mathcal{S}\left(\mathbf{u}_k + \sigma_w^{[n]2}\mathbf{n}, \lambda^{[n]}\right) - \mathbf{u}_k\right\|_2^2\right\}\right) \tag{3.18}$$

where $\mathbf{n}$ is a vector of zero-mean standard i.i.d. Gaussian random variables, i.e., $\mathbf{n} \sim \mathcal{N}(\mathbf{0}, \mathbf{I})$ and we have considered $\mathrm{E}\left\{(\mathbf{\Phi}^T\boldsymbol{\xi}_k)(\mathbf{\Phi}^T\boldsymbol{\xi}_k)^T\right\} = \frac{\sigma^2}{\mu}\mathbf{I}_N$ under Assumption 1. From (3.18), we can see that the SE also predicts the mean squared error (MSE) of the reconstructed signal in that the SE converges to the true MSE at every iteration as $N \longrightarrow \infty$ [70], i.e.,

$$\mathrm{E}\left\{\left\|\mathcal{S}\left(\mathbf{u}_k + \sigma_w^{[n]2}\mathbf{n}, \lambda^{[n]}\right) - \mathbf{u}_k\right\|_2^2\right\} = \frac{1}{N}\left\|\mathbf{u}_k - \hat{\mathbf{u}}_k^{[n]}\right\|_2^2 \tag{3.19}$$

provided that $\Psi\left(\sigma_w^{[n]2}\right) < \sigma_w^{[n]2}$ which should remain true for the SU measure of AMP to coincide with that of other methods, such as BP. It has been observed through extensive numerical simulations (see e.g., [36]) that SE fails to predict the performance of ITH algorithms. The reason is the correlation between $\mathbf{H}$ and $\hat{\mathbf{u}}_k^{[n]}$, which appears right after the first iteration and thus the above heuristics are not true for ITH algorithms. On the other hand, the SE predicts the performance of AMP exactly. The reason is that the CT removes or compensates for the correlation between $\mathbf{H}$ and $\hat{\mathbf{u}}_k^{[n]}$ at every iteration and thus the above heuristics regarding the reconstruction noise being Gaussian and the MSE convergence remain true. Thus the variance of each element of the vector $\mathbf{w}_k^{[n]}$ can be written as

$$\sigma_w^{[n]2} = \frac{1}{\mu}\left(\sigma^2 + \frac{1}{N}\left\|\mathbf{u}_k - \hat{\mathbf{u}}_k^{[n]}\right\|_2^2\right) \tag{3.20}$$

Note that the performance comparisons described above bring the thresholding policy to the foreground as well. It would suffice to say that the optimal thresholding value should be a function of the standard deviation $\sigma_w^{[n]}$, i.e., $\lambda^{[n]} = \tau\sigma_w^{[n]}$, where τ is a constant. We will describe the thresholding policy used for our purpose in Section 5.6.

GML based detection for multiple-frame reconstructed signals

Let us assume that the received signal was compressed at a compression rate μ and then reconstructed using AMP. Here we assume that the AMP algorithm has reached convergence and therefore drop the iteration indices from the variables. Let $\check{\mathbf{q}}_k$ be a $N_f N \times 1$ vector containing all reconstructed frame vectors $\check{\mathbf{u}}_k^{(j)}$, i.e., $\check{\mathbf{q}}_k \triangleq [\check{\mathbf{u}}_k^{(0)T}, \check{\mathbf{u}}_k^{(1)T}, \cdots, \check{\mathbf{u}}_k^{(N_f-1)T}]^T$. From Section 3.3.1, we may assume that the reconstruction error for each signal sample is i.i.d. Gaussian with variance σ_w^2. The pdf for the reconstructed signal from (3.16) can then be written as

$$p(\check{\mathbf{q}}_k|a_k, \mathbf{h}) = C\exp\left\{-\frac{1}{2\sigma_w^2}\|\check{\mathbf{q}}_k - \left[\mathbf{1}_{N_f\times 1} \otimes \mathbf{u}(a_k, \mathbf{h})\right]\|_2^2\right\} \tag{3.21}$$

where C is some positive constant. Using the GML criterion, it is clear that in order to maximize (3.21), we need to minimize the squared ℓ_2-norm, which can be expressed as

$$\begin{aligned}\Lambda(a_k, \mathbf{h}) &= \sum_{j=0}^{N_f-1} \sum_{l=0}^{L-1} (h_l^2 - 2h_l[\check{\mathbf{q}}_k]_{P_{j,l}}) \\ &= N_f \sum_{l=0}^{L-1} h_l^2 \; - \; \sum_{l=0}^{L-1} 2h_l \; \sum_{j=0}^{N_f-1} [\check{\mathbf{q}}_k]_{P_{j,l}}, \end{aligned} \tag{3.22}$$

where $P_{j,l} = jN + a_k N_{\mathcal{M}} + l$ is used for notational simplicity. Taking the partial derivative with respect to h_l while keeping a_k fixed, we obtain

$$\frac{\partial \Lambda(a_k, \mathbf{h})}{\partial h_l} \; = \; 2N_f h_l - 2 \sum_{j=0}^{N_f-1} [\check{\mathbf{q}}_k]_{P_{j,l}}.$$

Minimizing the cost function with respect to $\mathbf{h}$ would mean setting every gradient with respect to h_l to zero, which yields the following optimal estimate for h_l:

$$\hat{h}_l \; = \; \frac{1}{N_f} \sum_{j=0}^{N_f-1} [\check{\mathbf{q}}_k]_{P_{j,l}}. \tag{3.23}$$

Now substituting (3.23) in (3.22), we finally obtain

$$\Lambda(a_k, \hat{\mathbf{h}}) = -N_f \sum_{l=0}^{L-1} \hat{h}_l^2.$$

As a result, the symbol a_k can be found by solving the following problem

$$\min_{a_k} \; \Lambda(a_k, \hat{\mathbf{h}}) = \max_{a_k} \; \sum_{l=0}^{L-1} \hat{h}_l^2. \tag{3.24}$$

Given E_h to be the signal energy per frame, the instantaneous SNR for multiple frames can be defined as $\zeta \triangleq \frac{N_f E_h}{\sigma_w^2}$. From (3.24) and (3.23), it can then be observed that for the same instantaneous SNR ζ, the decision result will be independent of the number of frames N_f. This can be explained as follows. The estimate of $\hat{h}_l$ in (3.23) is obtained by averaging samples over different frames, which on one hand decreases the noise energy by a factor of N_f but on the other hand also decreases the signal energy by a factor of N_f due to the fact that the instantaneous SNR ζ is

kept constant [71]. Hence, the performance of the estimate of h_l does not change with N_f and thus also the solution to (3.24) does not change with N_f (i.e., the spreading factor) since it only involves the estimate of h_l. Replacing $\hat{h}_l$ in (3.24) by the value obtained from (3.23), the optimal energy detector for the reconstructed samples (R-ED) can be written as

$$\hat{a}_k^{(\mathrm{R-ED})} = \arg\max_{a_k} \sum_{l=0}^{L-1} \left[\frac{1}{N_f} \sum_{j=0}^{N_f-1} [\check{\mathbf{q}}_k]_{jN+a_kN_{\mathcal{M}}+l} \right]^2. \tag{3.25}$$

Replacing the reconstructed samples with Nyquist-rate samples in (3.25) gives the optimal Nyquist-rate energy detector (N-ED) [71]. So we can see that the optimal procedure consists of first averaging the signal components over different frames and then squaring, and the related performance is independent of the number of frames N_f if the instantaneous SNR ζ is kept constant. This is in contrast to the GML detector proposed in [49] for the Nyquist-rate sampled signal, which consists of first squaring and then averaging. For the reconstructed samples, it can be formulated as

$$\hat{a}_k^{(\mathrm{SR-ED})} = \arg\max_{a_k} \frac{1}{N_f} \sum_{j=0}^{N_f-1} \sum_{l=0}^{L-1} [\check{\mathbf{q}}_k]^2_{jN+a_kN_{\mathcal{M}}+l} \tag{3.26}$$

We refer to (3.26) as the spreading-factor dependent energy detector for the reconstructed samples (SR-ED). Replacing the reconstructed samples with the Nyquist-rate samples leads to the spreading-factor dependent Nyquist-rate energy detector (SN-ED) [49].

Averaging process in the compressed domain

We can see that the proposed detection procedure is practically feasible. We avoid Nyquist-rate sampling and the detection is carried out on the reconstructed samples. Still, it may require the reconstruction of all the frames which could be computationally expensive. Here we can benefit from the structure of our compressed detector and save a number of reconstruction steps by reconstructing only one (average) frame instead of all the frames. Since the transform operator $\mathbf{\Phi}$ is the same for all the frames, averaging the reconstructed frames should be similar to averaging the compressed frames and then reconstructing only one average frame. Now, by averaging the compressed frames $\mathbf{y}_k^{(j)}$, for $j = 0, \cdots, N_f - 1$, we can define

the compressed average frame by the $M \times 1$ vector $\bar{\mathbf{y}}_k$ as

$$\begin{aligned}\bar{\mathbf{y}}_k &\triangleq \frac{1}{N_f}\sum_{j=0}^{N_f-1}\left(\mathbf{\Phi}\mathbf{u}(a_k,\mathbf{h})+\boldsymbol{\xi}_k^{(j)}\right)\\ &= \mathbf{\Phi}\mathbf{u}(a_k,\mathbf{h})+\bar{\boldsymbol{\xi}}_k \end{aligned} \tag{3.27}$$

where $\bar{\boldsymbol{\xi}}_k = \frac{1}{N_f}\sum_{j=0}^{N_f-1}\boldsymbol{\xi}_k^{(j)}$, and from (3.4) or (3.5) the covariance matrix can be written as $\mathrm{E}\left\{\bar{\boldsymbol{\xi}}_k\bar{\boldsymbol{\xi}}_k^T\right\} \cong \frac{\sigma^2}{\mu N_f}\mathbf{I}_M$. AMP can help us compare the performance of the two approaches. From (3.16), we can see that it is sufficient to look at the reconstruction error/noise statistics resulting from the two approaches to assess the performance of the respective detectors. The error variance σ_w^2 in reconstruction via (3.27) can be written as

$$\sigma_w^2 = \frac{\sigma^2}{\mu N_f}+\frac{1}{\mu N}\left\|\mathbf{u}_k-\hat{\mathbf{u}}_k\right\|_2^2. \tag{3.28}$$

On the other hand, if each frame is first reconstructed from $\mathbf{y}_k^{(j)}$ with $j = 0, 1, \cdots, N_f - 1$, via AMP and then averaged, the variance of each element of the average noise vector $\bar{\mathbf{w}}_k \triangleq \frac{1}{N_f}\sum_{j=0}^{N_f-1}\mathbf{w}^{(j)}$ can be written as

$$\begin{aligned}\sigma_{\bar{w}}^2 &= \frac{\sigma^2}{\mu N_f}+\frac{1}{\mu N N_f}\sum_{j=0}^{N_f-1}\left\|\mathbf{u}_k-\hat{\mathbf{u}}_k^{(j)}\right\|_2^2\\ &\approx \frac{\sigma^2}{\mu N_f}+\frac{1}{\mu N}\|\mathbf{u}_k-\frac{1}{N_f}\sum_{j=0}^{N_f-1}\hat{\mathbf{u}}_k^{(j)}\|_2^2. \end{aligned} \tag{3.29}$$

Now assuming $\hat{\mathbf{u}}_k \approx \frac{1}{N_f}\sum_{j=0}^{N_f-1}\hat{\mathbf{u}}_k^{(j)}$, (3.29) is the same as (3.28). Thus the detectors based on both approaches will perform in a similar manner.

3.3.2 Direct Compressed Detectors

In the previous section we looked at detectors based on the reconstructed signals. Here we use GML to develop a detector based on the compressed signals directly, i.e., without reconstruction. Since we have assumed symbol level synchronization, the individual $\mathcal{M}$ pulse positions can also become accessible under Assumption 3. Further, as there is a linear transformation between the actual received signal and its compressed samples, we should be able to segregate the samples of each compressed received frame $\mathbf{y}_k^{(j)}$ for $j = 0, 1, \cdots, N_f - 1$, into $\mathcal{M}$ blocks. Thus,

each block would then represent the compressed samples corresponding to a pulse position of the actual received signal. Now considering a measurement matrix $\mathbf{\Phi}$ such that Assumption 2 and 3 hold true, we can write the pdf of the compressed received signal from (3.8) as

$$p(\mathbf{y}_k|a_k,\mathbf{x}) = D\exp\left\{-\frac{1}{2\sigma^2}\|\mathbf{y}_k - \left[\mathbf{1}_{N_f\times 1}\otimes\mathbf{\Phi}\mathbf{u}(a_k,\mathbf{h})\right]\|_2^2\right\} \tag{3.30}$$

where D is a constant and $\mathbf{x} \triangleq \tilde{\mathbf{\Phi}}\tilde{\mathbf{h}}$ is an $M_{\mathcal{M}}\times 1$ vector of the compressed samples corresponding to the block in $\mathbf{u}(a_k,\mathbf{h})$ carrying the transmitted pulse. Note that Assumption 2 is important here so that the compressed noise is i.i.d. and (3.30) can be formulated. Now in order to maximize (3.30), we need to minimize

$$\begin{aligned}\Lambda(a_k,\mathbf{x}) &= \sum_{j=0}^{N_f-1}\sum_{l=0}^{M_{\mathcal{M}}-1}\left([\mathbf{x}]_l^2 - 2[\mathbf{x}]_l[\mathbf{y}_k]_{P_{j,l}}\right)\\ &= N_f\sum_{l=0}^{M_{\mathcal{M}}-1}[\mathbf{x}]_l^2 \;-\; \sum_{l=0}^{M_{\mathcal{M}}-1}2[\mathbf{x}]_l\sum_{j=0}^{N_f-1}[\mathbf{y}_k]_{P_{j,l}},\end{aligned} \tag{3.31}$$

where $P_{j,l} = jM + a_kM_{\mathcal{M}} + l$. Taking the partial derivative with respect to $[\mathbf{x}]_l$ and setting the gradient equal to zero, yields the following estimate for $[\mathbf{x}]_l$

$$[\hat{\mathbf{x}}]_l \;=\; \frac{1}{N_f}\sum_{j=0}^{N_f-1}[\mathbf{y}_k]_{P_{j,l}}. \tag{3.32}$$

Substituting (3.32) in (3.31), we get the following compressed samples based energy detector (C-ED)

$$\hat{a}_k^{(\mathrm{C-ED})} = \arg\max_{a_k}\sum_{l=0}^{M_{\mathcal{M}}-1}\left[\frac{1}{N_f}\sum_{j=0}^{N_f-1}[\mathbf{y}_k]_{jM+a_kM_{\mathcal{M}}+l}\right]^2 \tag{3.33}$$

which is clearly independent of the spreading factor. Thus the energy detector based on the compressed signal directly can be realized by first averaging the compressed samples over the number of frames and then carrying out detection on the average compressed frame directly.

3.4 CS based Detection for a Deterministic Channel

In this section, we consider UWB communications over a deterministic channel. We derive BEP expressions for the CS-based detectors when detection is carried

out on the reconstructed signal as well as when it is carried out directly on the compressed signal. For simplicity we consider $\mathcal{M} = 2$, i.e., binary PPM.

3.4.1 Reconstruction Based Detection

In this section, we derive BEP expressions for the reconstruction based detector. We consider an average compressed frame for reconstruction. Thus the need to reconstruct all the frames has been alleviated except for one average frame. As explained in Section 3.3.1, the expressions obtained in this section should also be valid for the detector (3.25). Again we assume that the convergence stage has been reached for AMP so we will drop the iteration index. We can write the reconstructed symbol as

$$\check{\mathbf{u}}_k = \mathbf{u}(a_k, \mathbf{h}) + \mathbf{w}_k \tag{3.34}$$

where $\mathbf{w}_k \sim \mathcal{N}\left(\mathbf{0}, (\frac{\sigma^2}{\mu N_f} + \frac{1}{\mu N}\left\|\mathbf{u}_k - \hat{\mathbf{u}}_k\right\|_2^2)\mathbf{I}_N\right)$ under Assumption 1. Since $\mathcal{M} = 2$, every frame symbol has two pulse positions. Let us assume that the kth symbol is a 0, i.e., $a_k = 0$. This means we transmit the pulse in the first half of the signal frame, and we can partition the reconstructed symbol as

$$\check{\mathbf{u}}_{k,0} \triangleq [\check{\mathbf{u}}(0, \mathbf{h})]_{1:N/2} = \tilde{\mathbf{h}} + \tilde{\mathbf{w}}_{k,0} \tag{3.35}$$

where $\tilde{\mathbf{w}}_{k,0} \triangleq [\mathbf{w}_k]_{1:N/2}$, and

$$\tilde{\mathbf{u}}_{k,1} \triangleq [\check{\mathbf{u}}(0, \mathbf{h})]_{(N/2+1):N} = \tilde{\mathbf{w}}_{k,1} \tag{3.36}$$

where $\tilde{\mathbf{w}}_{k,1} \triangleq [\mathbf{w}_k]_{(N/2+1):N}$. Now the GML-based detector can be written as

$$U_{k,0} \underset{1}{\overset{0}{\gtrless}} U_{k,1} \tag{3.37}$$

where

$$U_{k,0} \triangleq \|\tilde{\mathbf{u}}_{k,0}\|_2^2 = E_h + 2\tilde{\mathbf{h}}^T\tilde{\mathbf{w}}_{k,0} + \|\tilde{\mathbf{w}}_{k,0}\|_2^2 \tag{3.38}$$

with $E_h \triangleq \|\tilde{\mathbf{h}}\|_2^2$ and

$$U_{k,1} \triangleq \|\tilde{\mathbf{u}}_{k,1}\|_2^2 = \|\tilde{\mathbf{w}}_{k,1}\|_2^2 . \tag{3.39}$$

Due to the statistical characterization of the reconstruction error by AMP, $\tilde{\mathbf{w}}_{k,0}$ and $\tilde{\mathbf{w}}_{k,1}$ are i.i.d. Gaussian. Now considering $\mathbf{h}$ as a deterministic channel, $U_{k,0}$ is a non-central chi-square distributed random variable and $U_{k,1}$ is a central chi-square distributed random variable, both with $N/2$ degrees of freedom. We can

see that finding a closed-form expression of the probability of error involving these two distributions is complicated. On the other hand, as we are dealing with the reconstructed signal consisting of N Nyquist-rate samples, where given the nature of UWB signals, it is known that $N \longrightarrow \infty$, we can rightly consider both $U_{k,0}$ and $U_{k,1}$ as Gaussian distributed by using the central limit theorem. Now to find a closed-form expression of the BEP, let us proceed by defining the variable

$$\Delta^{\text{recon}} \triangleq U_{k,0} - U_{k,1}. \tag{3.40}$$

Since $a_k = 0$ has been transmitted, the probability of error for the detector based on the reconstructed signal ($P_e^{(\text{R}-\text{BEP})}$) can be defined as

$$P_e^{(\text{R}-\text{BEP})} \triangleq P(\Delta^{\text{recon}} < 0). \tag{3.41}$$

Since $U_{k,0}$ and $U_{k,1}$ are assumed to be Gaussian distributed, the decision variable Δ^{recon} can also be considered Gaussian distributed. We now proceed to find its mean and variance.

Since $\text{E}\left\{\tilde{\mathbf{h}}^T\tilde{\mathbf{w}}_{k,0}\right\} = 0$, the mean of $U_{k,0}$ can be written as $\text{E}\{U_{k,0}\} = E_h + \text{E}\left\{\|\tilde{\mathbf{w}}_{k,0}\|_2^2\right\}$ and the mean of $U_{k,1}$ is given by, $\text{E}\{U_{k,1}\} = \text{E}\left\{\|\tilde{\mathbf{w}}_{k,1}\|_2^2\right\}$. Now since $\|\tilde{\mathbf{w}}_{k,i}\|_2^2$ for $i = 0, 1$, is a chi-square distributed random variable, its variance is given by, $\text{Var}\left\{\|\tilde{\mathbf{w}}_{k,i}\|_2^2\right\} = 2\frac{N}{2}\sigma_w^4$ where $\sigma_w^2 = \frac{\sigma^2}{\mu N_f} + \frac{1}{\mu N}\|\mathbf{u}_k - \hat{\mathbf{u}}_k\|_2^2$. We can further derive that, $\text{Var}\left\{\tilde{\mathbf{h}}^T\tilde{\mathbf{w}}_{k,0}\right\} = \sigma_w^2 E_h$ where we use the fact $\text{E}\left\{\tilde{\mathbf{w}}_{k,0}\tilde{\mathbf{w}}_{k,0}^T\right\} = \sigma_w^2\mathbf{I}_{N/2}$. Therefore, we obtain, $\text{Var}\{U_{k,0}\} = N\sigma_w^4 + 4\sigma_w^2 E_h$ and $\text{Var}\{U_{k,1}\} = N\sigma_w^4$. Thus the mean of the variable Δ^{recon} is

$$\text{E}\{\Delta^{\text{recon}}\} = \text{E}\{U_{k,0}\} - \text{E}\{U_{k,1}\} = E_h \tag{3.42}$$

and its variance is

$$\begin{aligned}\text{Var}\{\Delta^{\text{recon}}\} &= \text{Var}\{U_{k,0}\} + \text{Var}\{U_{k,1}\} \\ &= 2N\sigma_w^4 + 4\sigma_w^2 E_h.\end{aligned} \tag{3.43}$$

The probability of error for the reconstructed signal can therefore be approximated by

$$\begin{aligned}P_e^{(\text{R}-\text{BEP})} &= Q\left(\left[\frac{\text{Var}\{\Delta^{\text{recon}}\}}{(\text{E}\{\Delta^{\text{recon}}\})^2}\right]^{-\frac{1}{2}}\right) \\ &= Q\left(\left[4\frac{\sigma_w^2}{E_h} + 2N\left(\frac{\sigma_w^2}{E_h}\right)^2\right]^{-\frac{1}{2}}\right)\end{aligned} \tag{3.44}$$

which is the instantaneous BEP of a deterministic channel. Finding an analytical expression for the average BEP of (3.44) is quite complicated. Therefore, the average BEP ($P_e^{(\mathrm{R-ABEP})}$) can be approximated by numerically averaging $P_e^{(\mathrm{R-BEP})}$ over different channel realizations [72], i.e.,

$$P_e^{(\mathrm{R-ABEP})} = \frac{1}{N^{\mathrm{realiz}}} \sum_{i=0}^{N^{\mathrm{realiz}}-1} P_e^{(\mathrm{R-BEP})}(i) \tag{3.45}$$

where $P_e^{(\mathrm{R-BEP})}(i)$ is the instantaneous BEP for the ith channel realization and N^{realiz} is the total number of channel realizations.

The analysis provided above is for the case when $\mathcal{M} = 2$. Exact BEP expressions for the case when $\mathcal{M} > 2$ are again difficult to derive. Nonetheless, an upper bound (that is a union bound) on the BEP of $\mathcal{M}-1$ events can still be utilized [73], i.e.,

$$P_e^{(\mathrm{R-BEP})} \lessapprox \frac{\mathcal{M}}{2} Q\left(\left[4\frac{\sigma_w^2}{E_s} + 2N\left(\frac{\sigma_w^2}{E_s}\right)^2\right]^{-\frac{1}{2}}\right) \tag{3.46}$$

where $E_s \triangleq E_h \log_2 \mathcal{M}$. The bound becomes tighter with increasing SNR and is exact for the case $\mathcal{M} = 2$.

3.4.2 Direct Compressed Detection

To derive the BEP expressions for the direct compressed detector, we consider an average compressed frame. Now given that $a_k = 0$ and $\mathcal{M} = 2$, the average compressed frame $\bar{\mathbf{y}}_k$ can be partitioned into two equal parts under Assumption 3: the signal part $\bar{\mathbf{y}}_{k,0}$ and the non-signal part $\bar{\mathbf{y}}_{k,1}$, i.e.,

$$\bar{\mathbf{y}}_{k,0} \triangleq [\bar{\mathbf{y}}_k]_{1:M/2} = \tilde{\mathbf{\Phi}}\tilde{\mathbf{h}} + \tilde{\bar{\boldsymbol{\xi}}}_{k,0} \tag{3.47}$$

where $\tilde{\bar{\boldsymbol{\xi}}}_{k,0} \triangleq [\bar{\boldsymbol{\xi}}_k]_{1:M/2}$ and

$$\bar{\mathbf{y}}_{k,1} \triangleq [\bar{\mathbf{y}}_k]_{(M/2+1):M} = \tilde{\bar{\boldsymbol{\xi}}}_{k,1} \tag{3.48}$$

where $\tilde{\bar{\boldsymbol{\xi}}}_{k,1} \triangleq [\bar{\boldsymbol{\xi}}_k]_{(M/2+1):M}$. We know that $\tilde{\bar{\boldsymbol{\xi}}}_{k,i}$ for $i = 0, 1$, is zero-mean with covariance matrix, $\mathrm{E}\left\{\tilde{\bar{\boldsymbol{\xi}}}_{k,i}\tilde{\bar{\boldsymbol{\xi}}}_{k,i}^T\right\} = \frac{\sigma^2}{\mu N_f}\mathbf{I}_{M/2}$ under Assumption 2. The energies corresponding to (3.47) and (3.48) can be defined as

$$Y_{k,0} \triangleq \|\bar{\mathbf{y}}_{k,0}\|_2^2 = E_{\tilde{h}} + 2\tilde{\mathbf{h}}^T\tilde{\mathbf{\Phi}}^T\tilde{\bar{\boldsymbol{\xi}}}_{k,0} + \|\tilde{\bar{\boldsymbol{\xi}}}_{k,0}\|_2^2 \tag{3.49}$$

with $E_{\tilde{h}} = \|\tilde{\mathbf{\Phi}}\tilde{\mathbf{h}}\|_2^2$ and

$$Y_{k,1} \triangleq \|\bar{\mathbf{y}}_{k,1}\|_2^2 = \|\tilde{\bar{\boldsymbol{\xi}}}_{k,1}\|_2^2. \tag{3.50}$$

Now the GML-based energy detector for the compressed signal can be written as

$$Y_{k,0} \underset{1}{\overset{0}{\gtrless}} Y_{k,1} \tag{3.51}$$

and the bit error probability for the compressed detector $P_e^{(\mathrm{C-BEP})}$ can be defined as

$$P_e^{(\mathrm{C-BEP})} \triangleq P(\Delta^{\mathrm{comp}} < 0) \tag{3.52}$$

where

$$\Delta^{\mathrm{comp}} \triangleq Y_{0,0} - Y_{0,1}. \tag{3.53}$$

Now, due to Assumption 2, $\tilde{\bar{\boldsymbol{\xi}}}_{k,i}$ is still zero-mean i.i.d. Gaussian. Therefore, by using the central limit theorem, both $Y_{0,0}$ and $Y_{0,1}$ can be assumed to be Gaussian distributed as $M \longrightarrow \infty$, which implies that Δ^{comp} is also a Gaussian distributed random variable. We can find an approximate closed-form expression for the probability of error by finding the mean and the variance of the variable Δ^{comp}.

Since $\mathrm{E}\left\{\tilde{\mathbf{h}}^T\tilde{\mathbf{\Phi}}^T\tilde{\bar{\boldsymbol{\xi}}}_{k,0}\right\} = 0$ and $\mathrm{E}\left\{\|\tilde{\bar{\boldsymbol{\xi}}}_{k,0}\|_2^2\right\} = \frac{M}{2}\frac{\sigma^2}{\mu N_f}$, the mean of $Y_{k,0}$ can be calculated as $\mathrm{E}\{Y_{k,0}\} = E_{\tilde{h}} + \frac{M}{2}\frac{\sigma^2}{\mu N_f}$. Now, it can be proven that the $\mathrm{Var}\left\{\tilde{\mathbf{h}}^T\tilde{\mathbf{\Phi}}^T\tilde{\bar{\boldsymbol{\xi}}}_{k,0}\right\} = \frac{\sigma^2}{\mu N_f}E_{\tilde{h}}$ and since $\|\tilde{\bar{\boldsymbol{\xi}}}_0\|_2^2$ is a chi-square distributed random variable with $M/2$ degrees of freedom, $\mathrm{Var}\left\{\|\tilde{\bar{\boldsymbol{\xi}}}_{k,0}\|_2^2\right\} = 2\frac{M}{2}\frac{\sigma^4}{\mu^2 N_f^2}$. Thus, the variance of the decision variable $Y_{k,0}$ can be written as $\mathrm{Var}\{Y_{k,0}\} = 4\frac{\sigma^2}{\mu N_f}E_{\tilde{h}} + M\frac{\sigma^4}{\mu^2 N_f^2}$. Similarly, it can be shown that the mean of $Y_{k,1}$, $\mathrm{E}\{Y_{k,1}\} = \frac{M}{2}\frac{\sigma^2}{\mu N_f}$ and its variance $\mathrm{Var}\{Y_{k,1}\} = M\frac{\sigma^4}{\mu^2 N_f^2}$. Thus the mean of the variable Δ^{comp} is

$$\mathrm{E}\{\Delta^{\mathrm{comp}}\} = \mathrm{E}\{Y_{k,0}\} - \mathrm{E}\{Y_{k,1}\} = E_{\tilde{h}} \tag{3.54}$$

and its variance is

$$\begin{aligned}\mathrm{Var}\{\Delta^{\mathrm{comp}}\} &= \mathrm{Var}\{Y_{k,0}\} + \mathrm{Var}\{Y_{k,1}\} \\ &= 4\frac{\sigma^2}{\mu N_f}E_{\tilde{h}} + 2M\frac{\sigma^4}{\mu^2 N_f^2}.\end{aligned} \tag{3.55}$$

Since Δ^{comp} is a Gaussian distributed random variable, the approximate closed-form expression for the probability of error can be derived as

$$P_e^{(\text{C}-\text{BEP})} = Q\left(\left[4\frac{\sigma^2/\mu}{N_f E_{\tilde{h}}} + 2M\left(\frac{\sigma^2/\mu}{N_f E_{\tilde{h}}}\right)^2\right]^{-\frac{1}{2}}\right). \tag{3.56}$$

Note that (3.56) leads to the probability of error of the Nyquist-rate sampled received signal if M is replaced by N and $\mu = 1$. It is given by

$$P_e^{(\text{N}-\text{BEP})} = Q\left(\left[4\frac{\sigma^2}{N_f E_h} + 2N\left(\frac{\sigma^2}{N_f E_h}\right)^2\right]^{-\frac{1}{2}}\right). \tag{3.57}$$

We can see that (3.56) and (3.57) are expressions for the instantaneous BEP. Average BEP results can again be found by numerical averaging over different channel realizations as in (3.45).

3.5 CS based Detection for a Gaussian Distributed Channel

In this section, we derive the BEP expressions for the proposed CS-based detectors when the channel is Gaussian distributed. We assume that the channel elements are zero-mean i.i.d. Gaussian, i.e., $h_i \sim \mathcal{N}(0,1)$. For the ease of the derivations, we further assume that the channel spread $T_h = T_{\mathcal{M}}$ and thus, $L = N_{\mathcal{M}}$. The Gaussian assumption on the channel may not be realistic but it helps to provide some intuition regarding the influence of the channel on the average BEP. Here again, we consider $\mathcal{M} = 2$ and $a_k = 0$.

3.5.1 Reconstruction Based Detection

In this section, we look at the reconstruction based detector when the channel is Gaussian distributed and derive a closed-form expression of its theoretical BEP. Thus, in the context of (3.34), under Assumption 1 we can say from (3.35) and (3.36) that $\check{\mathbf{u}}_{k,0} \sim \mathcal{N}(\mathbf{0}, (1+\sigma_w^2)\mathbf{I}_{N/2})$ and $\check{\mathbf{u}}_{k,1} \sim \mathcal{N}(\mathbf{0}, \sigma_w^2\mathbf{I}_{N/2})$. From (3.38) and (3.39), this means that $U_{k,0}$ and $U_{k,1}$, both being the sum of Gaussian distributed random variables are chi-square distributed with $N/2$ degrees of freedom. The pdf of $U_{k,0}$ is given by [73]

$$p_{U_{k,0}}(u_{k,0}) = \frac{{u_{k,0}}^{\frac{N}{4}-1}}{{\sigma_r}^{\frac{N}{2}} 2^{\frac{N}{4}} \Gamma\left(\frac{N}{4}\right)} e^{\frac{-u_{k,0}}{2\sigma_r^2}}$$

where $\sigma_r^2 \triangleq 1 + \sigma_w^2$, and the pdf of $U_{k,1}$ is given by [73]

$$p_{U_{k,1}}(u_{k,1}) = \frac{u_{k,1}^{\frac{N}{4}-1}}{\sigma_w^{\frac{N}{2}} 2^{\frac{N}{4}} \Gamma\left(\frac{N}{4}\right)} e^{\frac{-u_{k,1}}{2\sigma_w^2}}.$$

Now from (3.37) the average BEP for the reconstruction based detector (R-ABEP), given a zero symbol is transmitted is

$$P_e^{(\mathrm{R-ABEP})} = P\left(U_{k,0} < U_{k,1} | a_k = 0\right). \tag{3.58}$$

The probability of a correct decision given that a zero is transmitted can then be written as

$$\begin{aligned}\bar{P}_c &= P\left(U_{k,1} < U_{k,0} | a_k = 0\right) \\ &= \int_0^{u_{k,0}} p_{U_{k,1}}(u_{k,1})\, du_{k,1}\end{aligned}$$

which can be simplified to

$$\bar{P}_c = \frac{\gamma\left(\frac{N}{4}, \frac{u_{k,0}}{2\sigma_w^2}\right)}{\Gamma\left(\frac{N}{4}\right)}$$

where $\gamma(.,.)$ is the lower-incomplete-gamma function and $\Gamma(.)$ is the gamma function such that $\gamma(n,u) = \int_0^u t^{n-1}e^{-t}dt$ and $\Gamma(n) = \int_0^\infty t^{n-1}e^{-t}dt$, [74]. The average BEP is therefore given by

$$\begin{aligned}P_e^{(\mathrm{R-ABEP})} &= 1 - \int_0^\infty \bar{P}_c\, p_{U_{k,0}}(u_{k,0}) du_{k,0} \\ &= 1 - \int_0^\infty \frac{\gamma(\frac{N}{4}, \frac{u_{k,0}}{2\sigma_w^2})}{\Gamma(\frac{N}{4})} \frac{{u_{k,0}}^{\frac{N}{4}-1}}{\sigma_r^{\frac{N}{2}} 2^{\frac{N}{4}} \Gamma\left(\frac{N}{4}\right)} e^{\frac{-u_{k,0}}{2\sigma_r^2}} du_{k,0}.\end{aligned} \tag{3.59}$$

By using [74, Eq. (6.455.2)], we can reduce (3.59) to the following closed-form expression

$$\begin{aligned}P_e^{(\mathrm{R-ABEP})} = 1 - &\frac{2\Gamma(\frac{N}{2})}{\frac{N}{2}[\Gamma(\frac{N}{4})]^2} \left[\frac{\sigma_r \sigma_w}{\sigma_r^2 + \sigma_w^2}\right]^{\frac{N}{2}} \\ &\times {}_2F_1\left(1, \frac{N}{2}; \frac{N}{4}+1; \frac{\sigma_r^2}{\sigma_r^2 + \sigma_w^2}\right),\end{aligned} \tag{3.60}$$

where ${}_2F_1(.,.;.;.)$ is the Gaussian hypergeometric function defined by [74, Eq. (9.14.2)]. Hence, we have obtained a closed-form expression for the average BEP of the reconstruction based energy detector for a channel with i.i.d. zero-mean Gaussian elements.

3.5.2 Direct Compressed Detection

In this section, we present the BEP expressions for the detector based on the compressed signals when the channel is Gaussian distributed. From (3.47), we can see that since $\tilde{\mathbf{h}}$ is Gaussian, $\tilde{\mathbf{\Phi}}\tilde{\mathbf{h}}$ will also be Gaussian with covariance matrix $\mathrm{E}\{(\tilde{\mathbf{\Phi}}\tilde{\mathbf{h}})(\tilde{\mathbf{\Phi}}\tilde{\mathbf{h}})^T\} = \frac{1}{\mu}\mathbf{I}_{M/2}$ under Assumptions 2 and 3. Consequently, $\bar{\mathbf{y}}_{k,0}$ will be zero-mean Gaussian distributed with covariance matrix $\mathrm{E}\{\bar{\mathbf{y}}_{k,0}\bar{\mathbf{y}}_{k,0}^T\} = \frac{1}{\mu}(1 + \frac{\sigma^2}{N_f})\mathbf{I}_{M/2}$. Thus we can write $\bar{\mathbf{y}}_{k,0} \sim \mathcal{N}(\mathbf{0}, \sigma_c^2\mathbf{I}_{M/2})$, where $\sigma_c^2 \triangleq \frac{1}{\mu}(1 + \frac{\sigma^2}{N_f})$ and from (3.48) we can write $\bar{\mathbf{y}}_{k,1} \sim \mathcal{N}(\mathbf{0}, \sigma_f^2\mathbf{I}_{M/2})$, where $\sigma_f^2 \triangleq \frac{\sigma^2}{\mu N_f}$. Therefore, from (3.49) and (3.50), we can say that $Y_{k,0}$ and $Y_{k,1}$ are chi-square distributed random variables, both with $M/2$ degrees of freedom.

Now from (3.51), we can observe that the average BEP for the compressed detector (C-ABEP), given a zero transmitted-symbol

$$P_e^{(\mathrm{C-ABEP})} = P\left(Y_{k,0}<Y_{k,1}|a_k = 0\right). \tag{3.61}$$

The probability of a correct decision given that a zero is transmitted can then be written as

$$\begin{aligned}\bar{P}_c &= P\left(Y_{k,1}<Y_{k,0}|a_k = 0\right)\\ &= \int_0^{y_{k,0}} p_{Y_{k,1}}\left(y_{k,1}\right) dy_{k,1}\\ &= \int_0^{y_{k,0}} \frac{y_{k,1}^{\frac{M}{4}-1}}{\sigma_f^{\frac{M}{2}} 2^{\frac{M}{4}}\Gamma\left(\frac{M}{4}\right)} e^{\frac{-y_{k,1}}{2\sigma_f^2}}\, dy_{k,1},\end{aligned}$$

which can be simplified to

$$\bar{P}_c = \frac{\gamma\left(\frac{M}{4}, \frac{y_{k,0}}{2\sigma_f^2}\right)}{\Gamma\left(\frac{M}{4}\right)}.$$

The average BEP is then given by

$$\begin{aligned}P_e^{(\mathrm{C-ABEP})} &= 1 - \int_0^{\infty} \bar{P}_c\, p_{Y_{k,0}}\left(y_{k,0}\right) dy_{k,0}\\ &= 1 - \int_0^{\infty} \frac{\gamma(\frac{M}{4}, \frac{y_{k,0}}{2\sigma_f^2})}{\Gamma(\frac{M}{4})} \frac{{y_{k,0}}^{\frac{M}{4}-1}}{\sigma_c^{\frac{M}{2}} 2^{\frac{M}{4}}\Gamma\left(\frac{M}{4}\right)} e^{\frac{-y_{k,0}}{2\sigma_c^2}}\, dy_{k,0}.\end{aligned} \tag{3.62}$$

By using [74, Eq. (6.455.2)], we can reduce (3.62) to

$$P_e^{(\mathrm{C-ABEP})} = 1 - \frac{2\Gamma(\frac{M}{2})}{\frac{M}{2}[\Gamma(\frac{M}{4})]^2}\left[\frac{\sigma_c\sigma}{\sigma_c^2+\sigma_f^2}\right]^{\frac{M}{2}} \times {}_2F_1\left(1, \frac{M}{2}; \frac{M}{4}+1; \frac{\sigma_c^2}{\sigma_c^2+\sigma_f^2}\right) \tag{3.63}$$

which is the closed-form expression for the average BEP of the optimal compressed energy detector for a channel with i.i.d. zero-mean Gaussian elements. Now from (3.63), the average BEP of the ED for the Nyquist-rate sampled received signal (N-ABEP) can be written as [75]

$$P_e^{(\mathrm{N-ABEP})} = 1 - \frac{2\Gamma(\frac{N}{2})}{\frac{N}{2}[\Gamma(\frac{N}{4})]^2}\left[\frac{\sigma_{c0}\sigma_{f0}}{\sigma_{c0}^2+\sigma_{f0}^2}\right]^{\frac{N}{2}} \times {}_2F_1\left(1, \frac{N}{2}; \frac{N}{4}+1; \frac{\sigma_{c0}^2}{\sigma_{c0}^2+\sigma_{f0}^2}\right) \tag{3.64}$$

where $\sigma_{c0}^2 \triangleq (1+\frac{\sigma^2}{N_f})$ and $\sigma_{f0}^2 \triangleq \frac{\sigma^2}{N_f}$.

3.6 Simulations

In this section, we present some simulation results for the different detectors developed in the previous sections for the binary PPM communications scenario. We provide two groups of simulations. One where we consider a deterministic channel and the other where we assume the channel to be Gaussian distributed. For the measurement matrices, Assumption 3 holds true in general. Further, we consider a measurement matrix whose elements are random Gaussian under Assumption 1 as well as a measurement matrix whose rows have been orthogonalized under Assumption 2.

For the reconstruction of the signal, AMP suggests an optimal thresholding policy in the form of the relationship $\lambda^{[n]} = \tau\sigma_w^{[n]}$ at the nth iteration, but it requires the knowledge of the original signal and therefore, it is not practically feasible. For our purpose, we use the following alternative relationship as suggested in [36]

$$\lambda^{[n]} = \lambda + \frac{1}{\mu}\lambda^{[n-1]}\left\langle \mathcal{S}'\left(\hat{\mathbf{u}}_k^{[n-1]} + \mathbf{\Phi}^T\mathbf{z}_k^{[n-1]}, \lambda^{[n-1]}\right)\right\rangle \tag{3.65}$$

where λ is a constant. Thus the threshold value keeps developing for every AMP iteration. Further, for the BEP expression of the spreading-factor dependent energy detector (3.26), we use the following expression from [49]

$$P_e^{(\mathrm{SN-BEP})} = Q\left(\left[4\frac{\sigma^2}{N_f E_h} + 4LN_f\left(\frac{\sigma^2}{N_f E_h}\right)^2\right]^{-\frac{1}{2}}\right) \tag{3.66}$$

and the corresponding average BEP ($P_e^{(\mathrm{SN-ABEP})}$) is obtained by averaging (3.66) over the channel realizations as in (3.45).

For Figures 3.4 to 3.8, we consider the IEEE 802.15.3a CM1 (line-of-sight) channel model [48]. The channel parameters are chosen as follows: the cluster arrival rate $\Lambda_{\mathrm{ch}} = 0.0233\mathrm{nsec}^{-1}$, the ray arrival rate within a cluster $\lambda_{\mathrm{ch}} = 2.5\mathrm{nsec}^{-1}$, the cluster decay factor $\Gamma_{\mathrm{ch}} = 2.5$ and the ray decay factor within a cluster $\gamma_{\mathrm{ch}} = 4.3$. The transmitted pulse waveform $q(t)$ is the second derivative of a Gaussian pulse of unit energy with pulse duration $T_q = 1$ nsec. In general, the frame length is taken as $T_f = 150$ nsec and a receive filter bandwidth of 3 GHz is considered. Thus each frame has $N = 900$ Nyquist-rate samples.

Figure 3.4 shows the instantaneous BER results for different detectors, i.e., C-ED, R-ED and N-ED, along with some theoretical BEP plots, i.e., SN-BEP, C-BEP, R-BEP and N-BEP, with a Gaussian distributed random measurement matrix (Assumption 1). Here, we consider signal transmission with a varying number of frames per symbol, i.e., $N_f = 1, 10, 20$. We can see that with increasing spreading factor, the SN-BEP keeps decreasing. Whereas the BEP results for the detectors with optimal frame combining remain consistent and do not vary with a varying number of frames. The performance of the R-ED follows the theoretical expression R-BEP exactly. The C-ED remains a bit away from the C-BEP because the Gaussian measurement matrix does not guarantee (3.5). Now with regard to the performance of the compressed detectors against the Nyquist-rate detectors, we see that at a compression ratio of $\mu = 0.5$, i.e., the sampling rate is only 50% of the Nyquist-rate, the compressed rate detectors offer a reasonably good performance (see [76] for details on the loss incurred due to CS). The C-ED performs better than the reconstructed version, i.e., the R-ED. The reason is that the reconstruction process loses some information whereas the compressed domain detection preserves the signal information albeit in a compressed form and gives a better performance. The difference between N-BEP and C-BEP is around 2 to 3 dB at a BER of 10^{-3}. Thus CS-based EDs are a viable option. For the sake of comparison, we also include in this figure the performance of matched filter (MF) based compressed de-

tectors (where it is assumed that the channel is known); when detection is carried out on the reconstructed signal (R-MF) and when it is carried out on the compressed signal directly (C-MF), along with the MF for the Nyquist-rate sampled signal (N-MF) and its theoretical plot (MF-BEP).

Figure 3.5 shows the instantaneous BER performance for different detectors when the measurement matrix has orthogonal rows (Assumption 2). Here $\mu = 0.5$ and $N_f = 1, 10, 20$. We see that the performance of C-ED has improved and it falls exactly on the C-BEP curve. R-ED does not coincide with R-BEP because the expression for the R-BEP is based on a random measurement matrix under Assumption 1, but its performance has also improved in comparison to the previous figure. The SN-BEP keeps again worsening with an increasing value of N_f.

Figure 3.6 shows a BER comparison of different detectors with varying compression ratios when the measurement matrix is Gaussian distributed (Assumption 1). We fix the SNR at 17 dB. Here we see that the performance of the R-ED and C-ED saturates after a certain compression ratio. The reason is that if N is not very large then as the number of measurements increases, the probability of having correlations within the measured values increases as well (see (3.6)). In Figure 3.7, we increase the frame time to $T_f = 300$ nsec. We can see that although the overall performance of all the detectors has been scaled, nonetheless R-ED and the C-ED show a tendancy of improvement for the larger value of N.

Figure 3.8 shows a BER comparison of different detectors with varying values of μ when the orthogonal measurement matrix is used (Assumption 2). We consider here an SNR of 17 dB. We can see that the performance of both the R-ED and C-ED has improved and does not saturate with increasing μ. C-ED follows C-BEP exactly but R-ED remains away from R-BEP because of the absence of a random measurement matrix.

From Figures 3.9 to 3.12, we consider a Gaussain distributed multipath channel, i.e., the channel samples are zero-mean, unit-variance Gaussian. Considering the limitations of the simulation software, i.e., Matlab, viz a viz (3.60), (3.63) and (3.64), we take a frame length of $T_f = 100$ nsec and a receive filter bandwidth of $B = 1$ GHz. Now every frame has $N = 200$ Nyquist-rate samples.

Figure 3.9 shows the average BER results for C-ED, R-ED and N-ED along with the theoretical BEPs i.e., SN-ABEP, C-ABEP, R-ABEP and N-ABEP, with a Gaussian distributed channel. SN-ABEP has been obtained by averaging the SN-BEP results over all channel realizations. We consider a random measurement matrix (Assumption 1) with the compression ratio $\mu = 0.5$ and $N_f = 1, 10, 20$. The simulation results for the detectors follow the BEP expressions quite closely.

We can see that the suboptimal detector SN-ABEP, once again falls a prey to the increasing spreading factor and its performance keeps decreasing. The proposed detectors remain unaffected by this factor. The R-ED follows the R-ABEP exactly but C-ED is a bit away from C-ABEP due to the randomness of the measurement matrix.

Figure 3.10 shows the average BER comparison of different detectors when an orthogonal measurement matrix is used (Assumption 2). Here again $\mu = 0.5$ and $N_f = 1, 10, 20$. We see that R-ED is away from R-ABEP but C-ED follows C-ABEP exactly due to the choice of the measurement matrix. In general the performance of the proposed CS-based energy detectors, C-ED and R-ED, remains reasonable in comparison to the Nyquist-rate based energy detector, N-ED.

Figures 3.11 and 3.12 show the average BER results for the presented detectors against a varying compression ratio at an SNR of 15 dB, for a random and an orthogonal measurement matrix, respectively. The number of frames per symbol is $N_f = 1$. We can see that with an increasing compression ratio the performance of the proposed detectors increases.

Discussion

From the above simulation results, we can see that C-ED performs better than R-ED in terms of BER. Therefore, a question arises as to what is the need of R-ED at all. First, it should be noted that despite a better performance, C-ED works under stringent constraints of exact synchronization. If full timing information is not available, the performance of C-ED will deteriorate. On the other hand, such constraints can be relaxed with respect to R-ED. Since R-ED has to reconstruct the received signal from its compressed samples as an initial step, the timing information can be extracted from the reconstructed signal by resorting to existing methods proposed for Nyquist-rate sampled signals. Secondly, note that the measurement process used in the paper is assumed to be identical (which usually will be the case) for each pulse position (i.e., over $T_{\mathcal{M}}$). If this process is changed either due to perturbations or on purpose, the performance of C-ED will be severely affected. On the other hand, the performance of R-ED is robust to changing measurement process. Thus, we can say that both proposed detectors are important and have their own merits. Table 3.1 provides a summary of the salient features of our proposed detectors.

Further, we would like to comment on the issue of narrow band interference (NBI) in UWB signals w.r.t. our proposed detectors. NBI has been one of the major

challenges as it reduces the dynamic range and necessitates more resolution bits for the effective detection of UWB signals [9, 77], causing an increase in ADC power consumption [2]. In this regard, the method presented in [59] to handle NBI can be easily incorporated in our proposed detection schemes. If the measurement matrix is designed as a Fourier ensemble with frequencies uniformly spaced over the signal bandwidth, then NBI can be identified by taking the square of the measurements. The measurements affected by NBI will have the highest magnitudes. The block of such contaminated measurements can be discarded and detection can be carried out on the rest of the measurements. Thus by adopting this idea, our proposed detectors can be robust against NBI as well.

3.7 Conclusions

In this paper we have developed compressive sampling based energy detectors to reduce the sampling rate much below the Nyquist rate. We have shown that compressive sampling helps in the realization of spreading-factor independent energy detectors. Our energy detectors work both on the reconstructed signal as well as on the compressed signal directly without reconstruction. We have derived theoretical BEP expressions to guage the performance of compressive sampling based energy detectors which can also be extended to Nyquist-rate sampling based energy detectors. Simulation results prove the validity of these expressions if the choice of measurement matrix follows the assumptions adopted in the theoretical derivations.

Table 3.1: Summary of the proposed detectors

Features	R-ED	C-ED
Sample Form	Reconstructed samples	Compressed samples
Theoretical BEP	Requires random $\mathbf{\Phi}$	Requires orthogonal $\mathbf{\Phi}$
Timing Information	Can be relaxed	Required
$\tilde{\mathbf{\Phi}}$ (over $T_{\mathcal{M}}$)	Independent	Must be identical

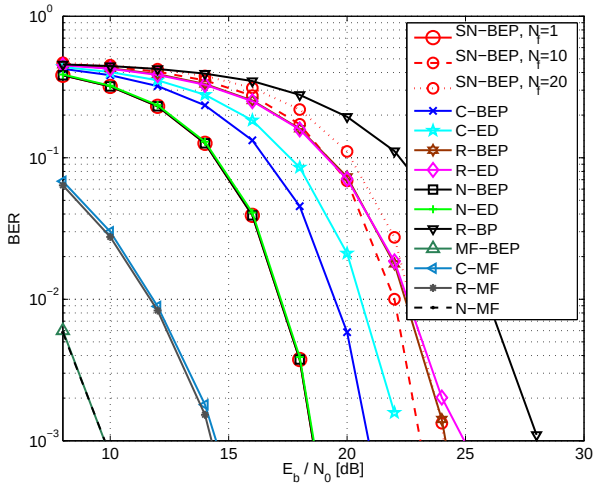

Figure 3.4: Comparison of different detectors with random measurement matrix and a deterministic channel

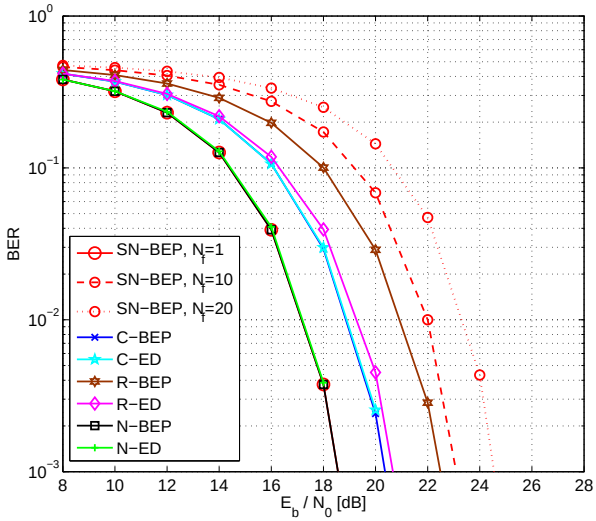

Figure 3.5: Comparison of different detectors with orthogonal measurement matrix and a deterministic channel

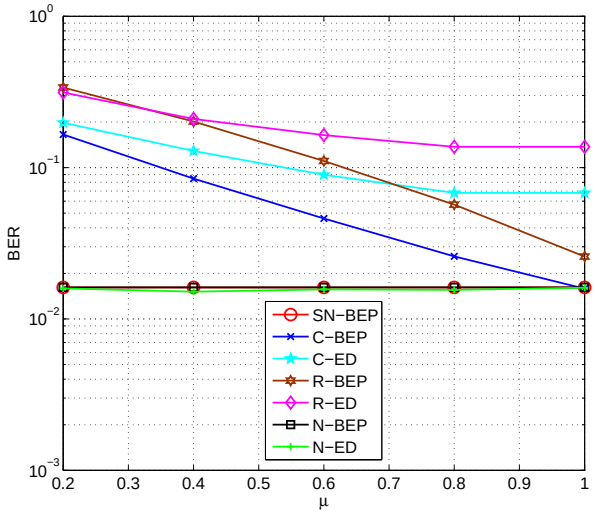

Figure 3.6: Comparison of detectors for varying compression ratio with random measurement matrix and a deterministic channel

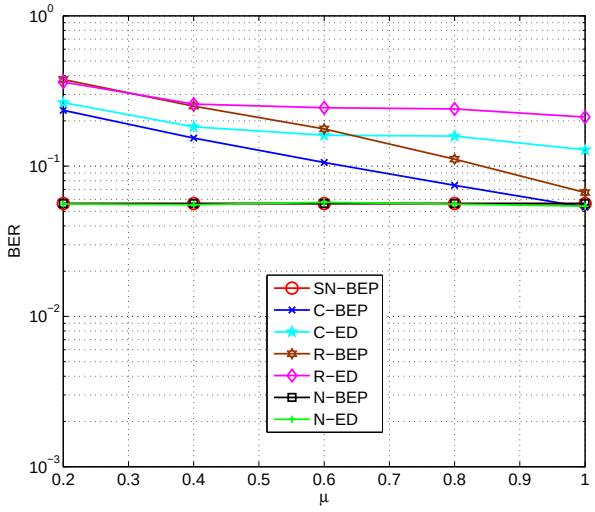

Figure 3.7: Comparison of detectors for varying compression ratio with random measurement matrix and a deterministic channel

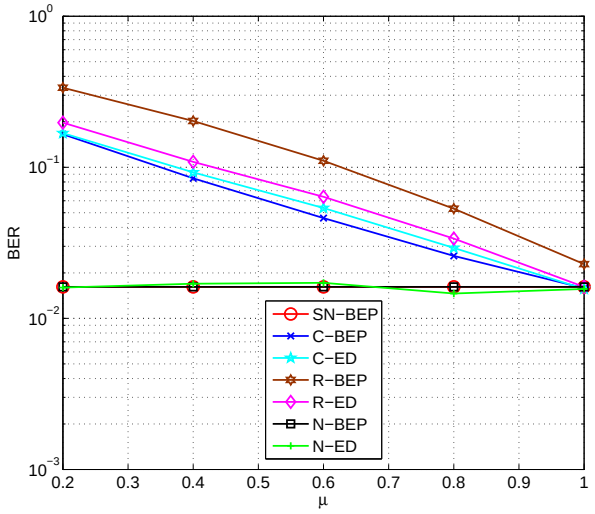

Figure 3.8: Comparison of detectors for varying compression ratio with orthogonal measurement matrix and a deterministic channel

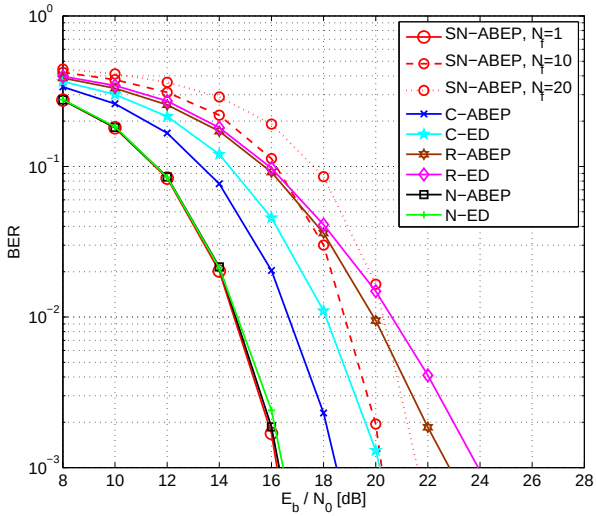

Figure 3.9: Comparison of different detectors with random measurement matrix and Gaussian channel

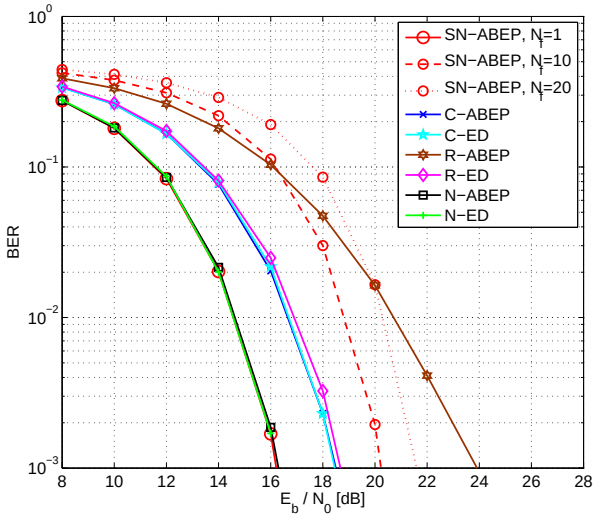

Figure 3.10: Comparison of different detectors with orthogonal measurement matrix and Gaussian channel

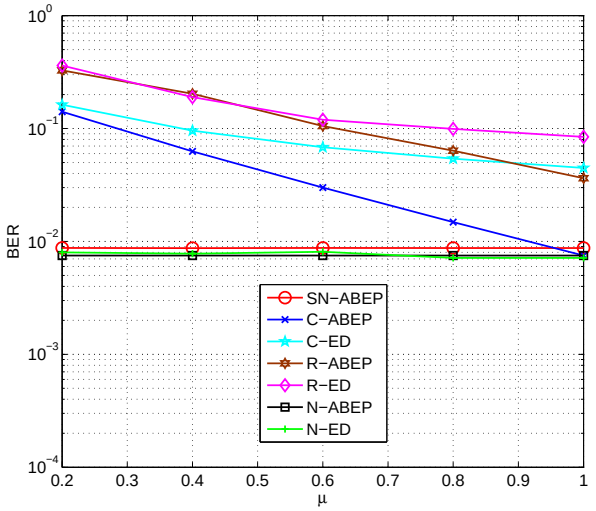

Figure 3.11: Comparison of detectors for varying compression ratio with random measurement matrix and Gaussian channel

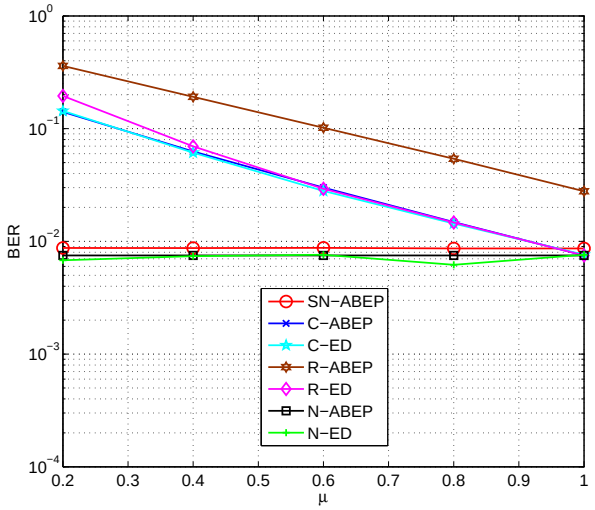

Figure 3.12: Comparison of detectors for varying compression ratio with orthogonal measurement matrix and Gaussian channel

Chapter 4

Compressive Sampling Based Differential Detection for UWB Impulse Radio Signals

Shahzad Gishkori, Geert Leus and Vincenzo Lottici

Abstract

Noncoherent detectors significantly contribute to the practical realization of the ultra-wideband (UWB) impulse-radio (IR) concept, in that they allow avoiding channel estimation and provide highly efficient reception capabilities. Complexity can be reduced even further by resorting to an all-digital implementation, but Nyquist-rate sampling of the received signal is still demanding. The current paper addresses this issue by proposing a novel differential detection (DD) scheme, which exploits the compressive sampling (CS) framework to reduce the sampling rate much below the Nyquist-rate. The optimization problem is formulated to jointly recover the sparse received signal as well as the differentially encoded data symbols, and compared with both the separate approach and the scheme using the compressed received signal without reconstruction. Finally, a maximum *a posteriori* based detector using the compressed symbols is developed for a Laplacian distributed channel, as a reference to compare the performance of the proposed approaches. Simulation results show that the proposed joint CS-based DD brings the considerable advantage of reducing sampling rate without degrading performance compared with the optimal MAP detector.

4.1 Introduction

Ultra-wideband (UWB) impulse-radio (IR) is a promising signaling scheme, particularly suitable for low-power-density short-range communications, in virtue of many appealing features, such as high user capacity, fine timing resolution, frequency overlay based coexistence with existing services, low probability of interception and detection [8],[45]. Rich multipath propagation, however, makes each transmitted pulse appear at the receiver as hundred of echoes [48]. Although Rake receivers allow to collect most of the energy conveyed by the multipath components [72], they require a large number of fingers together with intensive computational load and high sampling rate to perform channel estimation [78], thus contradicting the main requirement of simple transceiver devices. As suboptimal yet effective alternative, noncoherent receivers have been proposed in order to skip the difficult channel estimation task, in the form of autocorrelation based receivers (AcRs) [79]. We can refer to transmitted reference (TR), where a reference pulse is transmitted together with the data pulse [80]-[81], and differential detection (DD), which employs differential encoding [82]. Detection performance of DD schemes can be further improved with the multi-symbol DD approach (MSDD) [83]-[84], and its

variant based on symbol-level synchronization only [85], even though for an all-digital implementation they all are still affected by the basic issue of still requiring high rate analog-to-digital converters (ADCs).

Relations with prior work. The compressive sampling (CS) concept has been recently pursued as a powerful way to reduce the sampling rate of sparse signal much below the Nyquist rate without incurring in large performance degradations [5]-[6]. The key idea relies on representing a sparse signal with a few measurements only obtained via random projection in the analog domain [46]-[65], and then, reconstructing it through a sparse recovery method. Now, exploiting the fact that the received UWB signal can be considered to be sparse in the time domain [3], we can argue that the CS-based approach can be useful for data detection. Toward this direction, a few works have been recently appeared, as [86] for coherent receivers, [57] for joint time of arrival (ToA) estimation and data decoding, and [55] for a generalized likelihood ratio test (GLRT) detector based on the transmission of pilot symbols.

Purpose and contributions. In this paper, we focus on CS-based noncoherent receivers for differentially encoded UWB signals, as preliminarily discussed in [87]. A few important features are gained which differentiate our contributions from previous works.

1. The key to our method is the formulation of a cost function, as the composition of the sparse regularized least square error for two compressed-rate consecutive received signal waveforms combined with the squared DD error, which is minimized using an iterative efficient method derived form the elastic net optimization framework. Thus, reconstruction of the compressed signal samples and detection of encoded information is performed in a joint approach.

2. The proposed CS-based DD does not require any channel estimation as in [57] nor pilot symbols transmission as in [55].

3. A simpler two-step approach is formulated wherein first the sparse regularized least square error is minimized, and then, the recovered symbol waveforms are used to perform conventional DD.

4. A direct detection method working directly on the compressed samples is considered as well, which avoids signal reconstruction, and its limitations are clarified.

5. A compressed-rate MAP DD is derived as performance benchmark for the proposed detectors, assuming a Laplacian distributed channel response (i.e., the channel taps are Laplacian distributed).

Organization. The rest of the paper is organized as follows. Section 5.2 describes the signal model, Section 4.3 introduces the CS-based separate and joint reconstruction and detection methods, while Section 4.4 derives the MAP-based DDs at both Nyquist- and compressed-rate. Simulation results are discussed in Section 4.5, and finally concluding remarks are drawn in Section 5.7.

4.2 Signal Model

In the adopted IR-UWB signal model, each symbol is conveyed by a pulse $q(t)$ of duration T_q much less than the symbol interval T_s, i.e., $T_q \ll T_s$ [1]. The transmitted signal composed of a block of Q symbols takes the form

$$s(t) = \sum_{k=0}^{Q-1} b_k q(t - kT_s) \tag{4.1}$$

where $b_k \in \{\pm 1\}$ are the differentially encoded transmitted symbols, i.e., $b_k = b_{k-1}a_k$, $a_k \in \{\pm 1\}$ being the information symbols. As a reference transmitted symbol, without loss of generality we take $b_{-1} = 1$.

The signal travels through a slow-fading multipath channel, assumed to be time-invariant within the interval of Q consecutive symbols, and with delay spread smaller than T_s, so that inter symbol interference (ISI) is avoided. Let $g(t) \triangleq \sum_{l=0}^{L-1} \alpha_l \delta(t - \tau_l)$ represent the channel impulse response (CIR) with L paths, where α_l and τ_l are the gain and path delay of the lth path, respectively.

The received signal $r(t)$ can then be written as

$$r(t) = \underbrace{\sum_{k=0}^{Q-1} b_k h(t - kT_s)}_{\triangleq x(t)} + v(t) \tag{4.2}$$

where $h(t) \triangleq \sum_{l=0}^{L-1} \alpha_l q(t - \tau_l)$ is the received pulse, and $v(t)$ is the zero mean additive white Gaussian noise component with variance σ_v^2. Denoting the Nyquist

[1] Generalizations of the proposed framework to signaling based on multiple frames to comply with the FCC power spectral density requirements [7] can be easily performed, and so for the sake of simplicity, it will not be addressed.

sampling rate with $1/T = N/T_s$, the received signal in its sampled version can be written as $\mathbf{r} \triangleq [\mathbf{r}_0^T, \mathbf{r}_1^T, \cdots, \mathbf{r}_{Q-1}^T]^T$ where $\mathbf{r}_k \triangleq [r(kT_s), r(kT_s+T), \cdots, r(kT_s+NT-T)]^T$ collects the N Nyquist-rate samples corresponding to the kth symbol. In view of (5.6), it can be written

$$\mathbf{r}_k = \mathbf{x}_k + \mathbf{v}_k = b_k \mathbf{h} + \mathbf{v}_k \tag{4.3}$$

where $\mathbf{h} \triangleq [h(0), h(T), \cdots, h(NT-T)]^T$ is the sampled CIR whose entries are modeled as independent and identically distributed (i.i.d.) Laplacian random variables (owing to the sparse nature of the UWB channel), and $\mathbf{v}_k \triangleq [v(kT_s), v(kT_s+T), \cdots, v(kT_s+NT-T)]^T$ is a zero mean Gaussian random vector with covariance matrix $\mathrm{E}\{\mathbf{v}_k \mathbf{v}_k^T\} = \sigma_v^2 \mathbf{I}_N$.

We can observe that the signal vector $\mathbf{x}_k$ is generally sparse due to the fact that the channel $\mathbf{h}$ is sparse, i.e., most of its components are zero or negligible [48]. Thus, according to the CS framework theory [5, 6], it can be represented by M linear measurements, with $M \ll N$. This is generally obtained through analog processing of $r(t)$, as illustrated in [46, 65]. For the sake of convenience, however, the model we will adopt here is based on an operation that is performed on the Nyquist rate samples of $r(t)$. Hence, the compressed received signal within one symbol can be expressed as

$$\mathbf{y}_k = \mathbf{\Phi}_k \mathbf{r}_k = \mathbf{\Phi}_k \mathbf{x}_k + \boldsymbol{\xi}_k \tag{4.4}$$

where the $M \times N$ matrix $\mathbf{\Phi}_k$ is the measurement matrix at time instant k and $\boldsymbol{\xi}_k \triangleq \mathbf{\Phi}_k \mathbf{v}_k$ is the noise component. It is worth recalling that $\mathbf{\Phi}_k$ satisfies the restricted isometry property (RIP) [6], thus allowing the recovery of the received signal from its CS version in the asymptotic sense as a function of the number of measurements M, with $M \ll N$ [75]. A wide range of both random (Gaussian or Bernoulli) and structured (Fourier or identity) measurement matrices satisfy the RIP. Particularly, although the latter have been proved to be the better choice for smaller N. An important parameter that has a direct influence on the performance of CS-based systems is the compression ratio defined as $\mu \triangleq M/N$, with $\mu \in (0, 1]$. A higher value of μ implies a higher value of M and hence a better performance, whereas on the other side, a lower M is desirable to keep the sampling rate at affordable levels, although this is usually achieved at the price of a given performance degradation.

4.3 Compressed-Sensing Based Detection

Several methods are available to recover differentially encoded information from the samples of the received signal. Considering that each received symbol waveform is obtained in compressed form, data decoding may optionally require prior signal reconstruction followed by differential detection, or alternatively, a joint reconstruction and detection process, as illustrated in the sequel.

4.3.1 Conventional Differential Detection

Differential detection involves the correlation between consecutive symbols within a received block. In the case of Nyquist-rate differential detection (NDD), the estimate of the information symbol can be expressed as

$$\hat{a}_{k+1}^{(\mathrm{NDD})} = \mathrm{sign}\left(\arg\min_{a}\left\{\|\mathbf{r}_k - a\mathbf{r}_{k+1}\|_2^2\right\}\right). \tag{4.5}$$

Hence from (4.5), it can be seen that one possible yet coarse way of decoding information from the compressed received signal consists of performing correlation directly on the compressed samples. We will designate this approach as direct compressed differential detection (DC-DD), which can be described as

$$\hat{a}_{k+1}^{(\mathrm{DC-DD})} = \mathrm{sign}\left(\arg\min_{a}\left\{\|\mathbf{y}_k - a\mathbf{y}_{k+1}\|_2^2\right\}\right). \tag{4.6}$$

This method does not involve sparse reconstruction of the actual received signal, but exploits only the compressed waveform $\mathbf{y}_k$ given by (4.4). We note however that the DC-DD works under the condition that every compressed symbol waveform is the result of the same linear transformation of the received signal, otherwise it may exhibit strong limitations. We will come back to this aspect in the following subsections. Nevertheless, direct compressed detection can be favorably applied when synchronization requirements may be relaxed (and accordingly, signal reconstruction can be avoided), such as for instance in [85].

4.3.2 Overview of Reconstruction Techniques

Focusing on the reconstruction of $\mathbf{x}_k$, a naive way is to adopt the ordinary least squares (OLS) optimization method, thus obtaining from (4.4)

$$\hat{\mathbf{x}}_k^{(\mathrm{OLS})} = \arg\min_{\mathbf{x}_k}\left\{\|\mathbf{y}_k - \mathbf{\Phi}_k\mathbf{x}_k\|_2^2\right\}. \tag{4.7}$$

Due to the fact that the $M \times N$ measurement matrix $\mathbf{\Phi}_k$ is fat ($M \ll N$), and so not full column rank, the solution to the OLS problem in (4.7) is not unique. One way to circumvent this drawback is to use Tikhonov regularization based on the ℓ_2 norm, which penalizes the OLS cost function with a quadratic penalty, also known as ridge regression (RR), leading to

$$\hat{\mathbf{x}}_k^{(\mathrm{RR})} = \arg\min_{\mathbf{x}_k} \left\{ \|\mathbf{y}_k - \mathbf{\Phi}_k \mathbf{x}_k\|_2^2 + \lambda \|\mathbf{x}_k\|_2^2 \right\} \tag{4.8}$$

where λ is the Lagrangian constant. Although the RR solution is unique, it does not care about the sparsity of $\mathbf{x}_k$. A specific solution to this problem is the least absolute shrinkage and selection operator (LASSO) [37], which adopts a regularization term based on the ℓ_1 norm, as

$$\hat{\mathbf{x}}_k^{(\mathrm{LASSO})} = \arg\min_{\mathbf{x}_k} \left\{ \|\mathbf{y}_k - \mathbf{\Phi}_k \mathbf{x}_k\|_2^2 + \lambda \|\mathbf{x}_k\|_1 \right\} \tag{4.9}$$

where λ is again the Lagrangian constant. Due to the ℓ_1 regularization that induces sparsity, part of the entries of $\hat{\mathbf{x}}_k^{(\mathrm{LASSO})}$ will be switched off (hopefully the noisy or the non-significant ones), under the condition that the value of λ is properly chosen. This appealing feature explains why the interest in the LASSO technique is growing more and more whenever a sparse signal has to be reconstructed. The above fully motivates the adoption of LASSO, or its modified versions, to address the CS-based detection problem we are dealing with, as will be illustrated in the rest of this section.

4.3.3 Separate Reconstruction and Detection

According to the separate compressed differential detection approach (SC-DD), the sparse received signal is first reconstructed from the compressed samples applying the LASSO algorithm, and subsequently used to decode the information symbols through correlation of consecutive symbol waveforms. Among the various algorithms to solve the LASSO problem, we mention the LARS scheme [38], which has a low complexity but requires $M > N$, and the one proposed in [88], which is applicable for $M < N$ but is computationally intensive. On the other side, the pathwise coordinate descent (PCD) optimization idea is proposed in [39] as a way to solve the LASSO problem, and turns out to be particularly competitive as far as the computational complexity aspects are concerned. The PCD is based on optimizing one coordinate of $\mathbf{x}_k$ at-a-time, while all the others are kept at the values evaluated at the previous iteration, so that each update works as a warm start for

the next step. Hence, the PCD solution to (4.9) for the $(n+1)$th iteration, $n \geq 0$, and the jth coordinate, $1 \leq j \leq N$, of $\hat{\mathbf{x}}_{k+l}$, $l = 0, 1$ can be proved to be [39]

$$[\hat{\mathbf{x}}_{k+l}]_j(n+1) = \text{shrink}\left(\sum_{i=1}^{M}[\mathbf{\Phi}_{k+l}]_{i,j}\{[\mathbf{y}_{k+l}]_i - [\hat{\mathbf{y}}_{k+l}^{(j)}]_i(n+1)\}, \lambda\right) \quad (4.10)$$

where the "shrink" operator is defined as $\text{shrink}\,(z,\lambda) \triangleq \text{sign}(z)(|z|-\lambda)_+$, with the parameter λ optimized through a cross-validation (CV) approach (Sect. 4.5.1), and $[\hat{\mathbf{y}}_{k+l}^{(j)}]_i(n+1)$ is evaluated as

$$[\hat{\mathbf{y}}_{k+l}^{(j)}]_i(n+1) = \sum_{m<j}[\mathbf{\Phi}_{k+l}]_{i,m}[\hat{\mathbf{x}}_{k+l}]_m(n+1) + \sum_{m>j}[\mathbf{\Phi}_{k+l}]_{i,m}[\hat{\mathbf{x}}_{k+l}]_m(n), \quad (4.11)$$

i.e., excluding the effect of the jth coordinate $[\hat{\mathbf{x}}_{k+l}]_j(n)$, and using for the earlier $(j-1)$ entries the values updated at the current $(n+1)$th iteration, namely $[\hat{\mathbf{x}}_{k+l}]_1(n+1), [\hat{\mathbf{x}}_{k+l}]_2(n+1), \cdots, [\hat{\mathbf{x}}_{k+l}]_{j-1}(n+1)$, and for the remaining ones, namely $[\hat{\mathbf{x}}_{k+l}]_{j+1}(n), [\hat{\mathbf{x}}_{k+l}]_{j+2}(n), \cdots, [\hat{\mathbf{x}}_{k+l}]_N(n)$, those values updated at the previous iteration. The PCD iterations (4.10) and (4.11) continue till convergence, i.e., when a predefined tolerance level has been reached for each coordinate. Next, from the symbol waveform estimates $\hat{\mathbf{x}}_k(P)$ and $\hat{\mathbf{x}}_{k+1}(P)$ reconstructed after P iterations, we can obtain the detected symbol as

$$\hat{a}_{k+1}^{(\text{SC}-\text{DD})} = \text{sign}\left(\hat{\mathbf{x}}_{k+1}(P)^T\hat{\mathbf{x}}_k(P)\right). \quad (4.12)$$

The computational complexity required by the PCD algorithm for each reconstruction iteration can be shown to be $\mathcal{O}(NM)$ [89], while that for the detection step is simply equal to $\mathcal{O}(N)$. Therefore, the overall complexity of the SC-DD for P iterations amounts to $\mathcal{O}(PNM)$.

4.3.4 Joint Reconstruction and Detection

An alternative to the SC-DD approach is to perform joint reconstruction and detection, which will be referred to as the joint compressed differential detection (JC-DD) approach. Formally, the corresponding cost function of the JC-DD optimization problem to be minimized over $\mathbf{x}_k$, $\mathbf{x}_{k+1}$ and a_{k+1} can be formulated as

$$\mathcal{C}_{k+1}^{(\text{JC}-\text{DD})}(\mathbf{x}_k, \mathbf{x}_{k+1}, a_{k+1}) \triangleq \sum_{l=0}^{1}\left[\|\mathbf{y}_{k+l} - \mathbf{\Phi}_{k+l}\mathbf{x}_{k+l}\|_2^2 + \lambda\|\mathbf{x}_{k+l}\|_1\right] + \alpha\|\mathbf{x}_k - a_{k+1}\mathbf{x}_{k+1}\|_2^2 \quad (4.13)$$

where λ is the Lagrangian constant and α is a weight constant. The following remarks about the JC-DD are now of interest.

1. The parameter α has to be chosen by trading off the performance of the reconstruction against the detection steps. A higher value may result in a wrong correlation estimate due to excess noise on $\hat{\mathbf{x}}_k$ and $\hat{\mathbf{x}}_{k+1}$. Conversely, a lower value may be detrimental as well due to an accuracy loss in the estimate $\hat{a}_{k+1}$. Indeed, in that case the JC-DD collapses into the SC-DD approach, where we first reconstruct independent of detection, and then detect optimizing only with respect to a_{k+1}.

2. In view of the joint optimization, the reconstruction and detection steps reinforce each other during iterations. Therefore, improved performance over both the DC-DD and SC-DD is expected.

3. Several regression methods are available to minimize the cost function (4.13), even though we will show in a while that none of them exhibits the regularization features that properly match the JC-DD problem. Generally speaking, denoting with $\mathbf{u}$ and $\mathbf{z}$ the vectors with size M and N, collecting the received compressed samples and to be optimally reconstructed, respectively, and with $\mathbf{\Lambda}$ an $M \times N$ measurement matrix, we can basically enumerate the following three methods.

   - *Standard LASSO.* Taking into account (4.9), the standard LASSO can be put into the form

   $$\begin{cases} \hat{\mathbf{z}}^{(\mathrm{LASSO})} = \arg\min\limits_{\mathbf{z}} \left\{ \|\mathbf{u} - \mathbf{\Lambda}\mathbf{z}\|_2^2 \right\} \\ \text{s.t.} \qquad\qquad \|\mathbf{z}\|_1 \leq \gamma \end{cases} \tag{4.14}$$

   where γ is a given threshold. We note that the main effect of the constraint based on the ℓ_1 norm is to induce parsimony in the solution, in the sense that among all the feasible solutions (4.14) takes specific care of those solutions with higher sparsity. However, no quadratic constraint on the optimization variables is involved as required by the JC-DD cost function (4.13). Therefore, it can be concluded that the standard LASSO is of scarce utility for our purpose and some alternatives have to be searched for.

   - *Elastic Net.* Elastic Net (EN) is a modified version of LASSO where a

quadratic constraint is considered as well [43], according to the form

$$\begin{cases} \hat{\mathbf{z}}^{(\mathrm{EN})} = \arg\min\limits_{\mathbf{z}} \left\{ \|\mathbf{u} - \mathbf{\Lambda}\mathbf{z}\|_2^2 \right\} \\ \text{s.t.} \qquad \|\mathbf{z}\|_1 \leq \gamma_1 \\ \qquad\quad \|\mathbf{z}\|_2^2 \leq \gamma_2 \end{cases}, \tag{4.15}$$

with γ_1 and γ_2 being predefined thresholds. The added constraint has the effect of grouping the elements of the optimization vector $\mathbf{z}$, which adds to the action of favoring sparse solutions played by the ℓ_1-based constraint. The actual result is that parts of $\mathbf{z}$ will be different from zero and others will be negligible, thus matching the cluster-based propagation encountered in typical UWB environments [48], but again what is now lacking is the differential aspect related to the JC-DD cost function (4.13).

- *Fused LASSO.* An additional variant of LASSO is represented by the Fused LASSO (F-LASSO), which is proposed in [44] as

$$\begin{cases} \hat{\mathbf{z}}^{(\mathrm{F-LASSO})} = \arg\min\limits_{\mathbf{z}} \left\{ \|\mathbf{u} - \mathbf{\Lambda}\mathbf{z}\|_2^2 \right\} \\ \text{s.t.} \qquad \|\mathbf{z}\|_1 \leq \gamma_1 \\ \qquad\quad \sum_{j=2}^{N} |[\mathbf{z}]_j - [\mathbf{z}]_{j-1}| \leq \gamma_2 \end{cases}. \tag{4.16}$$

  The F-LASSO method penalizes the cost function with not only the sum of the absolute values of the coefficients of the optimization variable, i.e., $\|\mathbf{z}\|_1$, but also their differences. That way, sparsity is induced while "fusing" successive coefficients to each other, but again, these features are not exactly what is required.

4. From the regularization methods (4.14)-(4.16), it is apparent that none of them satisfies the requirements for the optimization of the JC-DD cost function, including both an ℓ_1-based as well as a squared differential penalty on two sets of optimization variables and not just one. Hence, this need fully motivates the development of a different method that we will focus on in the next subsection.

4.3.5 Differential Elastic Net

We propose here a novel regularization method, which we will designate as differential elastic net (DEN), and which can be formulated as

$$\begin{cases} (\hat{\mathbf{z}}_1, \hat{\mathbf{z}}_2, \hat{a})^{(\mathrm{DEN})} = \underset{\mathbf{z}_1, \mathbf{z}_2, a}{\arg\min} \left\{ \sum_{l=1}^{2} \left[\|\mathbf{u}_l - \mathbf{\Lambda}_l \mathbf{z}_l\|_2^2 \right] \right\} \\ \text{s.t.} \qquad \|\mathbf{z}_1\|_1 \leq \gamma_1 \\ \qquad\qquad \|\mathbf{z}_2\|_1 \leq \gamma_1 \\ \qquad\qquad \|\mathbf{z}_1 - a\mathbf{z}_2\|_2^2 \leq \gamma_2 \end{cases} \tag{4.17}$$

where $\mathbf{z}_1$ and $\mathbf{z}_2$ are the two sets of variables to be optimally reconstructed, each with size N, $\mathbf{u}_1$ and $\mathbf{u}_2$ are the two sets of compressed samples, each with size M, and $\mathbf{\Lambda}_1$ and $\mathbf{\Lambda}_2$ are the corresponding $M \times N$ measurement matrices. The rationale of the DEN method relies on searching the sparse solutions $\hat{\mathbf{z}}_1$ and $\hat{\mathbf{z}}_2$ while imposing at the same time fusion between their respective elements, together with deriving the optimal estimate $\hat{a}$ of the transmitted information symbol.

As an effective way to solve (4.17), we resort to the PCD algorithm illustrated in Sect. 4.3.3. Due to its iterative nature, convergence to a unique solution may be an issue. Indeed, convergence of the PCD is typically not ensured for non-differentiable cost functions. It has been proved, however, that an exception occurs whenever the non-differentiable part is separable in its variables [90]. Interesting to say, the ℓ_1 part in the cost function (4.13) just satisfies that condition, and accordingly, this proves the uniqueness of the PCD solution to (4.17). Now, the DEN solutions to (4.17) can be derived, as stated in the following proposition.

Proposition 4.3.1. *The jth entries of the solutions $\hat{\mathbf{z}}_1$ and $\hat{\mathbf{z}}_2$ to (4.17) at the $(n+1)$th iteration, $n \geq 0$, can be written as*

$$[\hat{\mathbf{z}}_1]_j(n+1) = \frac{\mathrm{shrink}\left(\sum_{i=1}^{M} [\mathbf{\Lambda}_1]_{i,j} \{ [\mathbf{u}_1]_i - [\hat{\mathbf{u}}_1^{(j)}(n+1)]_i \} + \alpha \hat{a}(n) [\hat{\mathbf{z}}_2]_j(n), \lambda \right)}{1+\alpha} \tag{4.18}$$

$$[\hat{\mathbf{z}}_2]_j(n+1) = \frac{\mathrm{shrink}\left(\sum_{i=1}^{M} [\mathbf{\Lambda}_2]_{i,j} \{ [\mathbf{u}_2]_i - [\hat{\mathbf{u}}_2^{(j)}(n+1)]_i \} + \alpha \hat{a}(n) [\hat{\mathbf{z}}_1]_j(n), \lambda \right)}{1+\alpha \hat{a}^2(n)} \tag{4.19}$$

$$\hat{a}(n+1) = \hat{\mathbf{z}}_2^T(n+1) \hat{\mathbf{z}}_1(n+1) \tag{4.20}$$

where

$$[\hat{\mathbf{u}}_l^{(j)}(n+1)]_i = \sum_{m<j} [\mathbf{\Lambda}_l]_{i,m} [\hat{\mathbf{z}}_l]_m (n+1) + \sum_{m>j} [\mathbf{\Lambda}_l]_{i,m} [\hat{\mathbf{z}}_l]_m (n), \ l = 1, 2. \tag{4.21}$$

Proof. The Lagrangian of the cost function in (4.17) is

$$\mathcal{L}(\mathbf{z}_1, \mathbf{z}_2, a) = \sum_{l=1}^{2} \left[\|\mathbf{u}_l - \mathbf{\Lambda}_l \mathbf{z}_l\|_2^2 + \lambda \|\mathbf{z}_l\|_1 \right] + \alpha \|\mathbf{z}_1 - a\mathbf{z}_2\|_2^2 \tag{4.22}$$

where λ and α are the Lagrangian constants, depending on the thresholds γ_1 and γ_2. Upon differentiating (4.22) with respect to the jth element of $\mathbf{z}_1$ and $\mathbf{z}_2$ and equating them to zero, it is easy to obtain (4.18) and (4.19), respectively. Then, (4.20) follows. □

Hence, in view of Proposition 4.3.1 and the structure of the cost function (4.13), the optimal solutions to the JC-DD problem can be readily derived by directly replacing, respectively: $\hat{\mathbf{z}}_1(n)$ and $\hat{\mathbf{z}}_2(n)$ with $\hat{\mathbf{x}}_k(n)$ and $\hat{\mathbf{x}}_{k+1}(n)$, $\mathbf{u}_1$ and $\mathbf{u}_2$ with $\mathbf{y}_k$ and $\mathbf{y}_{k+1}$, $\hat{\mathbf{u}}_1^{(j)}(n)$ and $\hat{\mathbf{u}}_2^{(j)}(n)$ with $\hat{\mathbf{y}}_k^{(j)}(n)$ and $\hat{\mathbf{y}}_{k+1}^{(j)}(n)$, and finally $\mathbf{\Lambda}_1$ and $\mathbf{\Lambda}_2$ with $\mathbf{\Phi}_k$ and $\mathbf{\Phi}_{k+1}$. To conclude, it is worth noting that the computational complexity of the JC-DD approach based on the PCD iterative algorithm for a total of P iterations results in $\mathcal{O}(PNM)$, and therefore, it is comparable with that of the SC-DD.

4.4 MAP detectors

In this section, MAP detectors will be derived as performance benchmarks assuming that the received signal is sampled at the Nyquist rate or at the compressed rate. Differently from [91], the channel response is Laplacian distributed so as to take into account its inherent sparsity.

4.4.1 Nyquist-rate MAP detector

The Nyquist-rate sampled waveform corresponding to two consecutive symbols can be written as

$$\mathbf{r} = (\mathbf{b} \otimes \mathbf{I}_N)\mathbf{h} + \mathbf{v} \tag{4.23}$$

where $\mathbf{r} \triangleq [\mathbf{r}_k^T, \mathbf{r}_{k+1}^T]^T$, with $\mathbf{r}_k$ being expressed by (4.3), $\mathbf{b} \triangleq [b_k, b_{k+1}]^T$ includes two consecutive differentially-encoded symbols, and $\mathbf{v} \triangleq [\mathbf{v}_k^T, \mathbf{v}_{k+1}^T]^T$ is the noise component. Hence, the Nyquist-rate MAP differential detector (N-MAP-DD) can be expressed as

$$\hat{\mathbf{b}} = \arg\max_{\mathbf{b}} \{p(\mathbf{r}|\mathbf{b})P(\mathbf{b})\} \tag{4.24}$$

where $P(\mathbf{b})$ is the *a priori* distribution of the transmitted symbols $\mathbf{b}$. Under some assumptions, it can be proved that the N-MAP-DD (4.24) takes a simple form, as illustrated in the following proposition.

Proposition 4.4.1. *Assuming a uniform distribution of the transmitted symbols* $\mathbf{b}$ *and Laplacian distribution of the channel response* $\mathbf{h}$*, the N-MAP-DD coincides with the conventional Nyquist-rate DD (4.5)*

$$\hat{a}_{k+1}^{(\mathrm{N-MAP-DD})} = \mathit{sign}\left(\mathbf{r}_{k+1}^T \mathbf{r}_k\right). \tag{4.25}$$

Proof. Upon representing the channel response as the product $\mathbf{h} = \rho\mathbf{n}$ between a Rayleigh random variable ρ and a joint normal random vector $\mathbf{n}$, the expression of $p(\mathbf{r}|\mathbf{b})$, as derived in Appendix 4.A, is

$$p(\mathbf{r}|\mathbf{b}) = \int_0^\infty p(\mathbf{r}|\mathbf{b},\rho)p(\rho)d\rho \tag{4.26}$$

where $p(\mathbf{r}|\mathbf{b},\rho)$ is the zero-mean joint normal distribution

$$p(\mathbf{r}|\mathbf{b},\rho) = \frac{1}{\pi^{2N}\sigma_v^2(\sigma_v^2+2\rho^2)} \exp\left\{-\frac{1}{\sigma_v^2}\mathbf{r}^T\left[\mathbf{I}_{2N} - \frac{\rho^2}{\sigma_v^2+2\rho^2}(\mathbf{b}\mathbf{b}^T\otimes\mathbf{I}_N)\right]\mathbf{r}\right\}. \tag{4.27}$$

Since $\mathbf{b}$ is assumed to be uniformly distributed, from (4.24) it can be argued that maximizing the product $p(\mathbf{r}|\mathbf{b})P(\mathbf{b})$ is equivalent to maximizing $p(\mathbf{r}|\mathbf{b})$ over $\mathbf{b}$. From (4.26), we can say that if the maximum of $p(\mathbf{r}|\mathbf{b},\rho)$ over $\mathbf{b}$ is independent of each value of ρ, then that is also the maximum of $p(\mathbf{r}|\mathbf{b})$. Now from (4.27), maximizing $p(\mathbf{r}|\mathbf{b},\rho)$ means that for a given $\mathbf{r}$ and ρ, finding the value of $\mathbf{b}$ that maximizes

$$\Gamma_{\mathrm{N}}(\mathbf{r}|\mathbf{b},\rho) \triangleq -\frac{1}{\sigma_v^2}\mathbf{r}^T\left[\mathbf{I}_{2N} - \frac{\rho^2}{\sigma_v^2+2\rho^2}(\mathbf{b}\mathbf{b}^T\otimes\mathbf{I}_N)\right]\mathbf{r}. \tag{4.28}$$

Dropping immaterial addends independent of $\mathbf{b}$, from (4.28) it can be obtained that the MAP estimate is the value of $\mathbf{b}$ maximizing the function (independent of ρ) defined as

$$\Psi_{\mathrm{N}}(\mathbf{r}|\mathbf{b}) \triangleq \mathbf{r}^T(\mathbf{b}\mathbf{b}^T\otimes\mathbf{I}_N)\mathbf{r} = b_{k+1}b_k\mathbf{r}_{k+1}^T\mathbf{r}_k. \tag{4.29}$$

Thus, in view of the differential encoding rule $a_{k+1} = b_{k+1}b_k$, (4.29) turns equivalently into

$$\Psi_{\mathrm{N}}(\mathbf{r}|\mathbf{b}) = a_{k+1}\mathbf{r}_{k+1}^T\mathbf{r}_k \tag{4.30}$$

which provides the desired result (4.25). □

4.4.2 Compressed-rate MAP detector

The signal model for two consecutive received symbol waveforms sampled at compressed rate can be formulated as

$$\mathbf{y} = \mathbf{\Phi}(\mathbf{b} \otimes \mathbf{I}_N)\mathbf{h} + \mathbf{\Phi}\mathbf{v} \tag{4.31}$$

where $\mathbf{y} \triangleq [\mathbf{y}_k^T, \mathbf{y}_{k+1}^T]^T$, with $\mathbf{y}_k$ being expressed by (4.4), $\mathbf{b}$ and $\mathbf{v}$ are defined as in (4.23), and $\mathbf{\Phi} \triangleq \text{diag}\{\mathbf{\Phi}_k, \mathbf{\Phi}_{k+1}\}$, with $\mathbf{\Phi}_{k+l}$, $l = 0, 1$ being the $M \times N$ measurement matrices for which we assume $\mathbf{\Phi}_{k+l}\mathbf{\Phi}_{k+l}^T = \mathbf{I}_M$, $l = 0, 1$. The compressed-rate MAP differential detector (C-MAP-DD) is given by

$$\hat{\mathbf{b}} = \arg\max_{\mathbf{b}} \{p(\mathbf{y}|\mathbf{b})P(\mathbf{b})\} \tag{4.32}$$

where $P(\mathbf{b})$ is the *a priori* distribution of the transmitted symbols $\mathbf{b}$. The structure of the C-MAP-DD scheme can be derived as illustrated in the sequel.

Proposition 4.4.2. *Assuming a uniform distribution of the transmitted symbols* $\mathbf{b}$ *and Laplacian distribution of the channel response* $\mathbf{h}$*, the C-MAP-DD rule results approximately in*

$$\hat{a}_{k+1}^{(\text{C}-\text{MAP}-\text{DD})} = \textit{sign}\left(\mathbf{y}_{k+1}^T \mathbf{\Phi}_{k+1}\mathbf{\Phi}_k^T \mathbf{y}_k\right). \tag{4.33}$$

Proof. Following the approach pursued in Proposition 4.4.1, in Appendix 4.B it is shown that

$$p(\mathbf{y}|\mathbf{b}) = \int_0^\infty p(\mathbf{y}|\mathbf{b}, \rho)p(\rho)d\rho \tag{4.34}$$

where ρ is a Rayleigh distributed random variable and $p(\mathbf{y}|\mathbf{b}, \rho)$ is the zero-mean joint normal distribution

$$\begin{aligned} p(\mathbf{y}|\mathbf{b}, \rho) = &\frac{1}{\pi^{2M}\sigma_v^{4M}|\mathbf{\Sigma}|} \\ &\times \exp\left\{-\frac{1}{\sigma_v^2}\mathbf{y}^T\left[\mathbf{I}_{2M} - \frac{\rho^2}{\sigma_v^2}\mathbf{\Phi}(\mathbf{b} \otimes \mathbf{I}_N)\mathbf{\Sigma}^{-1}(\mathbf{b} \otimes \mathbf{I}_N)^T\mathbf{\Phi}^T\right]\mathbf{y}\right\} \end{aligned} \tag{4.35}$$

with the $N \times N$ positive definite matrix $\mathbf{\Sigma}$ being defined as

$$\mathbf{\Sigma} \triangleq \mathbf{I}_N + \frac{\rho^2}{\sigma_v^2}\left(\mathbf{\Phi}_k^T\mathbf{\Phi}_k + \mathbf{\Phi}_{k+1}^T\mathbf{\Phi}_{k+1}\right). \tag{4.36}$$

Exploiting the assumption that $P(\mathbf{b})$ is independent of $\mathbf{b}$, from (4.32) it comes out that maximizing the product $p(\mathbf{y}|\mathbf{b})P(\mathbf{b})$ over $\mathbf{b}$ equals to doing the same with $p(\mathbf{y}|\mathbf{b})$ over $\mathbf{b}$. Now from (4.34), if the maximum of $p(\mathbf{y}|\mathbf{b},\rho)$ over $\mathbf{b}$ for each value of ρ is independent of ρ then that is also the maximum of $p(\mathbf{y}|\mathbf{b})$. From (4.35), finding the maximum of $p(\mathbf{y}|\mathbf{b},\rho)$ over $\mathbf{b}$ means maximizing

$$\Gamma_{\mathrm{C}}(\mathbf{y}|\mathbf{b},\rho) \triangleq -\frac{1}{\sigma_v^2}\mathbf{y}^T\left[\mathbf{I}_{2M} - \frac{\rho^2}{\sigma_v^2}\mathbf{\Phi}(\mathbf{b}\otimes\mathbf{I}_N)\mathbf{\Sigma}^{-1}(\mathbf{b}\otimes\mathbf{I}_N)^T\mathbf{\Phi}^T\right]\mathbf{y}, \quad (4.37)$$

or equivalently, the function obtained after dropping immaterial addends independent of $\mathbf{b}$ as

$$\Psi_{\mathrm{C}}(\mathbf{y}|\mathbf{b},\rho) \triangleq \mathbf{y}^T\mathbf{\Phi}(\mathbf{b}\otimes\mathbf{I}_N)\mathbf{\Sigma}^{-1}(\mathbf{b}\otimes\mathbf{I}_N)^T\mathbf{\Phi}^T\mathbf{y} \quad (4.38)$$

which, however, is still dependent on ρ due to the presence of $\mathbf{\Sigma}^{-1}$. Such a matrix inverse can be computed by exploiting the eigenvalue decomposition (EVD) of the $N\times N$ positive semi-definite matrix $\mathbf{\Phi}_k^T\mathbf{\Phi}_k + \mathbf{\Phi}_{k+1}^T\mathbf{\Phi}_{k+1}$ given by $\mathbf{Q}\mathbf{\Omega}\mathbf{Q}^T$, with $\mathbf{\Omega}$ having non-negative elements along its main diagonal and $\mathbf{Q}\mathbf{Q}^T = \mathbf{I}_N$. Thus, plugging the EVD into (4.38) yields

$$\Psi_{\mathrm{C}}(\mathbf{y}|\mathbf{b},\rho) \triangleq \mathbf{y}^T\mathbf{\Phi}(\mathbf{b}\otimes\mathbf{I}_N)\mathbf{Q}\left(\mathbf{I}_N + \frac{\rho^2}{\sigma_v^2}\mathbf{\Omega}\right)^{-1}\mathbf{Q}^T(\mathbf{b}\otimes\mathbf{I}_N)^T\mathbf{\Phi}^T\mathbf{y}. \quad (4.39)$$

Now, considering the fact that the diagonal matrix $\left(\mathbf{I}_N + \frac{\rho^2}{\sigma_v^2}\mathbf{\Omega}\right)^{-1}$ has entries which are strictly positive and less than unity, (4.39) can be approximated by its upper bound (independent of ρ)

$$\Upsilon_{\mathrm{C}}(\mathbf{y}|\mathbf{b}) \triangleq \mathbf{y}^T\mathbf{\Phi}(\mathbf{b}\otimes\mathbf{I}_N)(\mathbf{b}\otimes\mathbf{I}_N)^T\mathbf{\Phi}^T\mathbf{y}, \quad (4.40)$$

that can be properly rearranged as

$$\Upsilon_{\mathrm{C}}(\mathbf{y}|\mathbf{b}) = b_{k+1}b_k\mathbf{y}_{k+1}^T\mathbf{\Phi}_{k+1}\mathbf{\Phi}_k^T\mathbf{y}_k. \quad (4.41)$$

Thus, in view of the differential encoding rule $a_{k+1} = b_{k+1}b_k$, we end up with the desired result (4.33). □

Some remarks about the C-MAP-DD scheme can be of interest.

1. The OLS-DD estimate of the information symbol a_{k+1} is obtained from (4.7) as

$$\hat{a}_{k+1}^{\mathrm{OLS-DD}} = \mathrm{sign}\left((\mathbf{\Phi}_{k+1}^{+}\mathbf{y}_{k+1})^T(\mathbf{\Phi}_k^{+}\mathbf{y}_k)\right) \quad (4.42)$$

where $\mathbf{\Phi}_{k+l}^{+}$ is the pseudo-inverse of $\mathbf{\Phi}_{k+l}$, $l = 0, 1$. Since the measurement matrices have orthonormal rows, it can be shown that $\mathbf{\Phi}_{k+l}^{+} = \mathbf{\Phi}_{k+l}^{T}$, $l = 0, 1$. Therefore, we get

$$(\mathbf{\Phi}_{k+1}^{+}\mathbf{y}_{k+1})^{T}(\mathbf{\Phi}_{k}^{+}\mathbf{y}_{k}) = \mathbf{y}_{k+1}^{T}\mathbf{\Phi}_{k+1}\mathbf{\Phi}_{k}^{T}\mathbf{y}_{k}, \tag{4.43}$$

from which we argue that the OLS-DD coincides with the C-MAP-DD.

2. Assuming $\mathbf{\Phi}_{k+1} = \mathbf{\Phi}_{k}$ and exploiting $\mathbf{\Phi}_{k}\mathbf{\Phi}_{k}^{T} = \mathbf{I}_{M}$, we obtain from (4.33)

$$\mathbf{y}_{k+1}^{T}\mathbf{\Phi}_{k+1}\mathbf{\Phi}_{k}^{T}\mathbf{y}_{k} = \mathbf{y}_{k+1}^{T}\mathbf{y}_{k} \tag{4.44}$$

which means that, whenever the measurement matrices are invariant, the C-MAP-DD coincides with the DC-DD.

4.5 Simulation Results

The detectors we discussed in the previous sections are verified here by means of numerical simulations taking as performance quality the bit error rate (BER) metric as a function of both the ratio of the mean-received bit-energy and the noise spectral density ratio defined as $E_b/N_0 \triangleq \|\mathbf{h}\|_2^2/\sigma_v^2$, and the compression ratio μ. The conventional DD at Nyquist-rate (NDD) is compared with the compressed DD schemes based on the approaches of the direct type DC-DD in (4.6), the separate type SD-DD in (4.10)-(4.12) and the joint type JD-DD solved through the iterative method outlined in Proposition 4.3.1. The performance results of the compressed MAP DD derived in Proposition 4.4.2 and the least squares DD defined by (4.42), labelled as C-MAP-DD and OLS-DD, respectively, are also plotted as performance benchmarks.

4.5.1 Simulation Setup

The transmitted signal consists of differentially encoded symbols, each conveyed by an ultra short pulse traveling through a Laplacian distributed propagation channel. For the sake of simplicity, we assume that the channel response, identified as $\mathbf{h}$ in (4.3), includes the effects of the shaping filters at both the transmitter and receiver sides. The received symbol waveform sampled at Nyquist rate contains $N = 32$ samples, or alternatively, is compressed with a compression ratio μ, thus resulting in $M < N$ samples. The measurement matrix $\mathbf{\Phi}_{k}$ has zero-mean unit-variance i.i.d. normal entries with orthonormalized rows, and can be chosen within

consecutive symbols to be the same ($\mathbf{\Phi}_k = \mathbf{\Phi}_{k+1}$) or different from each other ($\mathbf{\Phi}_k \neq \mathbf{\Phi}_{k+1}$). The methods PCD in (4.10)-(4.11) and DEN in (4.18)-(4.20) are iterated for a maximum of 200 iterations or if a tolerance level of 10^{-5} is reached.

The optimal value of the parameter λ is selected for the SC-DD case by applying a $\mathcal{K}$-fold cross validation (CV) approach [92, Chapter 17]. For a given λ, the received samples $\mathbf{y}$ are subdivided into the sequence $\mathbf{y}_m$, $1 \leq m \leq \mathcal{K}$, each including $M/\mathcal{K}$ samples. Then, $\mathbf{y}_m$ is predicted as $\hat{\mathbf{y}}_m$ using the samples obtained by removing $\mathbf{y}_m$ itself from $\mathbf{y}$. The optimal λ is thus evaluated as the value minimizing the prediction error

$$\lambda^{(\text{opt})} = \arg\min_{\lambda} \left\{ \frac{1}{M} \sum_{m=1}^{\mathcal{K}} \|\mathbf{y}_m - \hat{\mathbf{y}}_m(\lambda)\|_2^2 \right\} \tag{4.45}$$

where $\mathcal{K} = 8$ and the trial values of λ are $1, 0.1, 0.01, 0.001$. Conversely, for the JC-DD the optimal λ is chosen as

$$\lambda^{(\text{opt})} = \arg\max_{\lambda} \{|\hat{a}_{k+1}(\lambda)|\} \tag{4.46}$$

where $\hat{a}_{k+1}$ is the DEN symbol soft estimate given by the correlation (4.20) of Proposition 4.4.2.

4.5.2 Performance Comparisons

Figs. 4.1 and 4.2 quantify the BER detection performance as a function of the E_b/N_0 ratio, assuming that the measurement matrices are chosen to be the same or different from each other, respectively. While the reference NDD works at Nyquist-rate, all the other schemes adopt a compression ratio of $\mu = 0.5$ or $\mu = 0.75$. Focusing in Fig. 4.1 on the case $\mu = 0.5$, it can be noted that the JC-DD closely follows the C-MAP-DD, but if compared to the NDD, it degrades approximately by 1.5 dB at a BER level of 10^{-2}. Further, the DC-DD overlaps with the C-MAP-DD, according to what we observed in remark 2) of Sect. 4.4.2, whereas the SC-DD lags behind by 1 dB. Increasing the compression ratio to $\mu = 0.75$, the JC-DD, DC-DD and SC-DD BER degradation from the reference NDD reduces to around 1dB, 1dB and 1.3 dB, respectively. Thus, we show that the above compressed detectors can trade off performance against complexity in terms of compression ratio.

The results of Fig. 4.2 confirm that: *i*) the scenario with different measurement matrices is more demanding than the one when they are the same as illustrated in Fig. 4.1, and *ii*) an increase of the compression ratio to $\mu = 0.75$ alleviates the performance gap from the conventional NDD at the price of increasing the complexity.

For $\mu = 0.5$ and a BER level of 10^{-2}, the JC-DD has a gap of approximately 1 dB from C-MAP-DD and 7.5 dB from the NDD, but shows a considerable edge over the separate approach SC-DD. Differently from Fig. 4.1, the direct scheme DC-DD completely misses detection and so turns out to be useless. This result proves that a reconstruction step, separate or better joint with detection, is clearly mandatory.

Further, from both Fig. 4.1 and Fig. 4.2 it is apparent that the performance of the OLS-DD equals that offered by the C-MAP-DD, as expected from remark 1) of Sect. 4.4.2. Nevertheless, we remark that the OLS-DD is considerably outperformed by the JC-DD and SC-DD in terms of sparse signal reconstruction, due to the intrinsic lack of inducing sparsity on the solutions exhibited by the least squares method.

Figs. 4.3 and 4.4 give a quantitative picture about the reconstruction performance of the JC-DD and SC-DD, respectively. We assume that the received waveforms without noise are $\mathbf{x}_k = \mathbf{h}$ and $\mathbf{x}_{k+1} = -\mathbf{h}$, $E_b/N_0 = 20$ dB, and λ is set to 0.1. In each figure, the upper part shows $\mathbf{h}$ and the reconstructed signal component $\hat{\mathbf{x}}_k$, whereas the lower part does the same for the adjacent symbol, namely $\mathbf{h}$ and $\hat{\mathbf{x}}_{k+1}$. For a given realization of $\mathbf{h}$, we obtain that out of $2N = 64$ signal samples for both symbols, the JC-DD forces $24/64 \approx 37\%$ components to zero and correctly reconstructs $31/64 \approx 48\%$ non-zero components, whereas the above percentages for the SC-DD turn into $36/64 \approx 56\%$ and $19/64 \approx 30\%$, respectively. These results make us argue that the SC-DD has a higher tendency of setting signal components to zero, whereas the JC-DD exploits its inherent fusion capabilities between the two sets of variables, leading not only to joint sparsity but also to a fair amount of reconstructed non-zero components. The different behavior plays a role in taking a correct decision based on correlation, and justifies the detection performance superiority of the joint approach on considering detection as a separate step from reconstruction.

Fig. 4.5 shows the sensitivity of the JC-DD scheme to the choice of the coefficient α which weighs the differential squared error in (4.13). It is apparent that better results over E_b/N_0 are obtained for values in the range around $\alpha = 100$. Finally, the effect of the compression ratio μ over the BER of the JC-DD is evaluated in Fig. 4.6 for an E_b/N_0 of 12 and 14 dB. As expected, it can be shown that smaller the μ the worse the BER level, and when μ approaches 1, the performance of the JC-DD tends to that of the NDD.

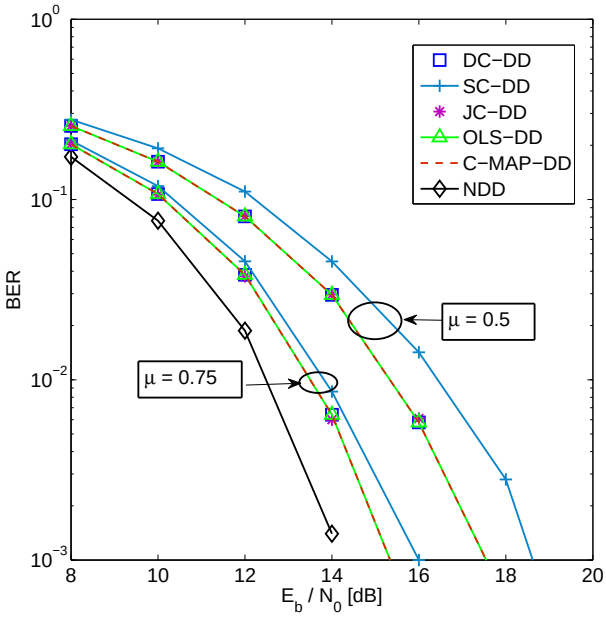

Figure 4.1: BER comparison for different detection methods with $\mathbf{\Phi}_k = \mathbf{\Phi}_{k+1}$ and compression ratio $\mu = 0.5, 0.75$.

4.6 Conclusions

In this paper, the compressive sampling framework has been applied to differentially encoded UWB signals. A joint reconstruction and detection method for the compressed symbol waveforms has been presented, which has been shown to outperform the simpler method based on a separate approach. Direct detection without reconstruction has been evaluated as well, whereas a compressed MAP differential detector has been derived to have a performance benchmark for the proposed detectors. Simulation results confirm that the major advantages we gain are *i*) the reduced sampling rate, *ii*) the ability to carry out the differential detection process in the digital domain, and *iii*) the option of a competitive performance in different scenarios where the measurement matrices are the same as well as different.

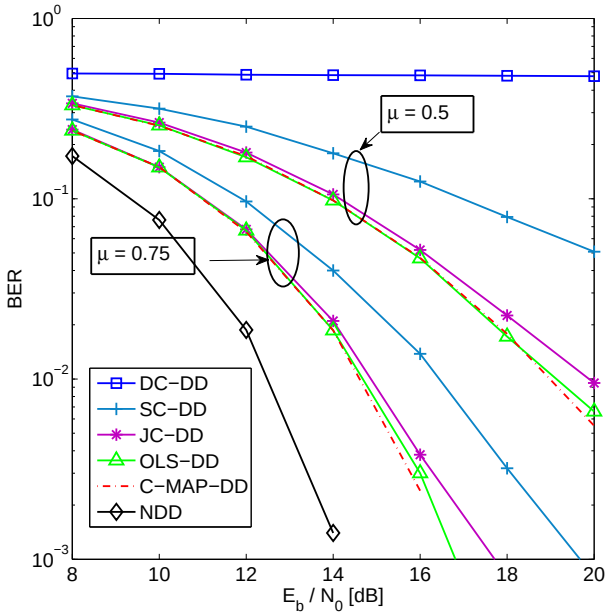

Figure 4.2: BER comparison for different detection methods with $\mathbf{\Phi}_k \neq \mathbf{\Phi}_{k+1}$ and compression ratio $\mu = 0.5, 0.75$.

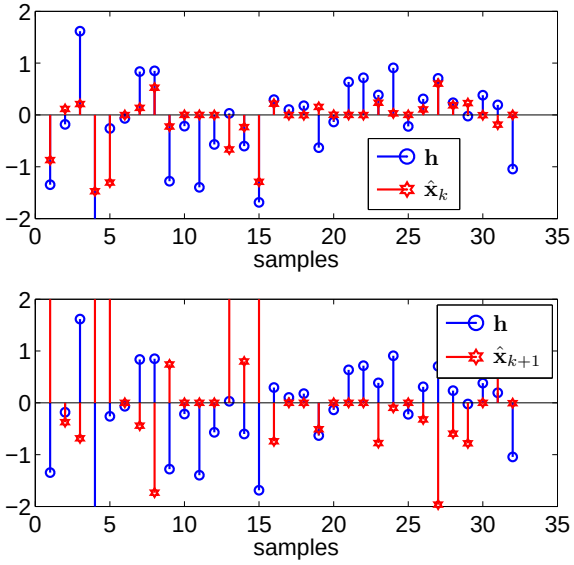

Figure 4.3: Reconstruction results of JC-DD at $10\log_{10}(E_b/N_0) = 20$ dB.

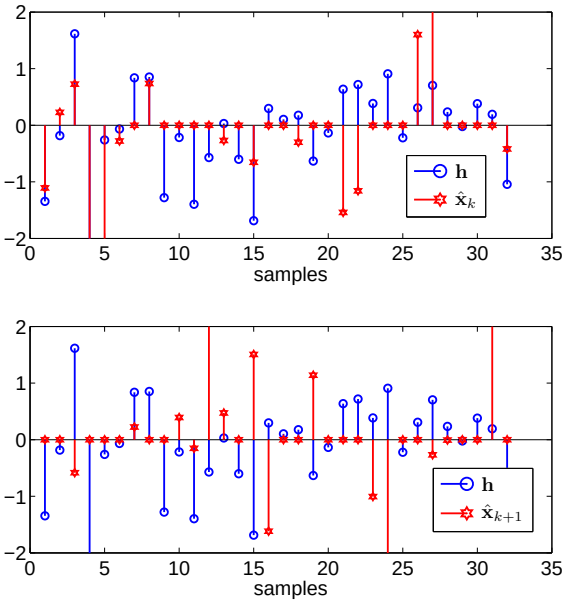

Figure 4.4: Reconstruction results of SC-DD at $10\log_{10}(E_b/N_0) = 20$ dB.

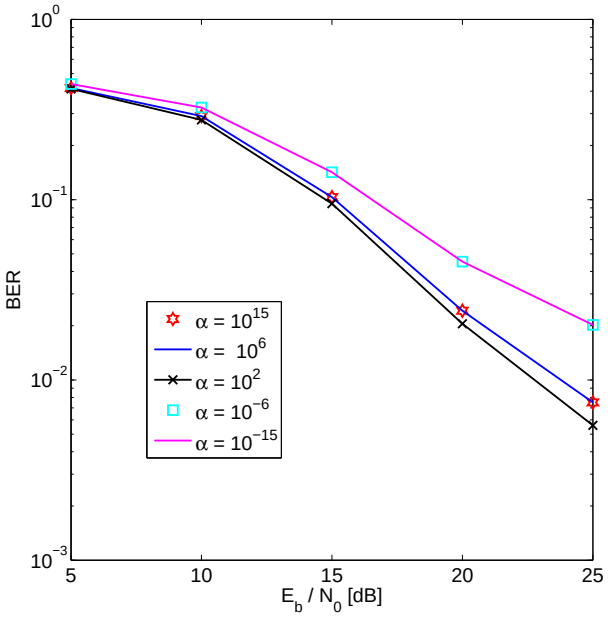

Figure 4.5: BER comparison of JC-DD for different weight coefficients α with $\mathbf{\Phi}_k \neq \mathbf{\Phi}_{k+1}$.

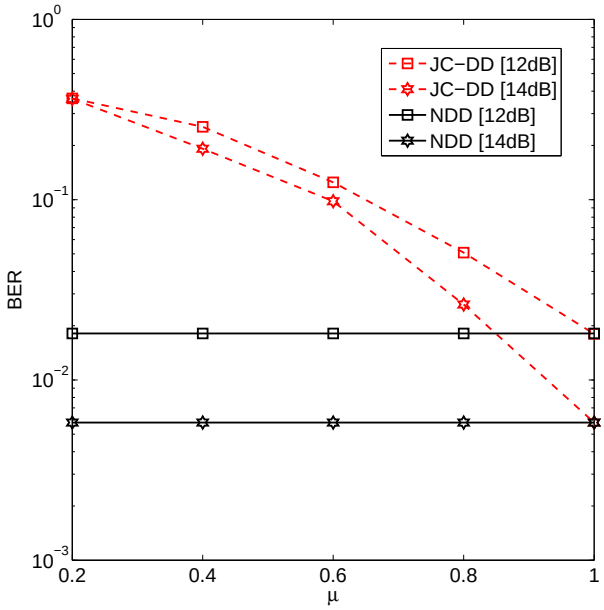

Figure 4.6: BER comparison of JC-DD and NDD for different compression ratios μ with $\mathbf{\Phi}_k \neq \mathbf{\Phi}_{k+1}$.

Appendix

4.A PDF of the Nyquist-rate sampled received signal

In order to evaluate the pdf of the received signal sampled at Nyquist rate, let us start from the result that a Laplacian distributed random variable can be represented as the product between a Rayleigh and a normal one [93]. The extension to the multivariate case allows us to write the channel response as $\mathbf{h} = \rho\mathbf{n}$, where the pdf of ρ is Rayleigh, i.e., $p(\rho) = \rho e^{-\rho^2/2}$, and $\mathbf{n}$ is a zero-mean joint normal random vector with covariance matrix $\mathbf{C_n} = \mathbf{I}_N$. Thus, the signal model for the Nyquist-rate sampled waveform corresponding to two consecutive received symbols can be formulated as

$$\mathbf{r} = (\mathbf{b} \otimes \mathbf{I}_N)\rho\mathbf{n} + \mathbf{v} \tag{4.47}$$

where $\mathbf{v}$ is the joint normal noise component with zero mean and covariance matrix $\mathbf{C_v} = \sigma_v^2\mathbf{I}_{2N}$, statistically independent of both ρ and $\mathbf{n}$. From (4.47), it is apparent that the pdf of $\mathbf{r}$ given $\mathbf{b}$ is expressed by

$$p(\mathbf{r}|\mathbf{b}) = \int_0^\infty p(\mathbf{r}|\mathbf{b},\rho)p(\rho)d\rho \tag{4.48}$$

where $p(\mathbf{r}|\mathbf{b},\rho)$ is the zero-mean joint normal distribution

$$p(\mathbf{r}|\mathbf{b},\rho) = \frac{1}{\pi^{2N}\left|\mathbf{C}_{\mathbf{r}|\mathbf{b},\rho}\right|} e^{-\mathbf{r}^T\mathbf{C}^{-1}_{\mathbf{r}|\mathbf{b},\rho}\mathbf{r}}, \tag{4.49}$$

with covariance matrix

$$\begin{aligned}\mathbf{C}_{\mathbf{r}|\mathbf{b},\rho} &= \mathrm{E}\{[(\mathbf{b}\otimes\mathbf{I}_N)\rho\mathbf{n}+\mathbf{v}]\,[(\mathbf{b}\otimes\mathbf{I}_N)\rho\mathbf{n}+\mathbf{v}]^T\} \\ &= \sigma_v^2\mathbf{I}_{2N} + \rho^2(\mathbf{b}\mathbf{b}^T\otimes\mathbf{I}_N).\end{aligned} \tag{4.50}$$

From the binomial inverse theorem, it can be obtained

$$\begin{aligned}\mathbf{C}^{-1}_{\mathbf{r}|\mathbf{b},\rho} &= \left[\sigma_v^2\mathbf{I}_{2N} + \rho^2(\mathbf{b}\mathbf{b}^T\otimes\mathbf{I}_N)\right]^{-1} \\ &= \left[\sigma_v^2\mathbf{I}_{2N} + \rho^2(\mathbf{b}\otimes\mathbf{I}_N)(\mathbf{b}\otimes\mathbf{I}_N)^T\right]^{-1} \\ &= \frac{1}{\sigma_v^2}\left\{\mathbf{I}_{2N} - \frac{\rho^2}{\sigma_v^2}(\mathbf{b}\otimes\mathbf{I}_N)\left[\mathbf{I}_N + \frac{\rho^2}{\sigma_v^2}(\mathbf{b}\otimes\mathbf{I}_N)^T(\mathbf{b}\otimes\mathbf{I}_N)\right]^{-1}(\mathbf{b}\otimes\mathbf{I}_N)^T\right\}.\end{aligned} \tag{4.51}$$

By exploiting the result

$$(\mathbf{b} \otimes \mathbf{I}_N)^T (\mathbf{b} \otimes \mathbf{I}_N) = 2\mathbf{I}_N, \tag{4.52}$$

(4.51) can be simplified into

$$\mathbf{C}^{-1}_{\mathbf{r}|\mathbf{b},\rho} = \frac{1}{\sigma_v^2}\left[\mathbf{I}_{2N} - \frac{\rho^2}{\sigma_v^2 + 2\rho^2}(\mathbf{b}\mathbf{b}^T \otimes \mathbf{I}_N)\right]. \tag{4.53}$$

Concerning the determinant of $\mathbf{C}_{\mathbf{r}|\mathbf{b},\rho}$, applying the Sylvester theorem yields

$$\begin{aligned}\left|\mathbf{C}_{\mathbf{r}|\mathbf{b},\rho}\right| &= \left|\sigma_v^2 \mathbf{I}_{2N} + \rho^2(\mathbf{b}\mathbf{b}^T \otimes \mathbf{I}_N)\right| \\ &= \sigma_v^{4N}\left|\mathbf{I}_N + \frac{\rho^2}{\sigma_v^2}(\mathbf{b} \otimes \mathbf{I}_N)^T(\mathbf{b} \otimes \mathbf{I}_N)\right| \\ &= \sigma_v^{4N}\left|\mathbf{I}_N + \frac{2\rho^2}{\sigma_v^2}\mathbf{I}_N\right| \\ &= \left(\sigma_v^4 + 2\sigma_v^2\rho^2\right)^N \end{aligned} \tag{4.54}$$

which turns out to be independent of $\mathbf{b}$.

4.B PDF of the compressed-rate sampled received signal

Following the approach of Appendix 4.A, let us consider the signal model corresponding to two consecutive received symbols sampled at compressed rate

$$\mathbf{y} = \mathbf{\Phi}(\mathbf{b} \otimes \mathbf{I}_N)\rho\mathbf{n} + \mathbf{\Phi}\mathbf{v} \tag{4.55}$$

where ρ, $\mathbf{n}$ and $\mathbf{v}$ are defined as in (4.47), and $\mathbf{\Phi}$ as in (4.31). According to (4.55), the pdf of $\mathbf{y}$ given $\mathbf{b}$ can be written as

$$p(\mathbf{y}|\mathbf{b}) = \int_0^\infty p(\mathbf{y}|\mathbf{b},\rho)p(\rho)d\rho \tag{4.56}$$

where $p(\mathbf{y}|\mathbf{b},\rho)$ is the zero-mean joint normal distribution

$$p(\mathbf{y}|\mathbf{b},\rho) = \frac{1}{\pi^{2M}\left|\mathbf{C}_{\mathbf{y}|\mathbf{b},\rho}\right|} e^{-\mathbf{y}^T\mathbf{C}^{-1}_{\mathbf{y}|\mathbf{b},\rho}\mathbf{y}}. \tag{4.57}$$

Taking into account that $\mathbf{\Phi}\mathbf{\Phi}^T = \mathbf{I}_{2M}$, the covariance matrix $\mathbf{C}_{\mathbf{y}|\mathbf{b},\rho}$ results in

$$\begin{aligned}\mathbf{C}_{\mathbf{y}|\mathbf{b},\rho} &= \mathrm{E}\{[\mathbf{\Phi}(\mathbf{b} \otimes \mathbf{I}_N)\rho\mathbf{n} + \mathbf{\Phi}\mathbf{v}]\,[\mathbf{\Phi}(\mathbf{b} \otimes \mathbf{I}_N)\rho\mathbf{n} + \mathbf{\Phi}\mathbf{v}]^T\} \\ &= \sigma_v^2\mathbf{I}_{2M} + \rho^2\mathbf{\Phi}(\mathbf{b}\mathbf{b}^T \otimes \mathbf{I}_N)\mathbf{\Phi}^T \end{aligned} \tag{4.58}$$

whereas its inverse can be computed from the binomial inverse theorem as

$$\begin{aligned}\mathbf{C}_{\mathbf{y}|\mathbf{b},\rho}^{-1} &= \left[\sigma_v^2\mathbf{I}_{2M} + \rho^2\mathbf{\Phi}(\mathbf{b}\mathbf{b}^T \otimes \mathbf{I}_N)\mathbf{\Phi}^T\right]^{-1} \\ &= \frac{1}{\sigma_v^2}\left[\mathbf{I}_{2M} - \frac{\rho^2}{\sigma_v^2}\mathbf{\Phi}(\mathbf{b}\otimes\mathbf{I}_N)\mathbf{\Sigma}^{-1}(\mathbf{b}\otimes\mathbf{I}_N)^T\mathbf{\Phi}^T\right] \quad (4.59)\end{aligned}$$

where

$$\begin{aligned}\mathbf{\Sigma} &\triangleq \mathbf{I}_N + \frac{\rho^2}{\sigma_v^2}(\mathbf{b}\otimes\mathbf{I}_N)^T\mathbf{\Phi}^T\mathbf{\Phi}(\mathbf{b}\otimes\mathbf{I}_N) \\ &= \mathbf{I}_N + \frac{\rho^2}{\sigma_v^2}\left(\mathbf{\Phi}_k^T\mathbf{\Phi}_k + \mathbf{\Phi}_{k+1}^T\mathbf{\Phi}_{k+1}\right). \quad (4.60)\end{aligned}$$

Finally, using the Sylvester theorem, the determinant of $\mathbf{C}_{\mathbf{y}|\mathbf{b},\rho}$ is given by

$$\begin{aligned}\left|\mathbf{C}_{\mathbf{y}|\mathbf{b},\rho}\right| &= \left|\sigma_v^2\mathbf{I}_{2M} + \rho^2\mathbf{\Phi}(\mathbf{b}\mathbf{b}^T\otimes\mathbf{I}_N)\mathbf{\Phi}^T\right| \\ &= \sigma_v^{4M}\left|\mathbf{I}_{2M} + \frac{\rho^2}{\sigma_v^2}\mathbf{\Phi}(\mathbf{b}\otimes\mathbf{I}_N)(\mathbf{b}\otimes\mathbf{I}_N)^T\mathbf{\Phi}^T\right| \\ &= \sigma_v^{4M}\left|\mathbf{I}_N + \frac{\rho^2}{\sigma_v^2}(\mathbf{b}\otimes\mathbf{I}_N)^T\mathbf{\Phi}^T\mathbf{\Phi}(\mathbf{b}\otimes\mathbf{I}_N)\right| \quad (4.61)\end{aligned}$$

or equivalently from (4.60),

$$\left|\mathbf{C}_{\mathbf{y}|\mathbf{b},\rho}\right| = \sigma_v^{4M}\left|\mathbf{I}_N + \frac{\rho^2}{\sigma_v^2}\left(\mathbf{\Phi}_k^T\mathbf{\Phi}_k + \mathbf{\Phi}_{k+1}^T\mathbf{\Phi}_{k+1}\right)\right| \quad (4.62)$$

which is independent of $\mathbf{b}$.

Chapter 5

Compressive Sampling Based Multiple Symbol Differential Detection for UWB Communications

Shahzad Gishkori, Vincenzo Lottici and Geert Leus

Abstract

Compressive sampling (CS) based multiple symbol differential detectors are proposed for impulse-radio ultra-wideband signaling, using the principles of generalized likelihood ratio tests. The CS-based detectors correspond to two communication scenarios. One, where the signaling is fully synchronized at the receiver and the other, where there exists a symbol level synchronization only. With the help of CS, the sampling rates are reduced much below the Nyquist rate to save on the high power consumed by the analog-to-digital converters. In stark contrast to the usual compressive sampling practices, the proposed detectors work on the compressed samples directly, thereby avoiding a complicated reconstruction step and resulting in a reduction of the implementation complexity. To resolve the detection of multiple symbols, compressed sphere decoders are proposed as well, for both communication scenarios, which can further help to reduce the system complexity. Differential detection directly on the compressed symbols is generally marred by the requirement of an identical measurement process for every received symbol. Our proposed detectors are valid for scenarios where the measurement process is the same as well as where it is different for each received symbol.

5.1 Introduction

Promising the prospects of high data rates, fine time resolution, multipath immunity and coexistence with legacy services via frequency overlay, ultra-wideband (UWB) impulse-radios (IRs) are deemed as strong candidates for short-range connectivity, location-aware wireless sensor networks and low-rate communications with ranging capability [8], [94]. Owing to the ultra-large bandwidth, each transmitted pulse arrives at the receiver scattered over hundreds of separable paths with possible severe pulse distortion [48], [95]. Under these harsh propagation conditions, the rich diversity of UWB channels can be exploited by employing detection strategies based on Rake receivers, which however, require a large number of correlator-based fingers combined with accurate channel estimation, thus resulting in an intensive computational load and a high power consumption [72], [78]. Such requirements are contrary to the UWB objectives that call for simple receiver processing units with moderate energy consumption. Therefore, efficient techniques are needed in order to overcome these impediments and facilitate a pervasive deployment of UWB-based networks.

Background and Prior Works. A number of viable yet sub-optimal receivers

based on noncoherent detection have been proposed in the literature for efficient energy capture while avoiding channel estimation [79]. In the transmitted reference (TR) scheme [80], [81], an extra information-free reference pulse is used as a channel template by the correlator to detect the information data, thereby causing wastage of transmitted power and a decrease in data rate. These drawbacks can be avoided by adopting differential detection (DD) [82], [81]. Differentially encoding the information symbols allows employing the signal received within the previous symbol interval as a channel template for detection, thus enabling potentially low-complexity and energy-efficient receivers. However, the template waveform in both TR and DD schemes is neither noise-free nor interference-free, which contributes to a substantial performance degradation. This prompted the use of enhanced DD methods in the form of multiple symbol differential detection (MSDD) [83], [84]. Instead of correlating only the consecutive symbol-long received waveforms, a block of differentially encoded symbols is detected jointly, offering improved performance over both severe multipath fading and interference-limited scenarios. Still, accurate pulse level timing information has to be acquired, which in view of the low-power and ultra-short transmitted pulses, again requires a considerable computational effort; see e.g. [96]-[97]. Hence, a variant of the MSDD scheme has recently been proposed in [85] to reduce the timing restrictions, by limiting the timing accuracy from pulse or frame level to symbol level only, while maintaining a competitive performance.

Despite the considerable advantages offered by the symbol level synchronization (SLS) MSDD, the delay components required by the correlation units (on the order of tens or even hundreds of nanoseconds) lead to hardware implementation issues. Indeed, the long and accurate delay lines are hard to realize in the analog domain, and a digital implementation based on Nyquist rate (NR) sampling can heavily stress the receiver analog-to-digital converter (ADC), thereby causing a high power consumption [98]. In order to facilitate the ADC implementation, some attractive novel theories can be of effective help on reducing the sampling frequency below the cornerstone NR threshold, e.g., those based on sampling at the rate of innovation (SRI) [3], [99] or compressive sampling (CS) [5], [6]. Capitalizing on suitable properties of the signal, like the sparsity exhibited in the time domain by the UWB signals [48], [95], the key idea is to extract a reduced set of compressed samples from the analog received signal, or in other words, converting it into the compressed domain through a few measurements taken in the analog domain; see e.g., [46], [65]. Then, a reconstruction step from the compressed samples may follow by applying one of the algorithms proposed in [6, 99], [15, 30]. Alter-

natively, the reconstruction step is skipped and the receiver processing is based on the compressed samples directly.

The SRI technique is applied in [54], [52] to UWB receivers that work at sub-NR sampling but also require channel estimation (CE). On the other side, the CS framework supports a large variety of sampling kernels, e.g., random sampling, and hence allows for a higher flexibility [5], [6]. Practical applications of CS to the UWB scenario can be found in [60]-[57], mostly again for coherent receivers, thereby requiring CE. Apart from the overhead involved in the transmission of extra information such as pilot or training symbols in these works, one inevitably has to suffer from the complexity load required by the reconstruction of the channel template.

A simpler yet performance competitive implementation, consists of combining the CS framework with noncoherent detection, as illustrated in [100]-[101]. In [100], noncoherent receivers for differentially encoded UWB signals are designed exploiting the CS techniques. Besides introducing a joint reconstruction and detection scheme, a direct compressed DD (DC-DD) is also presented, which skips the reconstruction step, hence reducing the complexity. Building upon the DC-DD, the work in [102] merges the concepts of CS and decision feedback DD (DF-DD) [103]. A power-efficient and low-complexity receiver is enabled, named as CS-based (sorted) DF-DD or csDF-DD in short, however it has to be emphasized that: *i*) its robustness to timing offsets is restricted to only a fraction of the symbol interval and, *ii*) the measurement matrix is required to be the same for all the symbols within each block.

Rationale of the Proposed Approach. The above facts indicate that CS-based noncoherent detection can lead to promising receiver schemes. Hence, the search for an effective way to reduce complexity while preserving performance, fully motivates the current paper to make a further contribution. The basic idea we pursue, in part traced back to [104], is threefold: *i*) instead of considering the DC-DD of a single information symbol as in [100], we cast the concept of MSDD into the CS framework, thus formalizing the CS-based MSDD (CMSDD) scheme at sub-NR sampling; *ii*) in order to relax the demanding prerequisite of sub-pulse level accuracy on the timing synchronization, we develop a modified version of the CMSDD which requires SLS only, in the sequel referred to as SLS-CMSDD; *iii*) aimed at skipping CE, we resort to the generalized likelihood ratio test (GLRT) principle [105] in line with [84] and [85], according to which the generalized log-likelihood metric (GLLM) is maximized not only over the information symbols but also over the unknown channel template. GLRT also helps alleviate the restrictions of the

measurement matrices to be the same for all symbols.
Contributions. The main features of our approach are detailed as follows.

1. The proposed MSDD-like schemes are derived by avoiding the reconstruction step, i.e., they work directly on the compressed signal samples. The result is that the sampling rate as well as the implementation complexity related to the evaluation of the correlation coefficients needed by the objective function, are both kept at affordable levels, in accordance with the UWB requirements.

2. Unlike the CS-based noncoherent receivers illustrated so far, the measurement process can be either the same or different from symbol to symbol, thus offering an additional degree of freedom that can help the receiver better adapt to various scenarios.

3. As briefly touched above, resorting to the SLS concept, the robustness to timing errors of the proposed CS-based schemes is brought from pulse or frame level to symbol level. This feature relaxes the performance of the timing synchronizer, so further lowering the overall receiver complexity.

4. A particular effort is put on cutting back the complexity required to optimize the objective function over each data block for both the ideally-synchronized CMSDD and the SLS-CMSDD, which grows exponentially in the block size[1]. To this end, a modified sphere decoding (SD) algorithm is derived enabling the joint detection of blocks of tens of symbols at polynomial complexity.

5. Comprehensive numerical simulation results obtained over realistic UWB scenarios corroborate our analytical findings and demonstrate that the proposed noncoherent detectors can deliver efficient performance versus complexity trade-offs, and are capable of jointly relaxing the stringent requirements of both the high sampling rate and the accurate timing synchronization.

Organization. The rest of the paper is organized as follows. Section 5.2 describes the signal model. After reviewing the MSDD scheme with ideal timing synchronization, Section 5.3 introduces the CS-based version. Section 5.4 extends the SLS

[1]We recall from [84] that the block size plays a role in determining the performance improvements against the DD scheme, in the sense that the longer the block the better performance.

variant of the MSDD to the CS framework, and Section 5.5 deals with a modified scheme of SD. The simulation results are illustrated in Section 5.6, and finally, in Section 5.7 some concluding remarks are drawn.

5.2 Signal Model

For the UWB-IR signal model, each symbol is represented by N_f frames with one pulse $q(t)$ per frame. The symbol, frame and pulse intervals are designated as T_s, T_f and T_q, respectively, satisfying $T_s = N_f T_f$, $T_q \ll T_f$. Denoting the symbol level waveform[2] as

$$s(t) \triangleq \sum_{j=0}^{N_f-1} q(t - jT_f), \tag{5.1}$$

the transmitted signal corresponding to a block of $Q+1$ consecutive symbols can be written as

$$u(t) = \sum_{k=0}^{Q} b_k s(t - kT_s) \tag{5.2}$$

where $b_k \in \{\pm 1\}$ are the transmitted symbols, which are differentially encoded according to the rule

$$b_k = b_{k-1} a_k \tag{5.3}$$

with $a_k \in \{\pm 1\}$ representing the information-bearing symbols. Without loss of generality, we consider $b_0 = 1$ as initial reference symbol.

The multipath channel is assumed to be time-invariant within an interval of length $(Q+1)T_s$, which is required to transmit (5.2). The delay spread is smaller than T_f such that the overall channel fits within a single frame and hence inter-symbol interference (ISI) is avoided. Under the assumption that the channel impulse response (CIR) has L paths, the received pulse is given by

$$h(t) \triangleq \sum_{\ell=0}^{L-1} \alpha_\ell q(t - \tau_{\ell,0}) \star h_{LP}(t), \tag{5.4}$$

where $h_{LP}(t)$ is the low-pass filter at the receiver with bandwidth W, $\tau_{\ell,0} \triangleq \tau_\ell - \tau$, $0 \le \ell \le L-1$, is the relative delay of the ℓth path with respect to the timing offset

[2] Our focus is on a single-user point-to-point link, so for simplicity of presentation, the time hopping (TH) code is not employed. Such an extension is easy to be included. However, frame averaging may not be possible in this case. Our model can also be extended to the multi-user scenario but it would necessitate a compressed user template to identify a specific user.

$\tau \triangleq \tau_0$ of the first path due to signal propagation, τ_ℓ is the actual delay of the ℓth path at the receiver and α_ℓ is the respective path gain. The symbol level received waveform can thus be expressed as

$$g(t) \triangleq \sum_{j=0}^{N_f-1} h(t - jT_f), \tag{5.5}$$

and correspondingly, after exploiting (5.2) and (5.4)-(5.5), the received signal $r(t)$ is given by

$$r(t) = \underbrace{\sum_{k=0}^{Q} b_k g(t - kT_s - \tau)}_{\triangleq x(t)} + v(t), \tag{5.6}$$

where $x(t)$ is the block level received signal and $v(t)$ is the zero-mean additive white Gaussian noise component with variance σ_v^2.

5.3 MSDD With Exact Timing Synchronization

In this section, we consider the MSDD scheme when exact timing information is available at the receiver, or equivalently, when the timing offset is $\tau = 0$, and accordingly $\tau_{\ell,0} = \tau_\ell$. As a first step, we revisit the MSDD scheme presented in [84] for NR sampled UWB signals and derive it in an algebraic form (which is needed to build mathematical foundations for the compressed version), and denote it for simplicity as NMSDD. Then, we propose the MSDD-based on the CS framework, referred to as CMSDD.

5.3.1 Nyquist-Rate MSDD

Denoting with $1/T \triangleq N/T_f$ the Nyquist sampling rate, the NR received signal (5.6) can be expressed as

$$\mathbf{r} \triangleq [\mathbf{r}_0^T, \mathbf{r}_1^T, \cdots, \mathbf{r}_Q^T]^T \tag{5.7}$$

where $\mathbf{r}_k \triangleq [\mathbf{r}_k^{(0)^T}, \mathbf{r}_k^{(1)^T}, \cdots, \mathbf{r}_k^{(N_f-1)^T}]^T$, with

$$\mathbf{r}_k^{(j)} \triangleq [r(kT_s + jT_f), r(kT_s + jT_f + T), \cdots, r(kT_s + jT_f + NT - T)]^T \tag{5.8}$$

collecting the N NR samples of the jth frame for the kth symbol. Similarly, we can define $\mathbf{x}$, $\mathbf{x}_k$ and $\mathbf{x}_k^{(j)}$ based on $x(t)$, and $\mathbf{v}$, $\mathbf{v}_k$ and $\mathbf{v}_k^{(j)}$ based on $v(t)$. From (5.6), we can then obtain that

$$\mathbf{r}_k = \mathbf{x}_k + \mathbf{v}_k, \quad 0 \leq k \leq Q, \tag{5.9}$$

where $\mathbf{x}_k \triangleq b_k(\mathbf{1}_{N_f \times 1} \otimes \mathbf{h})$ is the signal part of $\mathbf{r}_k$, with

$$\mathbf{h} \triangleq [h(0), h(T), \cdots, h(NT-T)]^T \tag{5.10}$$

made up of the NR samples of the received pulse waveform (5.4). Note that $\mathbf{v}_k$ is a zero-mean Gaussian distributed noise vector with covariance matrix $\mathbf{C}_{\mathbf{v}} \triangleq \mathrm{E}\{\mathbf{v}_k \mathbf{v}_k^T\} = \sigma_v^2 \mathbf{I}_{NN_f}$. Exploiting (5.7) and (5.9), the joint model for the block of $Q+1$ symbols can now be written as

$$\mathbf{r} = (\mathbf{b} \otimes \mathbf{I}_{NN_f})(\mathbf{1}_{N_f \times 1} \otimes \mathbf{h}) + \mathbf{v}, \tag{5.11}$$

where $\mathbf{b} \triangleq [b_0, b_1, \cdots, b_Q]^T$ denotes the transmitted symbols. Hence, after defining the vector of the information symbols as $\mathbf{a} \triangleq [a_1, a_2, \cdots, a_Q]^T$, the NMSDD scheme can be stated as follows.

Proposition 1: NMSDD. The GLRT NMSDD mixed-integer optimization problem (OP) is

$$\hat{\mathbf{a}}^{(\mathrm{NMSDD})} = \arg\max_{\mathbf{a}} \left\{ \max_{\mathbf{h}} \Lambda(\mathbf{r}|\mathbf{a}, \mathbf{h}) \right\}, \tag{5.12}$$

where the GLLM is

$$\Lambda(\mathbf{r}|\mathbf{a}, \mathbf{h}) \triangleq 2N_f \bar{\mathbf{r}}^T (\mathbf{b} \otimes \mathbf{I}_N)\mathbf{h} - (Q+1)N_f \mathbf{h}^T \mathbf{h}, \tag{5.13}$$

with $\bar{\mathbf{r}} \triangleq [\bar{\mathbf{r}}_0^T, \bar{\mathbf{r}}_1^T, \cdots, \bar{\mathbf{r}}_Q^T]^T$ and

$$\bar{\mathbf{r}}_k \triangleq \frac{1}{N_f} \sum_{j=0}^{N_f-1} \mathbf{r}_k^{(j)} \tag{5.14}$$

which represents the $N \times 1$ vector collecting the samples of the average frame for the kth symbol.

Proof. Under the joint NR sampled model (5.11), the GLLM can be written as

$$\begin{aligned}
\Lambda(\mathbf{r}|\mathbf{a}, \mathbf{h}) &\triangleq 2\mathbf{r}^T (\mathbf{b} \otimes \mathbf{I}_{NN_f})(\mathbf{1}_{N_f \times 1} \otimes \mathbf{h}) \\
&\quad - [(\mathbf{b} \otimes \mathbf{I}_{NN_f})(\mathbf{1}_{N_f \times 1} \otimes \mathbf{h})]^T [(\mathbf{b} \otimes \mathbf{I}_{NN_f})(\mathbf{1}_{N_f \times 1} \otimes \mathbf{h})] \\
&= 2\mathbf{r}^T (\mathbf{b} \otimes \mathbf{I}_{NN_f})(\mathbf{1}_{N_f \times 1} \otimes \mathbf{h}) \\
&\quad - (Q+1)(\mathbf{1}_{N_f \times 1} \otimes \mathbf{h})^T (\mathbf{1}_{N_f \times 1} \otimes \mathbf{h}),
\end{aligned} \tag{5.15}$$

which can be further simplified into (5.13). Since $\mathbf{b}$ is a function of $\mathbf{a}$ as described in (5.3), (5.12) can be solved into two steps according to the GLRT principle. First, the GLLM (5.13) is maximized over $\mathbf{h}$ by setting the corresponding gradient to zero, and then, it is optimized over $\mathbf{a}$. ■

5.3.2 Compressive Sampling MSDD

For the CMSDD, we assume that each received frame vector $\mathbf{r}_k^{(j)}$ given by (5.8) is compressed using the $M \times N$ frame level fat measurement matrix $\mathbf{\Phi}_k$ (i.e., $M < N$), such that $\mathbf{\Phi}_k \mathbf{\Phi}_k^T = \mathbf{I}_M$,

$$\mathbf{y}_k^{(j)} \triangleq \mathbf{\Phi}_k \mathbf{r}_k^{(j)}, \quad 0 \leq j \leq N_f - 1. \tag{5.16}$$

Note that the compression ratio $\mu \triangleq \dfrac{M}{N}$, with $0 < \mu \leq 1$, identifies how much one can economize the sampling rate, and accordingly, the computational load of the data detector.

Upon defining $\mathbf{y}_k \triangleq [\mathbf{y}_k^{(0)^T}, \mathbf{y}_k^{(1)^T}, \cdots, \mathbf{y}_k^{(N_f-1)^T}]^T$, the compressed received signal within the kth symbol can then be expressed by the $MN_f \times 1$ vector

$$\mathbf{y}_k = (\mathbf{I}_{N_f} \otimes \mathbf{\Phi}_k)\mathbf{r}_k = (\mathbf{I}_{N_f} \otimes \mathbf{\Phi}_k)\mathbf{x}_k + \boldsymbol{\xi}_k, \quad 0 \leq k \leq Q, \tag{5.17}$$

where $\boldsymbol{\xi}_k \triangleq (\mathbf{I}_{N_f} \otimes \mathbf{\Phi}_k)\mathbf{v}_k$ is the noise component with covariance matrix $\mathbf{C}_{\boldsymbol{\xi}} \triangleq \mathrm{E}\{\boldsymbol{\xi}_k \boldsymbol{\xi}_k^T\} = \sigma_v^2 \mathbf{I}_{MN_f}$. It should be noted that the measurement process in (5.16) is performed in the compressed analog domain; see [46]-[65] for details about possible analog implementations.

Now from (5.17), we can express the joint compressed model for the $Q+1$ symbols as

$$\mathbf{y} = \mathbf{\Psi}(\mathbf{b} \otimes \mathbf{I}_{NN_f})(\mathbf{1}_{N_f \times 1} \otimes \mathbf{h}) + \boldsymbol{\xi} \tag{5.18}$$

where $\mathbf{y} \triangleq [\mathbf{y}_0^T, \mathbf{y}_1^T, \cdots, \mathbf{y}_Q^T]^T$ and $\boldsymbol{\xi} \triangleq [\boldsymbol{\xi}_0^T, \boldsymbol{\xi}_1^T, \cdots, \boldsymbol{\xi}_Q^T]^T$ are the compressed $(M < N)$ $(Q+1)MN_f \times 1$ measurement and noise vectors, respectively, and

$$\mathbf{\Psi} \triangleq \mathrm{diag}\left\{\mathbf{I}_{N_f} \otimes \mathbf{\Phi}_0, \mathbf{I}_{N_f} \otimes \mathbf{\Phi}_1, \cdots, \mathbf{I}_{N_f} \otimes \mathbf{\Phi}_Q\right\} \tag{5.19}$$

is the $(Q+1)MN_f \times (Q+1)NN_f$ block level measurement matrix, such that $\mathbf{\Psi}\mathbf{\Psi}^T = \mathbf{I}_{(Q+1)MN_f}$. Hence, the CMSDD can be formulated as follows.

Proposition 2: CMSDD. The GLRT CMSDD integer OP is

$$\hat{\mathbf{a}}^{(\mathrm{CMSDD})} = \arg\max_{\mathbf{a}} \left\{\Delta(\mathbf{y}|\mathbf{a})\right\}, \tag{5.20}$$

where the objective function is

$$\Delta(\mathbf{y}|\mathbf{a}) = \sum_{k=0}^{Q}\sum_{\ell=0}^{Q} b_k b_\ell \bar{\mathbf{y}}_k^T \mathbf{\Phi}_k \mathbf{\Phi}_\ell^T \bar{\mathbf{y}}_\ell, \tag{5.21}$$

with

$$\bar{\mathbf{y}}_k \triangleq \frac{1}{N_f}\sum_{j=0}^{N_f-1} \mathbf{y}_k^{(j)} \tag{5.22}$$

being the $M \times 1$ vector collecting the samples of the average compressed frame for the kth symbol.

Proof. See Appendix 5.A. ■

A number of remarks about the CMSDD can now be highlighted.

1. If the frame level measurement matrices $\mathbf{\Phi}_k$ are all orthogonal to each other, i.e., $\mathbf{\Phi}_k \mathbf{\Phi}_\ell^T = \mathbf{0}_{M\times M}$, $\forall k, \ell$ with $0 \leq k, \ell \leq Q$, then $\Delta(\mathbf{y}|\mathbf{a})$ does not depend on $\mathbf{a}$, and accordingly the detector does not exist.

2. If the frame level measurement matrices $\mathbf{\Phi}_k$ are all the same for each symbol, i.e., $\mathbf{\Phi}_0 = \mathbf{\Phi}_1 = \cdots = \mathbf{\Phi}_Q$, then taking into account (5.3), $\Delta(\mathbf{y}|\mathbf{a})$ turns into

$$\Delta(\mathbf{y}|\mathbf{a}) = \sum_{k=1}^{Q}\sum_{\ell=0}^{k-1}\prod_{i=1}^{k-\ell} [\mathbf{a}]_{i+\ell} \bar{\mathbf{y}}_k^T \bar{\mathbf{y}}_\ell, \tag{5.23}$$

   whereas in the case they differ from symbol to symbol, $\Delta(\mathbf{y}|\mathbf{a})$ has the general form

$$\Delta(\mathbf{y}|\mathbf{a}) = \sum_{k=1}^{Q}\sum_{\ell=0}^{k-1}\prod_{i=1}^{k-\ell} [\mathbf{a}]_{i+\ell} \bar{\mathbf{y}}_k^T \mathbf{\Phi}_k \mathbf{\Phi}_\ell^T \bar{\mathbf{y}}_\ell. \tag{5.24}$$

3. By virtue of the CS framework, the CMSDD relies on the evaluation of the average frame in (5.22), which is performed for each symbol in the compressed domain. This is less demanding than the implementation of (5.14) based on the NR sampling. As an additional strength, the detection process of the CMSDD avoids a reconstruction step, which further helps in keeping the complexity at an affordable level.

4. Concerning the performance limits of the CMSDD, if the frame level measurement matrices are orthogonal to each other, then the CMSDD does not work, whereas better performance is expected if they are the same for each

symbol. However, for applications where choosing identical measurement matrices is not feasible, the CMSDD can still offer compressed detection.

5. The performance-versus-complexity trade-off enabled by the CMSDD is expected to be governed by the compression ratio μ as well. Indeed, the higher the μ, the lower the performance loss, till the performance approaches that of the NMSDD as $\mu \to 1$. This can be established mathematically by noting that when $\mu = 1$ (i.e., $M = N$) then $\mathbf{\Phi}_k^T \mathbf{\Phi}_k = \mathbf{I}_N$ (which is a general property of orthogonal matrices). Thus,

$$\bar{\mathbf{y}}_k^T \mathbf{\Phi}_k \mathbf{\Phi}_\ell^T \bar{\mathbf{y}}_\ell = (\mathbf{\Phi}_k \bar{\mathbf{r}_k})^T \mathbf{\Phi}_k \mathbf{\Phi}_\ell^T (\mathbf{\Phi}_l \bar{\mathbf{r}_l}) = \bar{\mathbf{r}}_k^T \bar{\mathbf{r}}_\ell$$

and the CMSDD in (5.24) reduces to the NMSDD.

5.4 MSDD with Symbol Level Synchronization

In Section 5.3, we assumed ideal timing synchronization. This assumption means that the receiver can recover an accurate estimate of the timing offset at the pulse level. In this section, we will relax this computationally demanding constraint: first, we re-describe in algebraic form the MSDD scheme with synchronization at symbol level as proposed in [85] using NR sampling, denoted as the SLS-NMSDD in short. Then, we extend the above CMSDD approach to symbol level synchronization, thus formulating the SLS-CMSDD scheme. A coarse symbol level synchronization is thought to be available, so that the timing offset τ is less than a symbol duration, i.e., $\tau \in [0, T_s)$. Furthermore, the observation window is increased to $Q + 1$ symbols in order to accommodate the residual (unknown) timing offset.

The key idea of the MSDD with SLS is to partition the received symbol waveform $g(t)$ given by (5.5) into the two parts $g_0(t)$ and $g_1(t)$, such that

$$g_0(t) \triangleq \begin{cases} 0 & t \in [0, \tau) \\ g(t-\tau) & t \in [\tau, T_s) \end{cases}, \tag{5.25}$$

$$g_1(t) \triangleq \begin{cases} g(t+T_s-\tau) & t \in [0, \tau) \\ 0 & t \in [\tau, T_s) \end{cases}, \tag{5.26}$$

as depicted in Fig. 5.1, for a single frame per symbol, i.e., $N_f = 1$. It is apparent from (5.25) and (5.26) that $g_0(t)$ and $g_1(t)$ depend upon τ and are orthogonal to each other.

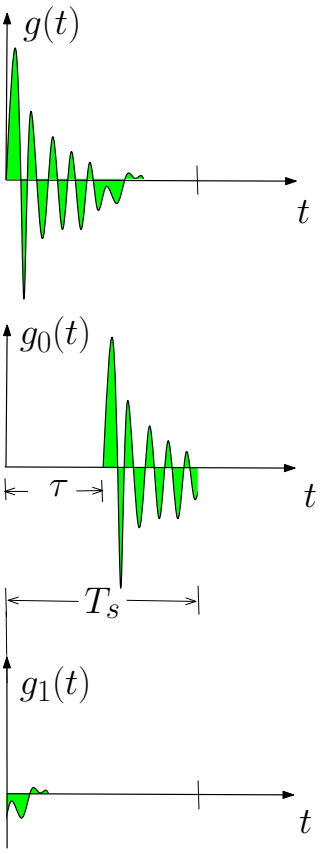

Figure 5.1: Partitioning of $g(t)$ into $g_0(t)$ and $g_1(t)$ for $N_f = 1$, in the presence of a timing offset τ.

5.4.1 Nyquist-rate MSDD with Symbol Level Synchronization

Denoting, $N_\tau \triangleq \lfloor \tau/T \rfloor$ and $\varepsilon \triangleq (\tau - N_\tau T)$, with $\varepsilon \in [0, T)$, the NR sampled symbol level versions of $g_0(t)$ and $g_1(t)$ are given by

$$\mathbf{g}_0 \triangleq [\mathbf{0}^T_{N_\tau \times 1}, g(-\varepsilon), g(T-\varepsilon), \cdots, g(NN_fT - N_\tau T - T - \varepsilon)]^T, \tag{5.27}$$

$$\begin{aligned}\mathbf{g}_1 \triangleq &[g(NN_fT - N_\tau T - \varepsilon), g(NN_fT - N_\tau T + T - \varepsilon), \\ &\cdots, g(NN_fT - T - \varepsilon), \mathbf{0}^T_{(NN_f - N_\tau)\times 1}]^T.\end{aligned} \tag{5.28}$$

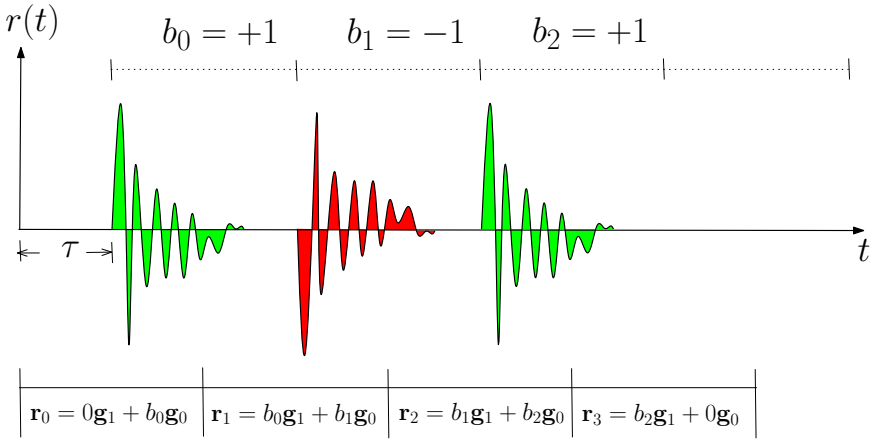

Figure 5.2: SLS model in the noiseless case with $Q = 2$, $N_f = 1$ and timing offset τ.

Thus, the NR sampled version of the kth received symbol waveform can be represented by the $NN_f \times 1$ vector

$$\mathbf{r}_k = b_k\mathbf{g}_0 + b_{k-1}\mathbf{g}_1 + \mathbf{v}_k, \quad 0 \le k \le Q+1, \tag{5.29}$$

where without loss of generality we assume $b_{-1} = b_{Q+1} = 0$. In view of (5.29), the joint SLS NR sampled model for the block of $Q+2$ symbols can be put into the form

$$\mathring{\mathbf{r}} = (\mathbf{b}_0 \otimes \mathbf{I}_{NN_f})\mathbf{g}_0 + (\mathbf{b}_1 \otimes \mathbf{I}_{NN_f})\mathbf{g}_1 + \mathring{\mathbf{v}}, \tag{5.30}$$

where $\mathbf{b}_0 \triangleq [b_0, b_1, \cdots, b_Q, b_{Q+1}]^T$ and $\mathbf{b}_1 \triangleq [b_{-1}, b_0, b_1, \cdots, b_Q]^T$ are the $(Q+2) \times 1$ extended differential symbol vectors, while $\mathring{\mathbf{r}} \triangleq [\mathbf{r}_0^T, \mathbf{r}_1^T, \cdots, \mathbf{r}_{Q+1}^T]^T$ and $\mathring{\mathbf{v}} \triangleq [\mathbf{v}_0^T, \mathbf{v}_1^T, \cdots, \mathbf{v}_{Q+1}^T]^T$. Fig. 5.2 sketches out the SLS model for a simple noiseless example with one frame per symbol ($N_f = 1$). Due to the presence of the residual timing offset $\tau \in [0, T_s)$, in order to detect $Q = 2$ transmitted symbols, $Q+2 = 4$ symbol intervals have to be collected, or equivalently, the sample vectors $\mathbf{r}_0, \mathbf{r}_1, \mathbf{r}_2, \mathbf{r}_3$. Hence, the SLS-NMSDD scheme can be formulated according to the following proposition.

Proposition 3: SLS-NMSDD. The GLRT SLS-NMSDD mixed-integer OP is

$$\hat{\mathbf{a}}^{(\mathrm{SLS-NMSDD})} = \arg\max_{\mathbf{a}} \left\{ \max_{\mathbf{g}_0, \mathbf{g}_1} \Lambda_{\mathrm{SLS}}(\mathring{\mathbf{r}}|\mathbf{a}, \mathbf{g}_0, \mathbf{g}_1) \right\}, \tag{5.31}$$

where the GLLM is

$$\begin{aligned}\Lambda_{\mathrm{SLS}}(\mathring{\mathbf{r}}|\mathbf{a},\mathbf{g}_0,\mathbf{g}_1) \triangleq\ & 2\mathring{\mathbf{r}}^T\left[(\mathbf{b}_0\otimes\mathbf{I}_{NN_f})\mathbf{g}_0+(\mathbf{b}_1\otimes\mathbf{I}_{NN_f})\mathbf{g}_1\right]\\ & -2\mathbf{g}_0^T(\mathbf{b}_0^T\mathbf{b}_1\otimes\mathbf{I}_{NN_f})\mathbf{g}_1\\ & -\left[\mathbf{g}_0^T(\mathbf{b}_0^T\mathbf{b}_0\otimes\mathbf{I}_{NN_f})\mathbf{g}_0+\mathbf{g}_1^T(\mathbf{b}_1^T\mathbf{b}_1\otimes\mathbf{I}_{NN_f})\mathbf{g}_1\right]. \quad (5.32)\end{aligned}$$

Proof. From the joint SLS NR sampled model (5.30), the GLLM can be expressed as

$$\begin{aligned}\Lambda_{\mathrm{SLS}}(\mathring{\mathbf{r}}|\mathbf{a},\mathbf{g}_0,\mathbf{g}_1) = 2\mathring{\mathbf{r}}^T & \left[(\mathbf{b}_0\otimes\mathbf{I}_{NN_f})\mathbf{g}_0+(\mathbf{b}_1\otimes\mathbf{I}_{NN_f})\mathbf{g}_1\right]\\ & -\left[(\mathbf{b}_0\otimes\mathbf{I}_{NN_f})\mathbf{g}_0+(\mathbf{b}_1\otimes\mathbf{I}_{NN_f})\mathbf{g}_1\right]^T\\ & \times\left[(\mathbf{b}_0\otimes\mathbf{I}_{NN_f})\mathbf{g}_0+(\mathbf{b}_1\otimes\mathbf{I}_{NN_f})\mathbf{g}_1\right], \quad (5.33)\end{aligned}$$

which after some algebra gives (5.32). ■

5.4.2 Compressive Sampling MSDD with Symbol Level Synchronization

Bearing in mind the CMSDD and SLS-NMSDD schemes discussed in Section 5.3.2 and Section 5.4.1, respectively, let us now combine the CS and SLS frameworks. Exploiting (5.17) and (5.29), the compressed waveform received within the kth symbol interval reads

$$\mathbf{y}_k = (\mathbf{I}_{N_f}\otimes\mathbf{\Phi}_k)[b_k\mathbf{g}_0+b_{k-1}\mathbf{g}_1]+\boldsymbol{\xi}_k, \quad 0\le k\le Q+1. \quad (5.34)$$

Accordingly, the joint compressed model for the $Q+2$ symbols takes the form

$$\mathring{\mathbf{y}} = \mathring{\mathbf{\Psi}}\left[(\mathbf{b}_0\otimes\mathbf{I}_{NN_f})\mathbf{g}_0+(\mathbf{b}_1\otimes\mathbf{I}_{NN_f})\mathbf{g}_1\right]+\mathring{\boldsymbol{\xi}}, \quad (5.35)$$

where $\mathring{\mathbf{y}} \triangleq [\mathbf{y}_0^T,\mathbf{y}_1^T,\cdots,\mathbf{y}_{Q+1}^T]^T$ and $\mathring{\boldsymbol{\xi}} \triangleq [\boldsymbol{\xi}_0^T,\boldsymbol{\xi}_1^T,\cdots,\boldsymbol{\xi}_{Q+1}^T]^T$ are the extended $(Q+2)MN_f\times 1$ compressed measurement and noise vectors, respectively, and

$$\mathring{\mathbf{\Psi}} \triangleq \mathrm{diag}\left\{\mathbf{I}_{N_f}\otimes\mathbf{\Phi}_0,\mathbf{I}_{N_f}\otimes\mathbf{\Phi}_1,\cdots,\mathbf{I}_{N_f}\otimes\mathbf{\Phi}_{Q+1}\right\} \quad (5.36)$$

is the $(Q+2)MN_f\times(Q+2)NN_f$ extended block level measurement matrix, such that $\mathring{\mathbf{\Psi}}\mathring{\mathbf{\Psi}}^T=\mathbf{I}_{(Q+2)MN_f}$. Thus, based on the joint model (5.35), the MSDD version adopting both SLS and CS can be stated as follows.

Proposition 4: SLS-CMSDD. The GLRT SLS-CMSDD integer OP is

$$\hat{\mathbf{a}}^{(\mathrm{SLS-CMSDD})} = \arg\max_{\mathbf{a}} \left\{ \Delta_{\mathrm{SLS}}(\mathring{\mathbf{y}}|\mathbf{a}) \right\}, \tag{5.37}$$

where the cost function is expressed as

$$\Delta_{\mathrm{SLS}}(\mathring{\mathbf{y}}|\mathbf{a}) \triangleq \sum_{k=0}^{Q} \sum_{\ell=0}^{Q} b_k b_\ell [\mathbf{y}_k^T (\mathbf{I}_{N_f} \otimes \mathbf{\Phi}_k \mathbf{\Phi}_\ell^T) \mathbf{y}_\ell + \mathbf{y}_{k+1}^T (\mathbf{I}_{N_f} \otimes \mathbf{\Phi}_{k+1} \mathbf{\Phi}_{\ell+1}^T) \mathbf{y}_{\ell+1}]. \tag{5.38}$$

Proof. See Appendix 5.B. ■

Some remarks about the SLS-CMSDD scheme are now in order.

1. When the frame level measurement matrices $\mathbf{\Phi}_k$ are all orthogonal to each other, i.e., $\mathbf{\Phi}_k \mathbf{\Phi}_\ell^T = \mathbf{0}_{M \times M}$, $\forall k, \ell$ with $0 \leq k, \ell \leq Q$, the detector again does not exist.

2. When the frame level measurement matrices are the same for all the symbols, i.e., $\mathbf{\Phi}_0 = \mathbf{\Phi}_1 = \cdots = \mathbf{\Phi}_Q$, the cost function (5.38) to be optimized takes the following simpler form

$$\Delta_{\mathrm{SLS}}(\mathring{\mathbf{y}}|\mathbf{a}) = \sum_{k=1}^{Q} \sum_{\ell=0}^{k-1} \prod_{i=1}^{k-\ell} [\mathbf{a}]_{i+\ell} \left(\mathbf{y}_k^T \mathbf{y}_\ell + \mathbf{y}_{k+1}^T \mathbf{y}_{\ell+1} \right), \tag{5.39}$$

   whereas in the case they differ from symbol to symbol its general form is

$$\Delta_{\mathrm{SLS}}(\mathring{\mathbf{y}}|\mathbf{a}) = \sum_{k=1}^{Q} \sum_{\ell=0}^{k-1} \prod_{i=1}^{k-\ell} [\mathbf{a}]_{i+\ell} [\mathbf{y}_k^T (\mathbf{I}_{N_f} \otimes \mathbf{\Phi}_k \mathbf{\Phi}_\ell^T) \mathbf{y}_\ell + \mathbf{y}_{k+1}^T (\mathbf{I}_{N_f} \otimes \mathbf{\Phi}_{k+1} \mathbf{\Phi}_{\ell+1}^T) \mathbf{y}_{\ell+1}]. \tag{5.40}$$

3. Similar to the CMSDD, the SLS-CMSDD shows the advantage of enabling data detection while skipping the reconstruction step, and its performance is basically dictated by the choice on both the measurement matrices and the compression ratio μ.

4. In view of relaxing the demanding constraints not only on the sampling rate but also on the timing synchronization accuracy, it is expected that SLS-CMSDD offers more competitive performance-versus-complexity trade-offs when compared to both the CMSDD and the SLS-NMSDD, which require either a higher timing accuracy or a higher sampling rate, respectively.

5.5 Compressed Sphere Decoder

Despite the major advantages of CMSDD and SLS-CMSDD as noncoherent differential detectors working directly on sub-NR sampled signals, it can be argued from the Propositions 2 and 4 that maximizing the objective functions (5.24) and (5.40) over all the possible realizations of $\mathbf{a}$ involves an exhaustive search that exhibits combinatorial complexity. Accordingly, such a route turns to be quite unfeasible even for short block sizes Q. In order to gain a manageable OP we resort to the SD.

Basics on SD. SD is an effective iterative decoding algorithm originally proposed to efficiently solve the shortest vector problem (SVP) in a lattice [106]-[107], i.e.,

$$\hat{\mathbf{s}}^{(\mathrm{SVP})} = \underset{\mathbf{s}\in\mathbb{Z}^{N\times 1}}{\arg\min}\left\{\|\mathbf{U}\mathbf{s}\|_2\right\}, \tag{5.41}$$

where $\mathbf{U}$ is the $M \times N$ full-rank generator matrix, whereas the lattice is defined as the set of $M \times 1$ vectors $\mathcal{L}(\mathbf{U}) \triangleq \left\{\mathbf{U}\mathbf{s} \,|\, \mathbf{s} \in \mathbb{Z}^{N\times 1}\right\}$. In the SD, only those lattice points are searched iteratively that lie within a sphere of radius ρ centered at $\mathbf{0}_{M\times 1}$, i.e., only the subset of $\hat{\mathbf{s}} \in \mathbb{Z}^{N\times 1}$ satisfying the condition $\|\mathbf{U}\mathbf{s}\|_2 \leq \rho$. Iteration after iteration, ρ is progressively made smaller and smaller, so that the search space is greatly reduced compared with a naive method based on exhaustive search. As a result, the SVP, which is NP hard as shown in [108], can be iteratively solved at low-degree polynomial complexity (cubic or higher) in the length N of the optimal vector to be searched for.

The SD algorithm was proposed for MSDD in [109], for frequency-flat Rayleigh fading channels to improve the performance over DF-DD [110], and successively, was extended to UWB detection in the MSDD scheme proposed in [84]. In the sequel, we will illustrate how to apply the SD framework to the CMSDD and SLS-CMSDD proposed in Section 5.3.2 and Section 5.4.2, respectively, leading thus to the concept of CS-based SD, or CSD for short.

CS based SD. To make our problem SD-compatible, let us reformulate the objective functions in (5.24) and (5.40) in an easy-to-evaluate form. In the case of the CMSDD, the maximum value of the objective function amounts to

$$\Delta_{\mathrm{Max}}(\mathbf{y}|\mathbf{a}) = \sum_{k=1}^{Q}\sum_{\ell=0}^{k-1} |\bar{\mathbf{y}}_k^T \mathbf{\Phi}_k \mathbf{\Phi}_\ell^T \bar{\mathbf{y}}_\ell|, \tag{5.42}$$

and subtracting (5.24) from (5.42) yields an equivalent objective function (to be minimized)

$$\breve{\Delta}(\mathbf{y}|\mathbf{a}) = \sum_{k=1}^{Q}\sum_{\ell=0}^{k-1} |\bar{\mathbf{y}}_k^T \mathbf{\Phi}_k \mathbf{\Phi}_\ell^T \bar{\mathbf{y}}_\ell| \left[1 - \mathrm{sign}\{\bar{\mathbf{y}}_k^T \mathbf{\Phi}_k \mathbf{\Phi}_\ell^T \bar{\mathbf{y}}_\ell\} \prod_{i=1}^{k-\ell} [\mathbf{a}]_{i+\ell}\right], \tag{5.43}$$

where, depending upon the sign of $\prod_{i=1}^{k-\ell}[\mathbf{a}]_{i+\ell}$, each term inside the square brackets takes a value in $\{0, 2\}$. Similarly, in the case of SLS-CMSDD, an equivalent objective function can be defined as

$$\breve{\Delta}_{\mathrm{SLS}}(\mathbf{y}|\mathbf{a}) = \sum_{k=1}^{Q}\sum_{\ell=0}^{k-1} |\mathbf{y}_k^T(\mathbf{I}_{N_f}\otimes\mathbf{\Phi}_k\mathbf{\Phi}_\ell^T)\mathbf{y}_\ell + \mathbf{y}_{k+1}^T(\mathbf{I}_{N_f}\otimes\mathbf{\Phi}_{k+1}\mathbf{\Phi}_{\ell+1}^T)\mathbf{y}_{\ell+1}| \times[1-\mathrm{sign}\{\mathbf{y}_k^T(\mathbf{I}_{N_f}\otimes\mathbf{\Phi}_k\mathbf{\Phi}_\ell^T)\mathbf{y}_\ell + \mathbf{y}_{k+1}^T(\mathbf{I}_{N_f}\otimes\mathbf{\Phi}_{k+1}\mathbf{\Phi}_{\ell+1}^T)\mathbf{y}_{\ell+1}\}\prod_{i=1}^{k-\ell}[\mathbf{a}]_{i+\ell}]. \quad (5.44)$$

For the ease of notation, let us now define

$$Z_{\ell,k} \triangleq \begin{cases} \bar{\mathbf{y}}_k^T\mathbf{\Phi}_k\mathbf{\Phi}_\ell^T\bar{\mathbf{y}}_\ell, & \mathrm{CMSDD} \\ \mathbf{y}_k^T(\mathbf{I}_{N_f}\otimes\mathbf{\Phi}_k\mathbf{\Phi}_\ell^T)\mathbf{y}_\ell + \mathbf{y}_{k+1}^T(\mathbf{I}_{N_f}\otimes\mathbf{\Phi}_{k+1}\mathbf{\Phi}_{\ell+1}^T)\mathbf{y}_{\ell+1}, & \mathrm{SLS-CMSDD} \end{cases} \quad (5.45)$$

Hence, the OP related to the CMSDD or SLS-CMSDD results in the general form

$$\hat{\mathbf{a}}_{\mathrm{opt}} = \arg\min_{\mathbf{a}}\{\Xi(\mathbf{y}|\mathbf{a})\}, \quad (5.46)$$

where

$$\Xi(\mathbf{y}|\mathbf{a}) \triangleq \sum_{k=1}^{Q}\sum_{\ell=0}^{k-1}\eta_{\ell,k}|Z_{\ell,k}|, \quad (5.47)$$

with

$$\eta_{\ell,k} \triangleq \left[1-\mathrm{sign}\{Z_{\ell,k}\}\prod_{i=1}^{k-\ell}[\mathbf{a}]_{i+\ell}\right] \quad (5.48)$$

and $Z_{\ell,k}$ given by (5.45). From (5.46)-(5.48), the following remarks can be obtained: *i*) the objective function (5.47) consists of the sum of the non-negative coefficients $|Z_{\ell,k}|$, weighted by the unknowns $\eta_{\ell,k} \in \{0, 2\}$; *ii*) the partial objective

$$\Xi_j(\mathbf{y}|\mathbf{a}_j) \triangleq \sum_{k=1}^{j}\sum_{\ell=0}^{k-1}\eta_{\ell,k}|Z_{\ell,k}|, \quad 1 \le j \le Q, \quad (5.49)$$

depends only on $\mathbf{a}_j \triangleq [[\mathbf{a}]_1, [\mathbf{a}]_2, \cdots, [\mathbf{a}]_j]^T$ and given $\mathbf{a}_{j-1}$, $\mathbf{a}_j$ depends only on $[\mathbf{a}]_j$; *iii*) in light of features *i*) and *ii*), (5.47) defines a sphere in the Q-dimensional lattice of the vectors $\mathbf{a} \in \{\pm 1\}^Q$ [108]. Therefore, (5.46)-(5.48) combined with remarks *i*)-*iii*) fully comply with the SD framework, and as a consequence our OP

Table 5.1: Pseudo-Code for CS-based SD

Pseudo-Code for CSD
Input: $Z_{\ell,k}$, for $k = 1, \cdots, Q,\ \ \ell = 0, \cdots, k-1$
Initialize: $n = 0$, $\hat{\mathbf{a}}^{(0)} = \hat{\mathbf{a}}^{\mathrm{DC-DD}},\ \ \rho^{(0)} = \Xi(\mathbf{y}\|\hat{\mathbf{a}}^{\mathrm{DC-DD}})$
Repeat
Candidate set for $[\hat{\mathbf{a}}^{(n)}]_1$:
$\mathcal{A}_1^{(n)} = \{[\hat{\mathbf{a}}^{(n)}]_1 \in \{\pm 1\} \| \Xi_1(\mathbf{y}\|\hat{\mathbf{a}}_1^{(n)}) \leq \rho^{(n)}\}$
Choose a tentative estimate of $[\hat{\mathbf{a}}^{(n)}]_1$ from $\mathcal{A}_1^{(n)}$
Candidate set for $[\hat{\mathbf{a}}^{(n)}]_2$ given $[\hat{\mathbf{a}}^{(n)}]_1$:
$\mathcal{A}_2^{(n)} = \{[\hat{\mathbf{a}}^{(n)}]_2 \in \{\pm 1\} \| \Xi_2(\mathbf{y}\|\hat{\mathbf{a}}_2^{(n)}) \leq \rho^{(n)}\}$
Choose a tentative estimate of $[\hat{\mathbf{a}}^{(n)}]_2$ from $\mathcal{A}_2^{(n)}$
$\vdots$
Candidate set for $[\hat{\mathbf{a}}^{(n)}]_Q$ given $[\hat{\mathbf{a}}^{(n)}]_1, \cdots, [\hat{\mathbf{a}}^{(n)}]_{Q-1}$:
$\mathcal{A}_Q^{(n)} = \{[\hat{\mathbf{a}}^{(n)}]_Q \in \{\pm 1\} \| \Xi_Q(\mathbf{y}\|\hat{\mathbf{a}}_Q^{(n)}) \leq \rho^{(n)}\}$
Choose a tentative estimate of $[\hat{\mathbf{a}}^{(n)}]_Q$ from $\mathcal{A}_Q^{(n)}$
$\hat{\mathbf{a}}_{\mathrm{opt}} \leftarrow \hat{\mathbf{a}}^{(n)}$
$\rho^{(n+1)} \leftarrow \Xi_Q(\mathbf{y}\|\hat{\mathbf{a}}^{(n)}) = \Xi(\mathbf{y}\|\hat{\mathbf{a}}_{\mathrm{opt}})$
Set $n = n + 1$
Until $\mathcal{A}_1^{(n)} = \emptyset$
Output: $\hat{\mathbf{a}}_{\mathrm{opt}}$

is amenable to be solved. It is worth mentioning that the above formulation of our objective function is not the same as the conventional SD since it is a nonlinear function of $\mathbf{a}$. Nonetheless, the possibility of estimating an element of $\mathbf{a}$ based on the previously estimated elements in a sequential manner, makes it solvable as an SD problem.

Implementation of CSD. Concerning the implementation of the iterative algorithm, at the generic nth SD iteration, a *necessary condition* for any tentative estimate $\hat{\mathbf{a}}^{(n)}$ to lie inside the sphere of radius $\rho^{(n)} > 0$ is given by

$$\Xi_j(\mathbf{y}\|\hat{\mathbf{a}}_j^{(n)}) \leq \rho^{(n)}, \quad 1 \leq j \leq Q. \tag{5.50}$$

Based on condition (5.50), the CSD can be computationally arranged according to the pseudo-code outlined in Tab. 5.1. We note that the CSD algorithm is initialized

by the solution $\hat{\mathbf{a}}^{\mathrm{DC-DD}}$ obtained by applying the low-complexity DC-DD scheme proposed in [100], which also gives the initial radius $\rho^{(0)}$ by evaluating (5.47). The iterations go on with a smaller and smaller sphere as search space, with the candidate $\hat{\mathbf{a}}_Q^{(n)}$ found at the previous iterations lying on its surface. When at a given iteration, for a certain j, condition (5.50) is satisfied for both values of $[\hat{\mathbf{a}}^{(n)}]_j$, i.e., $\{\pm 1\}$, a random value is taken from the candidate set $\mathcal{A}_j^{(n)}$, and if none of the values satisfies (5.50), j is decreased by 1 and $[\hat{\mathbf{a}}^{(n)}]_{j-1}$ is tried with the other value from the candidate set. Eventually, the algorithm stops when the candidate set $\mathcal{A}_1^{(n)}$ results to be empty, i.e., all the conditions on the candidate sets have been checked without reducing the sphere radius, thus meaning that the objective has safely reached its minimum value. It is worth mentioning that the set of coefficients $Z_{\ell,k}$ can be precomputed before the iterations, or even can be hard-quantized to two levels, and the unknowns $\eta_{\ell,k}$ take non-negative integer-values so checking the Q conditions at each iteration in Tab. 5.1 requires only real or integer format additions combined with logical operations, thus contributing in keeping the complexity at affordable levels in solving the OP (5.46)-(5.48).

5.6 Simulation Results

In this section, the proposed sub-NR MSDD schemes are tested through numerical simulations over realistic multipath environments. In particular, the bit error rate (BER) metric is quantified as a function of either the mean-bit-energy-to-noise-spectral-density ratio defined as $E_b/N_0 \triangleq N_f||\mathbf{h}||_2^2/\sigma_v^2$ or the compression ratio μ, for different values of the block size Q and frame number N_f, with ideal pulse level or coarse symbol level timing synchronization.

5.6.1 Simulation Setup

The transmitted signal consists of a number of bursts including Q consecutive differentially encoded binary symbols according to rule (5.3). In each symbol interval, the frame length is chosen to be $T_f = 50\,\mathrm{ns}$, whereas the transmitted pulse per frame $q(t)$ is selected as the second derivative of a Gaussian shape with width $T_q = 1\mathrm{ns}$. The slow-fading channel is assumed to be time-invariant within each burst, but randomly varying from burst to burst according to the IEEE 802.15.3a CM1 model [95], whose maximum delay spread is $25\,\mathrm{ns}$. The bandwidth of the receive low-pass filter is taken as $W = 2\,\mathrm{GHz}$, and consequently, the NR is $4\,\mathrm{GHz}$., i.e, $N = 200$ samples per frame. Therefore, assuming a compression ratio of μ

means that only $M = \mu N$ samples are employed by the detection algorithm. Further, we consider frame level measurement matrices $\mathbf{\Phi}_k$, $0 \leq k \leq Q$. We initially generate them as having zero-mean equi-distributed Gaussian entries and later orthonormalize the rows. Two different options are considered for compressing each symbol within the burst: *i*) same measurement matrix (SMM), i.e., $\mathbf{\Phi}_k = \mathbf{\Phi}_{k+1}$, $0 \leq k \leq Q-1$; *ii*) different measurement matrix (DMM), i.e., $\mathbf{\Phi}_k \neq \mathbf{\Phi}_{k+1}$, $0 \leq k \leq Q-1$.

5.6.2 BER with Ideal Timing Synchronization

Figs. 5.3 and 5.4 depict the BER metric versus the E_b/N_0 ratio for the SMM and DMM options, respectively, for the compression ratio $\mu = 0.5$, and block sizes $Q = 1, 10, 15$. The number of frames per symbol is set to $N_f = 1$ since for ideal timing synchronization the frame averaging in (5.14) or (5.22) is such that higher values are expected not to affect the performance, as confirmed by Tab. 6.1. For both figures, increasing Q gives reasonably better performance when compared with $Q = 1$, namely the conventional DD, regardless of choosing SMM or DMM. Indeed, at the BER of 10^{-3}, when moving from $Q = 1$ to $Q = 15$ both the NMSDD and CMSDD gain around 4 dB, regardless whether we choose SMM or DMM. Given that the channel stays invariant at least within the block interval, i.e., $(Q+1)N_f T_f$, the above behavior is basically due to the multi-symbol structure of both the algorithms, which advantageously exploit the signal correlation not only between adjacent symbols as the DD does, but also between many other symbols up to the block size apart. Further, in spite of the 2 dB loss suffered by the CMSDD against the NMSDD in case of SMM, the former presents the advantage of halving the sampling rate, thus reducing the computational load required to detect each data burst. It is further to be remarked that changing the setup from SMM to DMM, i.e., passing from Fig. 5.3 to Fig. 5.4, causes the performance of CMSDD to deteriorate by 3 dB. It can be imagined that the limiting case of this scenario will be in line with the first remark made both in Section 5.3.2 and Section 5.4.2, explaining that frame level orthogonal measurement matrices can make the detector independent of the differential symbols, and thus ineffective. Note that for the sake of comparison, we also plot in Fig. 5.3 the results of using sorted block-wise DF-DD (sbDF-DD) [103] and its compressed version CS-based DF-DD (csDF-DD) [102] (both in dotted lines). The results point out that the proposed CSD-based detector has a slight edge over the csDF-DD. Although, both require ideal timing recovery, the latter is further limited to the SMM scenario. On the other side, as quantified in

Section 5.6.3, the SLS-CMSDD is the only scheme that can considerably relax the timing accuracy, thereby enabling good performance-versus-complexity trade-off solutions. However, it is worth mentioning that our proposed schemes, CMSDD and SLS-CMSDD are not restricted to be used only with CSD as an alternative to exhaustive search, but other strategies, e.g., DF can also be opted. Figs. 5.5 and 5.6 show the BER versus the compression ratio μ at $E_b/N_0 = 10\,\text{dB}$, for both the NMSDD and CMSDD, with $Q = 1, 10, 15$, and adopting the SMM and DMM options, respectively. As expected, increasing μ, the CMSDD performance improves till it approaches that of the NMSDD when $\mu = 1$.

5.6.3 BER with Coarse Symbol Level Timing Synchronization

Concerning the SLS-based detectors, we choose $N_f = 10$ frames per symbol since in this configuration the timing offset is acquired with a coarse accuracy at symbol level, and thus, the value of N_f is expected to affect performance (as will be shown in a while). Figs. 5.7 and 5.8 quantify the BER in case the SMM and DMM options are adopted, respectively, with each figure referring to both SLS-NMSDD and SLS-CMSDD schemes, with block sizes $Q = 1, 10, 15$, and compression ratio $\mu = 0.5$. Given that the timing offset of each received burst is uniformly distributed over the symbol interval to comply with the condition of asynchronous access to the channel and in line with the assumption that timing synchronization is performed at symbol level only, the BER curves are averaged over the uniformly distributed timing offset $\tau \in [0.1T_s, 0.9T_s]$. Similar to the NMSDD and CMSDD, it is apparent that the performance of the SLS detectors at both NR and CS sampling improves using a larger block size Q, whereas the DMM incurs again a loss of around 3 dB with respect to the SMM option. It is worth emphasizing that the advantages of the SLS-CMSDD are twofold, in the sense that it can relax the stringent requirements on both the sampling rate and the timing accuracy at an affordable performance loss against the more demanding NMSDD and CMSDD schemes. In addition, similar to Figs. 5.5 and 5.6, it can be proved that as $\mu \to 1$ the SLS-CMSDD and SLS-NMSDD meet at the same BER level. Fig. 5.9 shows the averaged BER for the SLS-NMSDD and SLS-CMSDD, with SMM, $Q = 10$ and different values of the frame number, namely $N_f = 1, 5, 10$. It can be argued that the performance improves when N_f decreases given the corresponding decrease in noise accumulation in the absence of frame averaging.

In Figs. 5.10 and 5.11, we give the complexity performance of CSD against NR SD, for varying SNR and μ, respectively. We define the Complexity metric as

the total number of sum operations consumed during a search (since there are no multiplications in our cost functions). As expected, the CSD has a comparatively higher Complexity but decreases with increasing SNR and/or μ, thereby indicating a trade-off between performance and complexity.

Finally, in Fig. 5.12, we show a BER performance of CMSDD when using different types of samplers (i.e., measurement matrices). Although, we use a Gaussian sub-NR sampler in general but other samplers can also be used. Fig. 5.12 shows the BER performance when the Gaussian, regular and random sub-NR samplers are used, respectively. We see that the Gaussian sampler shows better performance than the regular sub-NR sampler especially at lower values of μ, whereas the random sub-NR sampler lags behind the other two.

5.7 Conclusions

In this paper, we have presented compressive sampling based multiple symbol differential detectors using the GLRT approach, both in the presence of full timing information as well as with symbol-level synchronization only. The detectors avoid an explicit reconstruction step and operate on the compressed samples directly. The detectors perform better when the measurement matrices are the same for each symbol within the block but have the ability to work even when they are different. The detectors do not exist for the case of orthogonal measurement matrices. Combined with sphere decoding, the proposed detectors offer very low complexity and power efficient detection possibilities.

Appendix

5.A Proof of Proposition 2

From the joint compressed model (5.18), the GLLM given $\mathbf{a}$ and $\mathbf{h}$ can be written as

$$\begin{aligned}\Omega(\mathbf{y}|\mathbf{a},\mathbf{h}) \triangleq\ & 2\mathbf{y}^T\boldsymbol{\Psi}(\mathbf{b}\otimes\mathbf{I}_{NN_f})(\mathbf{1}_{N_f\times 1}\otimes\mathbf{h}) \\ & -[(\mathbf{b}\otimes\mathbf{I}_{NN_f})(\mathbf{1}_{N_f\times 1}\otimes\mathbf{h})]^T\boldsymbol{\Psi}^T \\ & \times\boldsymbol{\Psi}[(\mathbf{b}\otimes\mathbf{I}_{NN_f})(\mathbf{1}_{N_f\times 1}\otimes\mathbf{h})],\end{aligned} \tag{5.51}$$

which, in view of the structure of $\mathbf{y}$, can be rearranged as

$$\begin{aligned}\Omega(\mathbf{y}|\mathbf{a},\mathbf{h}) &= 2\mathbf{y}^T\boldsymbol{\Psi}(\mathbf{b}\otimes\mathbf{I}_{NN_f})(\mathbf{1}_{N_f\times 1}\otimes\mathbf{h}) \\ &\quad -(\mathbf{1}_{N_f\times 1}\otimes\mathbf{h})^T(\mathbf{b}\otimes\mathbf{I}_{NN_f})^T\boldsymbol{\Psi}^T\boldsymbol{\Psi}(\mathbf{b}\otimes\mathbf{I}_{NN_f})(\mathbf{1}_{N_f\times 1}\otimes\mathbf{h}) \\ &= 2N_f\bar{\mathbf{y}}^T\boldsymbol{\Phi}(\mathbf{b}\otimes\mathbf{I}_N)\mathbf{h} - N_f\mathbf{h}^T(\mathbf{b}\otimes\mathbf{I}_N)^T\boldsymbol{\Phi}^T\boldsymbol{\Phi}(\mathbf{b}\otimes\mathbf{I}_N)\mathbf{h}\end{aligned} \tag{5.52}$$

where $\boldsymbol{\Phi} \triangleq \text{diag}\,\{\boldsymbol{\Phi}_0,\boldsymbol{\Phi}_1,\cdots,\boldsymbol{\Phi}_Q\}$ is a $(Q+1)M\times(Q+1)N$ block-diagonal matrix, $\bar{\mathbf{y}} \triangleq [\bar{\mathbf{y}}_0^T,\bar{\mathbf{y}}_1^T,\cdots,\bar{\mathbf{y}}_Q^T]^T$, with $\bar{\mathbf{y}}_k$ given by (5.22).

Following the GLRT principle, the first step is to maximize (5.52) over $\mathbf{h}$. Thus, setting the gradient with respect to $\mathbf{h}$ to zero yields

$$2N_f\bar{\mathbf{y}}^T\boldsymbol{\Phi}(\mathbf{b}\otimes\mathbf{I}_N) - 2N_f\mathbf{h}^T[(\mathbf{b}\otimes\mathbf{I}_N)^T\boldsymbol{\Phi}^T\boldsymbol{\Phi}(\mathbf{b}\otimes\mathbf{I}_N)] = \mathbf{0}^T, \tag{5.53}$$

which leads to the estimate

$$\hat{\mathbf{h}} = \mathbf{H}\bar{\mathbf{y}}, \tag{5.54}$$

where

$$\mathbf{H} \triangleq \left[(\mathbf{b}\otimes\mathbf{I}_N)^T\boldsymbol{\Phi}^T\boldsymbol{\Phi}(\mathbf{b}\otimes\mathbf{I}_N)\right]^{-1}\left[\boldsymbol{\Phi}(\mathbf{b}\otimes\mathbf{I}_N)\right]^T. \tag{5.55}$$

Then, after plugging (5.54) into (5.52), we obtain the cost function

$$\begin{aligned}\Gamma(\mathbf{y}|\mathbf{a}) \triangleq\ & 2N_f\bar{\mathbf{y}}^T\boldsymbol{\Phi}(\mathbf{b}\otimes\mathbf{I}_N)\mathbf{H}\bar{\mathbf{y}} \\ & -N_f\left[\mathbf{H}\bar{\mathbf{y}}\right]^T(\mathbf{b}\otimes\mathbf{I}_N)^T\boldsymbol{\Phi}^T\boldsymbol{\Phi}(\mathbf{b}\otimes\mathbf{I}_N)\mathbf{H}\bar{\mathbf{y}}.\end{aligned} \tag{5.56}$$

Considering that

$$\begin{aligned}-N_f\left[\mathbf{H}\bar{\mathbf{y}}\right]^T & (\mathbf{b}\otimes\mathbf{I}_N)^T\boldsymbol{\Phi}^T\boldsymbol{\Phi}(\mathbf{b}\otimes\mathbf{I}_N)\mathbf{H}\bar{\mathbf{y}} \\ &= -N_f\bar{\mathbf{y}}^T\boldsymbol{\Phi}(\mathbf{b}\otimes\mathbf{I}_N)\left[(\mathbf{b}\otimes\mathbf{I}_N)^T\boldsymbol{\Phi}^T\boldsymbol{\Phi}(\mathbf{b}\otimes\mathbf{I}_N)\right]^{-1} \\ &\qquad \times\left[(\mathbf{b}\otimes\mathbf{I}_N)^T\boldsymbol{\Phi}^T\boldsymbol{\Phi}(\mathbf{b}\otimes\mathbf{I}_N)\right]\mathbf{H}\bar{\mathbf{y}} \\ &= -N_f\bar{\mathbf{y}}^T\boldsymbol{\Phi}(\mathbf{b}\otimes\mathbf{I}_N)\mathbf{H}\bar{\mathbf{y}},\end{aligned} \tag{5.57}$$

after some algebra and dropping the immaterial factor N_f, (5.56) can be reformulated as

$$\Gamma[\mathbf{y}|\mathbf{a}] = \bar{\mathbf{y}}^T \mathbf{\Phi}(\mathbf{b} \otimes \mathbf{I}_N)\mathbf{S}^{-1}(\mathbf{b} \otimes \mathbf{I}_N)^T \mathbf{\Phi}^T \bar{\mathbf{y}}, \tag{5.58}$$

where

$$\mathbf{S} \triangleq (\mathbf{b} \otimes \mathbf{I}_N)^T \mathbf{\Phi}^T \mathbf{\Phi}(\mathbf{b} \otimes \mathbf{I}_N) = \sum_{k=0}^{Q} \mathbf{\Phi}_k^T \mathbf{\Phi}_k \tag{5.59}$$

is a positive (semi-)definite matrix[3] depending only on the measurement matrices $\mathbf{\Phi}_k$, $0 \leq k \leq Q$. Intensive numerical simulations have shown that the presence of $\mathbf{S}$ in (5.58) affects the differential detection of $\mathbf{a}$ only in a weak way, i.e., a specific $\hat{\mathbf{a}}$ maximizing (5.58) also (approximately) maximizes

$$\Delta[\mathbf{y}|\mathbf{a}] = \bar{\mathbf{y}}^T \mathbf{\Phi}(\mathbf{b} \otimes \mathbf{I}_N)(\mathbf{b} \otimes \mathbf{I}_N)^T \mathbf{\Phi}^T \bar{\mathbf{y}}. \tag{5.60}$$

Hence, after rearranging (5.60) according to $\bar{\mathbf{y}}$ and $\mathbf{\Phi}$, the objective function of the CMSDD OP takes the form of (5.21), which concludes the proof.

5.B Proof of Proposition 4

From the joint compressed model (5.35), the GLLM given $\mathbf{a}$, $\mathbf{g}_0$ and $\mathbf{g}_1$ for the SLS-CMSDD can be put into the form

$$\begin{aligned}\Omega_{\mathrm{SLS}}(\mathring{\mathbf{y}}|\mathbf{a}, \mathbf{g}_0, \mathbf{g}_1) \triangleq\ & 2\mathring{\mathbf{y}}^T \mathring{\mathbf{\Psi}} \left[(\mathbf{b}_0 \otimes \mathbf{I}_{NN_f})\mathbf{g}_0 + (\mathbf{b}_1 \otimes \mathbf{I}_{NN_f})\mathbf{g}_1\right] \\ & - \left[(\mathbf{b}_0 \otimes \mathbf{I}_{NN_f})\mathbf{g}_0 + (\mathbf{b}_1 \otimes \mathbf{I}_{NN_f})\mathbf{g}_1\right]^T \mathring{\mathbf{\Psi}}^T \\ & \times \mathring{\mathbf{\Psi}} \left[(\mathbf{b}_0 \otimes \mathbf{I}_{NN_f})\mathbf{g}_0 + (\mathbf{b}_1 \otimes \mathbf{I}_{NN_f})\mathbf{g}_1\right]. \end{aligned} \tag{5.61}$$

After some algebra, (5.61) can be rearranged as

$$\begin{aligned}\Omega_{\mathrm{SLS}}(\mathring{\mathbf{y}}|\mathbf{a}, \mathbf{g}_0, \mathbf{g}_1) =\ & 2\mathring{\mathbf{y}}^T \mathring{\mathbf{\Psi}} \left[(\mathbf{b}_0 \otimes \mathbf{I}_{NN_f})\mathbf{g}_0 + (\mathbf{b}_1 \otimes \mathbf{I}_{NN_f})\mathbf{g}_1\right] \\ & - 2\mathbf{g}_0^T (\mathbf{b}_0 \otimes \mathbf{I}_{NN_f})^T \mathring{\mathbf{\Psi}}^T \mathring{\mathbf{\Psi}} (\mathbf{b}_1 \otimes \mathbf{I}_{NN_f})\mathbf{g}_1 \\ & - [\mathbf{g}_0^T (\mathbf{b}_0 \otimes \mathbf{I}_{NN_f})^T \mathring{\mathbf{\Psi}}^T \mathring{\mathbf{\Psi}} (\mathbf{b}_0 \otimes \mathbf{I}_{NN_f})\mathbf{g}_0 \\ & + \mathbf{g}_1^T (\mathbf{b}_1 \otimes \mathbf{I}_{NN_f})^T \mathring{\mathbf{\Psi}}^T \mathring{\mathbf{\Psi}} (\mathbf{b}_1 \otimes \mathbf{I}_{NN_f})\mathbf{g}_1], \end{aligned} \tag{5.62}$$

where $\mathring{\mathbf{y}}$ and $\mathring{\mathbf{\Psi}}$ are the extended measurement vector and block level measurement matrix, respectively, defined in Section 5.4.2. It is worth observing in (5.62) that

$$\mathbf{g}_0^T (\mathbf{b}_0 \otimes \mathbf{I}_{NN_f})^T \mathring{\mathbf{\Psi}}^T \mathring{\mathbf{\Psi}} (\mathbf{b}_1 \otimes \mathbf{I}_{NN_f})\mathbf{g}_1 = \sum_{\ell=1}^{Q} [\mathbf{a}]_\ell \varpi_l, \tag{5.63}$$

[3] As detailed in [100], the positive (semi-)definite property of $\mathbf{S}$ can be easily shown through the eigenvalue decomposition (EVD).

where $\varpi_l \triangleq \mathbf{g}_0^T(\mathbf{I}_{N_f} \otimes \mathbf{\Phi}_\ell^T\mathbf{\Phi}_\ell)\mathbf{g}_1$. Note that due to the orthogonality of $\mathbf{g}_0$ and $\mathbf{g}_1$, ϖ_l will have very few addends[4]. Now given that it is equally probable for a_l to be $+1$ or -1, we can expect that the result can (on the average) be considered as vanishing for a sufficiently large block size Q. Hence, the objective function in (5.62) can be further simplified as

$$\begin{aligned}\Omega_{\mathrm{SLS}}(\mathring{\mathbf{y}}|\mathbf{a},\mathbf{g}_0,\mathbf{g}_1) \simeq 2\mathring{\mathbf{y}}^T\mathring{\mathbf{\Psi}}\left[(\mathbf{b}_0\otimes\mathbf{I}_{NN_f})\mathbf{g}_0+(\mathbf{b}_1\otimes\mathbf{I}_{NN_f})\mathbf{g}_1\right]\\ -[\mathbf{g}_0^T(\mathbf{b}_0\otimes\mathbf{I}_{NN_f})^T\mathring{\mathbf{\Psi}}^T\mathring{\mathbf{\Psi}}(\mathbf{b}_0\otimes\mathbf{I}_{NN_f})\mathbf{g}_0\\ +\mathbf{g}_1^T(\mathbf{b}_1\otimes\mathbf{I}_{NN_f})^T\mathring{\mathbf{\Psi}}^T\mathring{\mathbf{\Psi}}(\mathbf{b}_1\otimes\mathbf{I}_{NN_f})\mathbf{g}_1]. \quad (5.64)\end{aligned}$$

In accordance with the GLRT principle, setting the gradient of (5.64) to zero with respect to $\mathbf{g}_0$ and $\mathbf{g}_1$ gives

$$\hat{\mathbf{g}}_i = \mathbf{G}_i\mathring{\mathbf{y}}, \quad i=0,1, \quad (5.65)$$

where

$$\mathbf{G}_i \triangleq \left[(\mathbf{b}_i\otimes\mathbf{I}_{NN_f})^T\mathring{\mathbf{\Psi}}^T\mathring{\mathbf{\Psi}}(\mathbf{b}_i\otimes\mathbf{I}_{NN_f})\right]^{-1}\left[\mathring{\mathbf{\Psi}}(\mathbf{b}_i\otimes\mathbf{I}_{NN_f})\right]^T, \quad i=0,1. \quad (5.66)$$

Thus, upon plugging (5.65) into (5.64), after some algebra we obtain

$$\begin{aligned}\Gamma_{\mathrm{SLS}}(\mathring{\mathbf{y}}|\mathbf{a}) \triangleq \mathring{\mathbf{y}}^T\mathring{\mathbf{\Psi}}(\mathbf{b}_0\otimes\mathbf{I}_{NN_f})\mathbf{S}_0^{-1}(\mathbf{b}_0\otimes\mathbf{I}_{NN_f})^T\mathring{\mathbf{\Psi}}^T\mathring{\mathbf{y}}\\ +\mathring{\mathbf{y}}^T\mathring{\mathbf{\Psi}}(\mathbf{b}_1\otimes\mathbf{I}_{NN_f})\mathbf{S}_1^{-1}(\mathbf{b}_1\otimes\mathbf{I}_{NN_f})^T\mathring{\mathbf{\Psi}}^T\mathring{\mathbf{y}}, \quad (5.67)\end{aligned}$$

where $\mathbf{S}_0$ and $\mathbf{S}_1$ are defined, respectively, as

$$\mathbf{S}_0 \triangleq (\mathbf{b}_0\otimes\mathbf{I}_{NN_f})^T\mathring{\mathbf{\Psi}}^T\mathring{\mathbf{\Psi}}(\mathbf{b}_0\otimes\mathbf{I}_{NN_f}) = \mathbf{I}_{N_f}\otimes\sum_{k=0}^{Q}\mathbf{\Phi}_k^T\mathbf{\Phi}_k, \quad (5.68)$$

$$\mathbf{S}_1 \triangleq (\mathbf{b}_1\otimes\mathbf{I}_{NN_f})^T\mathring{\mathbf{\Psi}}^T\mathring{\mathbf{\Psi}}(\mathbf{b}_1\otimes\mathbf{I}_{NN_f}) = \mathbf{I}_{N_f}\otimes\sum_{k=1}^{Q+1}\mathbf{\Phi}_k^T\mathbf{\Phi}_k. \quad (5.69)$$

From (5.68)-(5.69), it can be remarked that: *i*) $\mathbf{S}_0$ and $\mathbf{S}_1$ are independent of both $\mathbf{b}_0$ and $\mathbf{b}_1$; *ii*) applying the EVD, it can be proved that $\mathbf{S}_0$ and $\mathbf{S}_1$ are positive (semi-)definite matrices; *iii*) it can be shown that the inverses of $\mathbf{S}_0$ and $\mathbf{S}_1$ affect the

[4]If $\mathbf{\Phi}_l$ are the same, for $l=1,\cdots,Q$, then ϖ_ls would also be the same, and (5.63) will result in a summation over $[\mathbf{a}]_l$s scaled by a constant value. If $\mathbf{\Phi}_l$ are different, for $l=1,\cdots,Q$, then ϖ_ls would produce a scrambling effect over $[\mathbf{a}]_l$s.

Table 5.2: BER performance of CMSDD with varying N_f and $Q = 10$

E_b/N_0 [dB]	$N_f = 1$	$N_f = 5$	$N_f = 10$
4	0.4009	0.4031	0.4038
6	0.3053	0.3074	0.3072
8	0.1558	0.1587	0.1582
10	0.0376	0.0384	0.0365
12	0.0034	0.0032	0.0032

maximization of (5.67) in a weak way (in terms of $\mathbf{a}$). Hence, collecting together the above results, we are left with the approximate cost function

$$\Delta_{\text{SLS}}(\mathring{\mathbf{y}}|\mathbf{a}) \triangleq \mathring{\mathbf{y}}^T \mathring{\mathbf{\Psi}}[(\mathbf{b}_0 \otimes \mathbf{I}_{NN_f})(\mathbf{b}_0 \otimes \mathbf{I}_{NN_f})^T + (\mathbf{b}_1 \otimes \mathbf{I}_{NN_f})(\mathbf{b}_1 \otimes \mathbf{I}_{NN_f})^T]\mathring{\mathbf{\Psi}}^T \mathring{\mathbf{y}}. \quad (5.70)$$

Finally, similar to the approach pursued for the CMSDD, (5.70) can be reformulated in the equivalent form given by (5.38), thus concluding the proof.

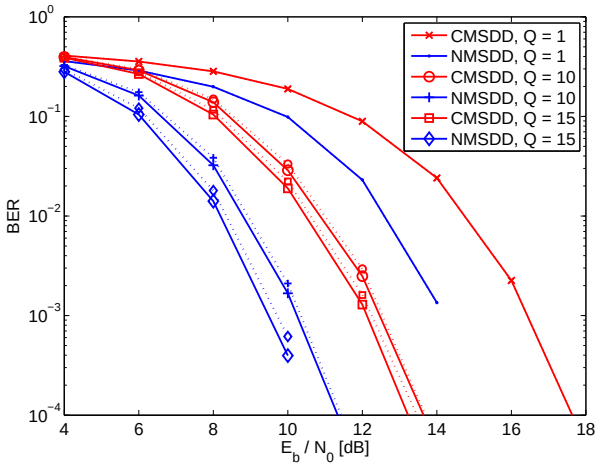

Figure 5.3: BER comparison of NMSDD and CMSDD with SMM, along with sbDF-DD and csDF-DD (dotted lines), different block sizes, $N_f = 1$ and $\mu = 0.5$.

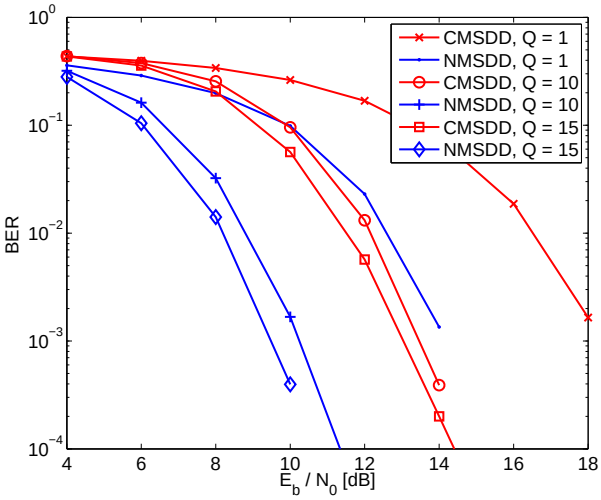

Figure 5.4: BER comparison of NMSDD and CMSDD with DMM, different block sizes, $N_f = 1$ and $\mu = 0.5$.

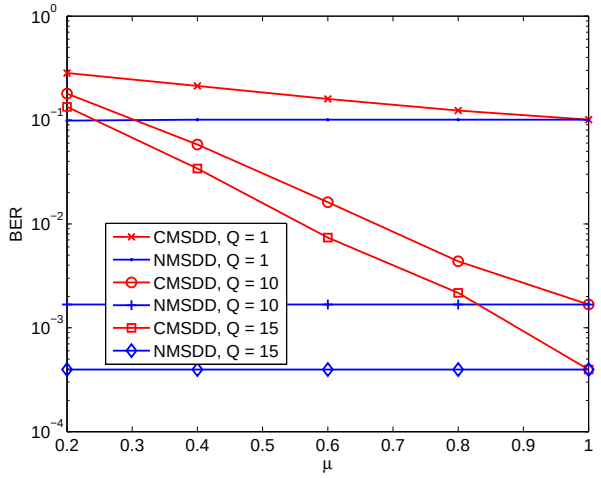

Figure 5.5: BER comparison of NMSDD and CMSDD with SMM, different block sizes, $N_f = 1$, different values of μ and $E_b/N_0 = 10\,\text{dB}$.

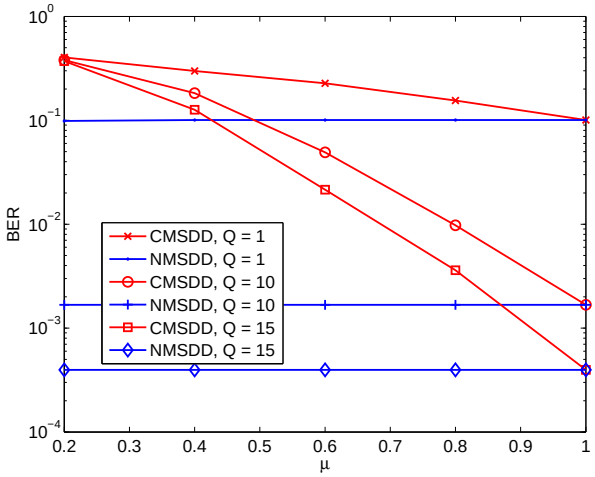

Figure 5.6: BER comparison of NMSDD and CMSDD with DMM, different block sizes, $N_f = 1$, different values of μ and $E_b/N_0 = 10\,\text{dB}$.

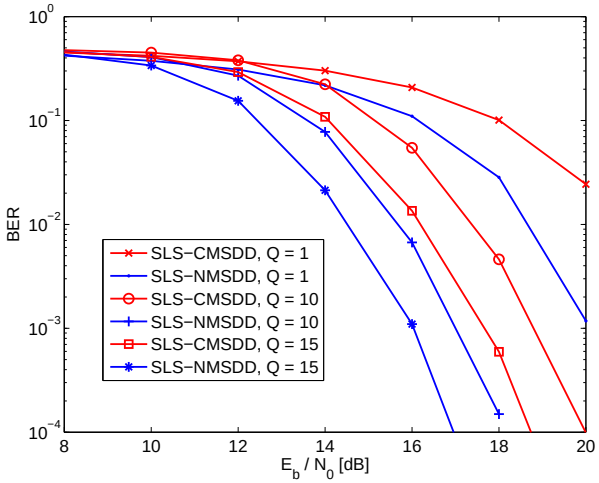

Figure 5.7: BER comparison of SLS-NMSDD and SLS-CMSDD with SMM, different block sizes, $N_f = 10$, $\mu = 0.5$ and $\tau \in [0.1T_s, 0.9T_s]$.

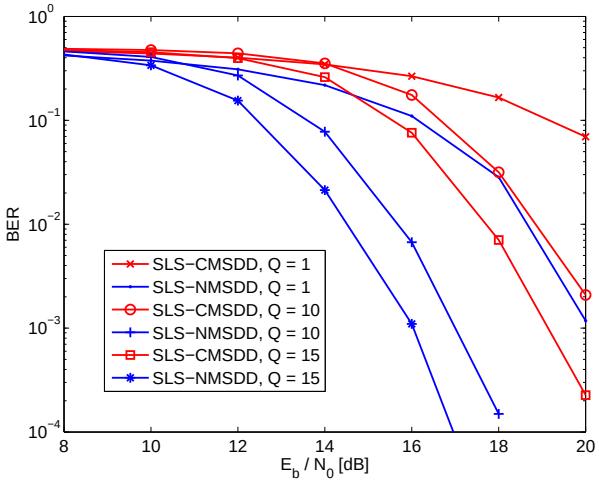

Figure 5.8: BER comparison of SLS-NMSDD and SLS-CMSDD with DMM, different block sizes, $N_f = 10$, $\mu = 0.5$ and $\tau \in [0.1T_s, 0.9T_s]$.

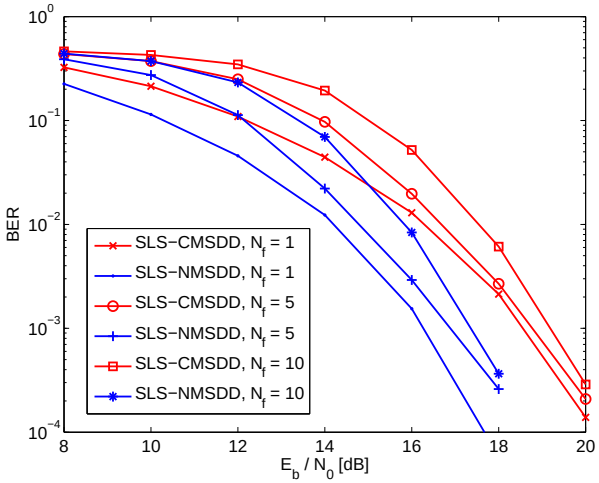

Figure 5.9: BER comparison of SLS-NMSDD and SLS-CMSDD with SMM, $Q = 10$, $\mu = 0.5$, different values of N_f and $\tau \in [0.1T_s, 0.9T_s]$.

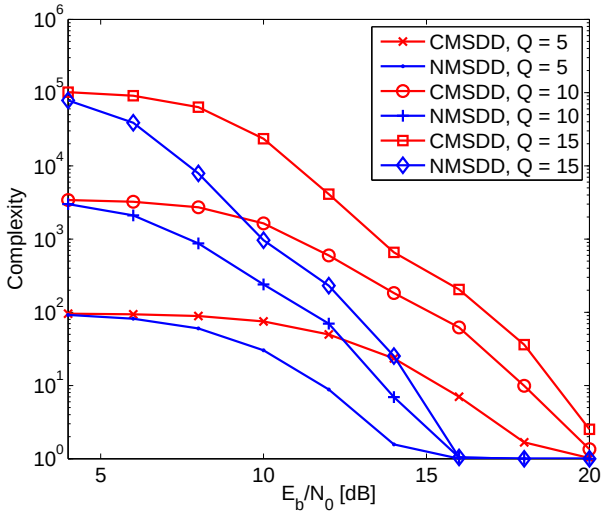

Figure 5.10: Complexity comparison of SD against compressed and Nyquist rate symbols, different block sizes, SMM, $N_f = 1$.

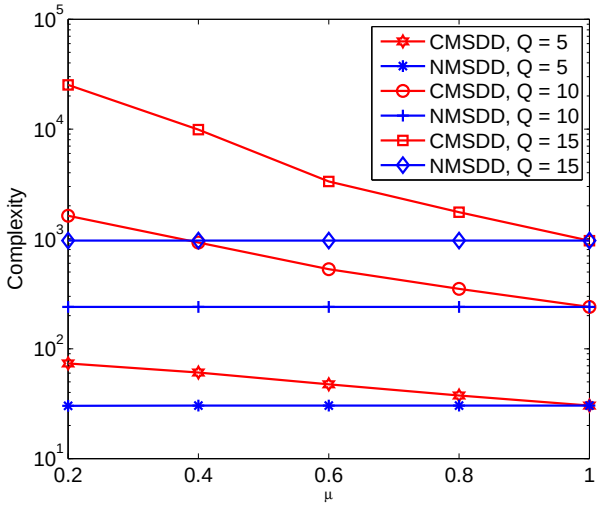

Figure 5.11: Complexity comparison of SD against compressed and Nyquist rate symbols, different block sizes, varying μ, SMM, $E_b/N_0 = 10$dB, $N_f = 1$.

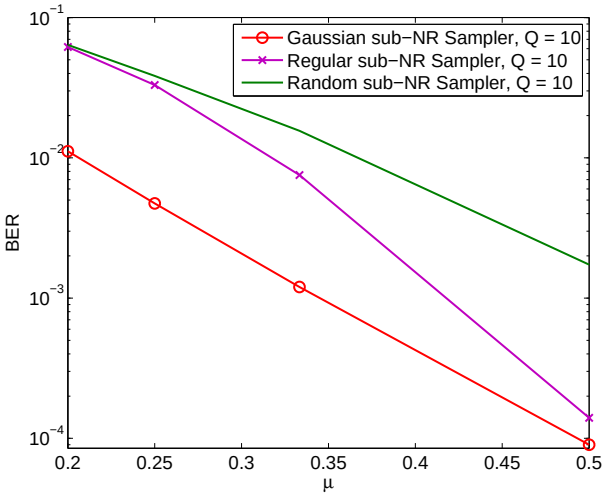

Figure 5.12: BER comparison of CMSDD with Gaussian, regular and random sub-NR sampler, different block sizes, SMM, $N_f = 1$, different values of μ and $E_b/N_0 = 14\,\text{dB}$.

Chapter 6

Compressed Sensing for Block-Sparse Smooth Signals

Shahzad Gishkori and Geert Leus

Abstract

We present reconstruction algorithms for smooth signals with block sparsity from their compressed measurements. We tackle the issue of varying group size via the group-sparse least absolute shrinkage selection operator (LASSO) as well as via latent group LASSO regularizations. We achieve smoothness in the signal via fusion. We develop low-complexity solvers for our proposed formulations through the alternating direction method of multipliers.

6.1 Introduction

Compressed sensing (CS) [5, 6] is one of the most exciting topics of present-day signal processing. Signal reconstruction from its low-dimensional representation becomes a possibility, given the sparse nature of the signal and, incoherence and/or restricted isometry property (RIP) [6] of the sensing/measurement process. In this regard, a number of approaches can be used, e.g., basis pursuit (BP) [15], least absolute shrinkage and selection operator (LASSO) [37] and greedy algorithms [30]. In order to exploit the structure of the signal being sensed, a number of variants of LASSO have become popular, e.g., group LASSO (G-LASSO) [41], sparse group LASSO (SG-LASSO) [42] and fused LASSO (F-LASSO) [44], etc. In this paper we propose new LASSO formulations to handle block sparse smooth signals. Smooth signals are often encountered in a wide range of engineering and biological fields. In engineering, signals observed in image processing, control systems and environment monitoring are often smooth or piece-wise smooth. In biology, a similar structure is observed, e.g., in protein mass spectroscopy [44]. The goal is to recover such structured signals from noisy and/or under-sampled measurements. A related topic is signal smoothing which deals with removing random outliers. Apart from being smooth, such signals can often be represented as sparse in some basis. This sparsity pattern normally varies in terms of the location and block size of the sparse coefficients. The challenge for signal reconstruction is to exploit the block sparsity with varying block sizes, while keeping smoothness intact and using fewer measurements, but all at low complexity. In the CS domain, signal smoothness has been handled by using a fusion constraint in [44]. The fusion is also known as total variation (TV) in the image processing literature. Apart from fusion, [44] also proposes an ℓ_1-norm penalty to cater for signal sparsity. However, since most of the signals are block sparse, [44] cannot give efficient results. To cater for the block sparsity, one can replace the ℓ_1-norm penalty with a group penalty. Although this

approach can handle the block sparsity very well, it only offers fixed group sizes and causes complete groups to be zero or nonzero. To avoid elimination of small sets of nonzero elements, a very small group size is opted but that can make the algorithm inefficient in eliminating large blocks of zero elements. In this regard, we propose to use a moderate group size along with an ℓ_1-norm penalty over the signal, to create sparsity within the groups. Thus by using fusion in combination with an ℓ_1-norm penalty and a moderate group size, a smooth signal can be reconstructed with high accuracy. The problem of varying group sizes can also be handled by using the concept of latent groups, see [111] and references therein. These are basically overlapping groups, with recurring signal elements in possibly multiple groups. Thus, an element lost in one group may resurface through another group after reconstruction. So we also propose to use such latents groups in combination with a fusion constraint to recover block sparse smooth signals with varying block sizes. Note that a work on using overlapping groups over the fusion function instead of the signal structure has appeared in [112], which however requires complete signal samples. Instead, we propose overlapping groups and fusion penalties over the actual signal for under-determined systems. Thus, we exploit the actual structure of the signal rather than the difference of elements. Further, in order to solve the proposed formulations, we derive low-complexity algorithms based on the alternating direction method of multipliers (ADMM) [113]. The reason for using this version of the augmented Lagrangian methods is primarily the non-separability of the fusion penalty in terms of the elements of the signal. Thus, the general convergence properties of ADMM can be used to guarantee optimal results for our proposed algorithms.

6.2 Signal Reconstruction

Let $\mathbf{x}$ be the $N \times 1$ recoverable signal. Given M measurements, the sensed signal can be written as

$$\mathbf{y} = \mathbf{\Phi}\mathbf{x} + \mathbf{v} \tag{6.1}$$

where $\mathbf{y}$ is an $M \times 1$ measurement vector, $\mathbf{\Phi}$ is an $M \times N$ measurement matrix ($M < N$) with compression ratio $\mu \triangleq M/N$ and $\mathbf{v}$ is an $M \times 1$ zero-mean additive white Gaussian noise vector with variance σ_v^2. To recover the signal from the compressed measurements while keeping the signal structure in tact, we propose below, two LASSO formulations.

6.2.1 Sparse Group LASSO with Fusion

Through sparse group fused LASSO (SGF-LASSO), we can resolve the issue of signal smoothness, as well as, that of fixed group sizes. The optimization problem can be formulated as

$$\hat{\mathbf{x}} = \arg\min_{\mathbf{x}} \frac{1}{2}\|\mathbf{y} - \mathbf{\Phi}\mathbf{x}\|_2^2 + \lambda_e \|\mathbf{x}\|_1^1 + \lambda_g \sum_{i=0}^{G-1} \|\mathbf{x}_i\|_2^1 + \lambda_f \sum_{j=1}^{N-1} \|[\mathbf{x}]_j - [\mathbf{x}]_{j-1}\|_1^1 \tag{6.2}$$

where $\mathbf{x}_i$ is an $N/G \times 1$ sub-vector of $\mathbf{x}$, representing one of G groups over the elements of $\mathbf{x}$, i.e., $\mathbf{x} = [\mathbf{x}_0^T, \mathbf{x}_1^T, \cdots, \mathbf{x}_{G-1}^T,]^T$. We can see from (6.2) that $\lambda_g \sum_{i=0}^{G-1} \|\mathbf{x}_i\|_2^1$ accounts for group sparsity, $\lambda_e \|\mathbf{x}\|_1^1$ for element-wise sparsity and $\lambda_f \sum_{j=1}^{N-1} \|[\mathbf{x}]_j - [\mathbf{x}]_{j-1}\|_1^1$ accounts for fusion within the elements of $\mathbf{x}$, such that the effect of each penalty becomes severer with increasing penalty parameters, i.e., λ_g, λ_e and λ_f, respectively. For a moderate value of G, the proposed formulation can tackle the varying group size problem by creating sparsity within the group along with fusing consecutive elements. Note that, for $\lambda_g = \lambda_f = 0$, (6.2) reduces to the standard LASSO problem, for $\lambda_f = 0$, (6.2) reduces to SG-LASSO, for $\lambda_e = \lambda_f = 0$, (6.2) takes the shape of G-LASSO and for $\lambda_g = 0$, (6.2) becomes F-LASSO.

Solver for SGF-LASSO

In order to solve the SGF-LASSO problem via ADMM, we introduce two auxiliary variables $\mathbf{u}$ and $\mathbf{z}$ of size $N \times 1$. Thus, (6.2) can be written as

$$[\hat{\mathbf{x}}, \hat{\mathbf{u}}, \hat{\mathbf{z}}] = \arg\min_{\mathbf{x},\mathbf{u},\mathbf{z}} \frac{1}{2}\|\mathbf{y} - \mathbf{\Phi}\mathbf{x}\|_2^2 + \lambda_e \|\mathbf{u}\|_1^1 + \lambda_g \sum_{i=0}^{G-1} \|\mathbf{u}_i\|_2^1 + \lambda_f \|\mathbf{z}\|_1^1 \quad \text{s.t.} \quad \mathbf{u}_i = \mathbf{x}_i,\ 0 \le i \le G-1,\ \ \mathbf{z} = \mathbf{D}\mathbf{x} \tag{6.3}$$

where $\mathbf{u}_i$ is an $N/G \times 1$ sub-vector of $\mathbf{u}$, i.e., $\mathbf{u} = [\mathbf{u}_0^T, \mathbf{u}_1^T, \cdots, \mathbf{u}_{G-1}^T,]^T$, and $\mathbf{D}$ is the difference matrix with $[\mathbf{D}]_{j,j} = -1$, $[\mathbf{D}]_{j,j+1} = 1$, for $0 \le j \le N-2$ and $[\mathbf{D}]_{N-1,N-1} = 1$, such that $\|\mathbf{D}\mathbf{x}\|_1^1$ equals the element-wise fusion. From (6.3),

the Lagrangian problem can be written as

$$\begin{aligned}\mathcal{L}(\mathbf{x},\mathbf{u},\mathbf{z},\boldsymbol{\rho}_u,\boldsymbol{\rho}_z) =& \frac{1}{2}\|\mathbf{y}-\boldsymbol{\Phi}\mathbf{x}\|_2^2+\lambda_e\|\mathbf{u}\|_1^1 \\ &+\lambda_g\sum_{i=0}^{G-1}\|\mathbf{u}_i\|_2^1+\lambda_f\|\mathbf{z}\|_1^1 \\ &+\sum_{i=0}^{G-1}\boldsymbol{\rho}_{u_i}^T(\mathbf{u}_i-\mathbf{x}_i)+\frac{c_u}{2}\sum_{i=0}^{G-1}\|\mathbf{u}_i-\mathbf{x}_i\|_2^2 \\ &+\boldsymbol{\rho}_z^T(\mathbf{z}-\mathbf{D}\mathbf{x})+\frac{c_z}{2}\|\mathbf{z}-\mathbf{D}\mathbf{x}\|_2^2 \end{aligned} \tag{6.4}$$

where $\boldsymbol{\rho}_u$ (with sub-vectors $\boldsymbol{\rho}_{u_i}$, for $0 \leq i \leq G-1$) and $\boldsymbol{\rho}_z$ are Lagrange multipliers and, c_u and c_z are positive constants. The solution of (6.3) is generated by the following successive approximations

$$\mathbf{x}^{[n]} = \arg\min_{\mathbf{x}} \mathcal{L}\left(\mathbf{x},\mathbf{u}^{[n-1]},\mathbf{z}^{[n-1]},\boldsymbol{\rho}_u^{[n-1]},\boldsymbol{\rho}_z^{[n-1]}\right) \tag{6.5}$$

$$\mathbf{u}^{[n]} = \arg\min_{\mathbf{u}} \mathcal{L}\left(\mathbf{x}^{[n-1]},\mathbf{u},\boldsymbol{\rho}_u^{[n-1]}\right) \tag{6.6}$$

$$\mathbf{z}^{[n]} = \arg\min_{\mathbf{z}} \mathcal{L}\left(\mathbf{x}^{[n-1]},\mathbf{z},\boldsymbol{\rho}_z^{[n-1]}\right) \tag{6.7}$$

and the multipliers are updated as

$$\boldsymbol{\rho}_u^{[n]} = \boldsymbol{\rho}_u^{[n-1]} + c_u(\mathbf{x}^{[n]}-\mathbf{u}^{[n]}) \tag{6.8}$$

$$\boldsymbol{\rho}_z^{[n]} = \boldsymbol{\rho}_z^{[n-1]} + c_z(\mathbf{D}\mathbf{x}^{[n]}-\mathbf{z}^{[n]}). \tag{6.9}$$

The closed-form solution for (6.5) at the nth iteration can be derived to be

$$\begin{aligned}\mathbf{x}^{[n]} =& \left(\boldsymbol{\Phi}^T\boldsymbol{\Phi}+c_z\mathbf{D}^T\mathbf{D}+c_u\mathbf{I}_N\right)^{-1} \\ &\times\left(\boldsymbol{\Phi}^T\mathbf{y}-\mathbf{D}^T\boldsymbol{\rho}_z^{[n-1]}+c_z\mathbf{D}^T\mathbf{z}^{[n-1]}-\boldsymbol{\rho}_u^{[n-1]}+c_u\mathbf{u}^{[n-1]}\right).\end{aligned} \tag{6.10}$$

We can see from (6.10) that the matrix inversion part does not change during the iterations so that it can be performed off-line, resulting in reduced complexity. Note that the matrix inversion lemma can be used to further ease the computations involved in the inversion operation. For $\mathbf{u}$, note that the optimization involves two penalties, i.e., apart from penalizing each element of $\mathbf{u}$ for sparsity, we need to optimize on each of its sub-groups as well. Since both penalties are non-differentiable, we utilize the fact that soft thresholding generates a minimizer for the cost function involving $\lambda_e\|\mathbf{u}_i\|_1^1$ [37], and for the cost function involving $\lambda_g\|\mathbf{u}_i\|_2^1$, the minimizer is $\mathbf{s}_u = \mathbf{u}_i/\|\mathbf{u}_i\|_2^2$ in case $\|\mathbf{u}_i\|_2^2 \neq 0$ and the minimizer is a vector $\mathbf{s}_u$ such

that $\|\mathbf{s}_u\|_2^1 < 1$ in case $\|\mathbf{u}_i\|_2^2 = 0$ [42]. Thus the closed-form solution of (6.6) for the ith subgroup at the nth iteration can be written as

$$\mathbf{u}_i^{[n]} = \left(\|\mathcal{S}\left(\mathbf{x}_i^{[n-1]} + \frac{\boldsymbol{\rho}_{u_i}^{[n-1]}}{c_u}, \frac{\lambda_e}{c_u}\right)\|_2^2 - \frac{\lambda_g}{c_u} \right)_+ \times \frac{\mathcal{S}\left(\mathbf{x}_i^{[n-1]} + \frac{\boldsymbol{\rho}_{u_i}^{[n-1]}}{c_u}, \frac{\lambda_e}{c_u}\right)}{\|\mathcal{S}\left(\mathbf{x}_i^{[n-1]} + \frac{\boldsymbol{\rho}_{u_i}^{[n-1]}}{c_u}, \frac{\lambda_e}{c_u}\right)\|_2^2} \tag{6.11}$$

for $0 \leq i \leq G-1$, where $\mathcal{S}(\mathbf{s}, \lambda) \triangleq \text{sign}(\mathbf{x})(\mathbf{x} - \lambda)_+$ is the soft thresholding operator. Thus the estimate of $\mathbf{u}$ can be obtained as

$$\mathbf{u}^{[n]} = [\mathbf{u}_0^{[n]T}, \mathbf{u}_1^{[n]T}, \cdots, \mathbf{u}_{G-1}^{[n]T}]^T \tag{6.12}$$

which along with $\mathbf{x}^{[n]}$ is used to update $\boldsymbol{\rho}_u^{[n]}$ in (6.8). Now from (6.7), the closed-form expression for the estimate of $\mathbf{z}$ at the nth iteration can be derived as

$$\mathbf{z}^{[n]} = \mathcal{S}\left(\mathbf{D}\mathbf{x}^{[n-1]} + \frac{\boldsymbol{\rho}_z^{[n-1]}}{c_z}, \frac{\lambda_f}{c_z}\right) \tag{6.13}$$

which subsequently updates $\boldsymbol{\rho}_z^{[n]}$ in (6.9).

6.2.2 Latent Group LASSO with Fusion

For the latent group fused LASSO (LGF-LASSO), the signal is segmented into many overlapping groups of certain sizes[1]. In contrast to the disjoints groups, overlapping groups can reselect the elements from other groups. We create $\tilde{G}$ overlapping groups through an $N/G \times N$ sub-selection matrix $\mathbf{W}_i$ which selects N/G rows from an identity matrix $\mathbf{I}_N$. An overlapping group can then be obtained by the relation, $\mathbf{W}_i\mathbf{x}$, for $0 \leq i \leq \tilde{G}-1$, where $\mathbf{W}_i$ is such that $\mathbf{W} \triangleq [\mathbf{W}_0^T, \mathbf{W}_1^T, \cdots, \mathbf{W}_{\tilde{G}}^T]^T$. Each sub-selection matrix $\mathbf{W}_i$ repeats K rows of $\mathbf{W}_{i-1}$, where K is the overlapping factor and $1 \leq K \leq N-1$. Figure 6.1 schematically shows the difference between disjoint ($K = 0$) and overlapping groups (for $K = N/(2G)$). We can see that the overlapping groups can solve the problem of the fixed group size but the price to be paid is in terms of computational complexity which increases excessively with the factor K due to the related increase in $\tilde{G}$. Now, the optimization problem for LGF-LASSO can be formulated as

[1] In this paper, we consider overlapping groups of fixed sizes, but the concept can easily be extended to varying sizes as well.

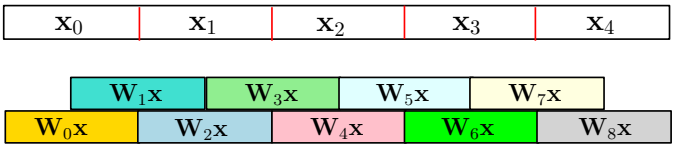

Figure 6.1: *Above*: Disjoint groups. *Below*: Overlapping groups.

$$\hat{\mathbf{x}} = \arg\min_{\mathbf{x}} \frac{1}{2}\|\mathbf{y} - \mathbf{\Phi}\mathbf{x}\|_2^2 + \lambda_g \sum_{i=0}^{\tilde{G}-1} \|\mathbf{W}_i\mathbf{x}\|_2^1 + \lambda_f \|\mathbf{D}\mathbf{x}\|_1^1. \tag{6.14}$$

Solver for LGF-LASSO

To solve the LGF-LASSO problem, we again turn to ADMM. By introducing a new auxiliary variable $\tilde{\mathbf{u}}$ of size $\tilde{G}N/G$, (6.14) can be written as

$$\begin{aligned}[\hat{\mathbf{x}}, \hat{\tilde{\mathbf{u}}}, \hat{\mathbf{z}}] = \arg\min_{\mathbf{x},\tilde{\mathbf{u}},\mathbf{z}} &\frac{1}{2}\|\mathbf{y} - \mathbf{\Phi}\mathbf{x}\|_2^2 + \lambda_g \sum_{i=0}^{\tilde{G}-1} \|\tilde{\mathbf{u}}_i\|_2^1 + \lambda_f \|\mathbf{z}\|_1^1 \\ \text{s.t.} \quad &\tilde{\mathbf{u}}_i = \mathbf{W}_i\mathbf{x},\ 0 \le i \le \tilde{G}-1,\ \ \mathbf{z} = \mathbf{D}\mathbf{x}\end{aligned} \tag{6.15}$$

where $\tilde{\mathbf{u}}_i$ is an $N/G \times 1$ sub-vector of $\tilde{\mathbf{u}}$, i.e., $\tilde{\mathbf{u}} = [\tilde{\mathbf{u}}_0^T, \tilde{\mathbf{u}}_1^T, \cdots, \tilde{\mathbf{u}}_{\tilde{G}-1}^T,]^T$. Now the Lagrangian for (6.15) can be written as

$$\begin{aligned}\mathcal{L}(\mathbf{x}, \tilde{\mathbf{u}}, \mathbf{z}, \boldsymbol{\rho}_{\tilde{u}}, \boldsymbol{\rho}_z) = &\frac{1}{2}\|\mathbf{y} - \mathbf{\Phi}\mathbf{x}\|_2^2 + \lambda_g \sum_{i=0}^{\tilde{G}-1} \|\tilde{\mathbf{u}}_i\|_2^1 + \lambda_f \|\mathbf{z}\|_1^1 \\ &+ \sum_{i=0}^{\tilde{G}-1} \boldsymbol{\rho}_{\tilde{u}_i}^T(\tilde{\mathbf{u}}_i - \mathbf{W}_i\mathbf{x}) + \frac{c_u}{2}\sum_{i=0}^{\tilde{G}-1} \|\tilde{\mathbf{u}}_i - \mathbf{W}_i\mathbf{x}\|_2^2 \\ &+ \boldsymbol{\rho}_z^T(\mathbf{z} - \mathbf{D}\mathbf{x}) + \frac{c_z}{2}\|\mathbf{z} - \mathbf{D}\mathbf{x}\|_2^2\end{aligned} \tag{6.16}$$

where $\boldsymbol{\rho}_{\tilde{u}}$ collects the Lagrangian multipliers with sub-vectors $\boldsymbol{\rho}_{\tilde{u}_i}$ for $0 \le i \le \tilde{G}-1$. Now the successive approximations for the solution of (6.16) w.r.t. $\mathbf{x}$, $\tilde{\mathbf{u}}$ and $\boldsymbol{\rho}_{\tilde{u}}$ can easily be obtained by solving

$$\mathbf{x}^{[n]} = \arg\min_{\mathbf{x}} \mathcal{L}\left(\mathbf{x}, \tilde{\mathbf{u}}^{[n-1]}, \mathbf{z}^{[n-1]}, \boldsymbol{\rho}_{\tilde{u}}^{[n-1]}, \boldsymbol{\rho}_z^{[n-1]}\right) \tag{6.17}$$

$$\tilde{\mathbf{u}}^{[n]} = \arg\min_{\mathbf{u}} \mathcal{L}\left(\mathbf{x}^{[n-1]}, \tilde{\mathbf{u}}, \boldsymbol{\rho}_{\tilde{u}}^{[n-1]}\right) \tag{6.18}$$

$$\boldsymbol{\rho}_{\tilde{u}}^{[n]} = \boldsymbol{\rho}_{\tilde{u}}^{[n-1]} + c_u(\mathbf{x}^{[n]} - \tilde{\mathbf{u}}^{[n]}) \tag{6.19}$$

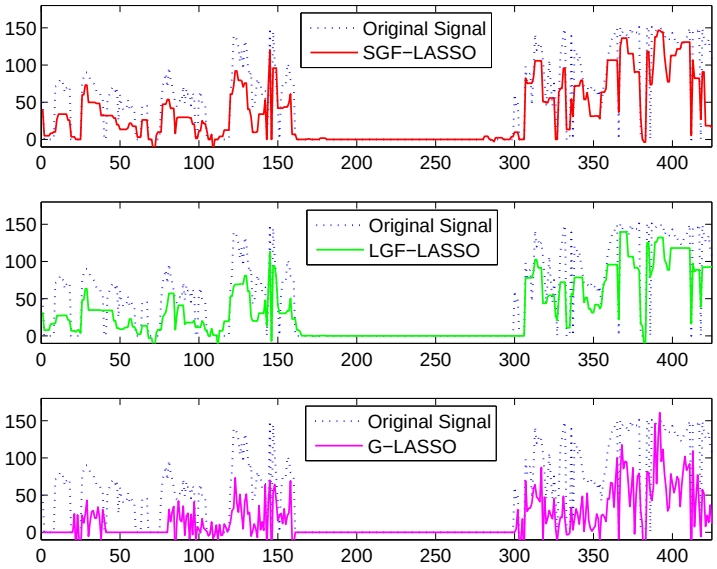

Figure 6.2: Comparison of SGF-LASSO, LGF-LASSO and G-LASSO

whereas, the estimates of $\mathbf{z}$ and $\boldsymbol{\rho}_z$ are the same as in (6.7) and (6.9), respectively.

6.3 Simulations

In this section, we present some simulation results to compare the performance of our proposed algorithms. We compare the performance of SGF-LASSO, LGF-LASSO and G-LASSO. We consider a cloud reflectivity data from the Earth System Research Laboratory (ESRL) [114]. This data basically shows variations in cloud reflectivity over time (around 12 hours) for different cloud heights above ground level (AGL). We consider it to be the ground truth and try to estimate it in the presence of noise of variance $\sigma^2 = 0.25$. There are $N = 425$ reflectivity samples corresponding to each height. We limit ourselves to the data of $N_{CH} = 50$ levels of cloud heights. A signal $\mathbf{x}$ is sensed separately per height, through the same measurement matrix $\boldsymbol{\Phi}$ (where each row may correspond to a sensor), which has been drawn from a zero-mean Gaussian distribution with variance $1/M$. We have further orthogonalized the rows of the measurement matrix $\boldsymbol{\Phi}$.

The penalty parameters for the simulations have been considered as $\lambda_e = 5$, $\lambda_g = 35$ and $\lambda_f = 10$. In general, these parameters can be selected from a given

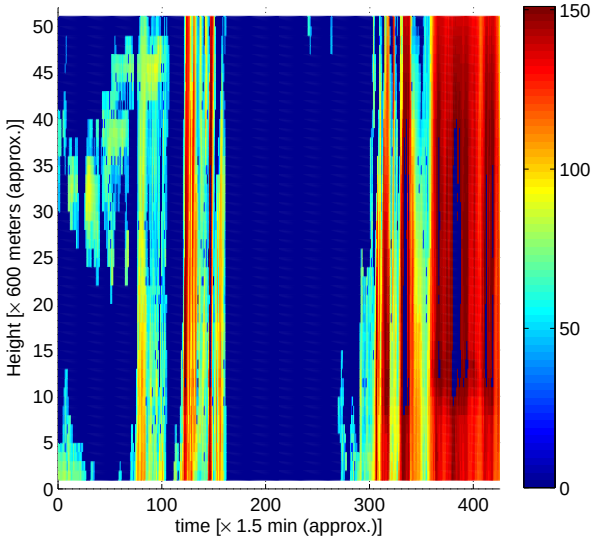

Figure 6.3: Original Signal

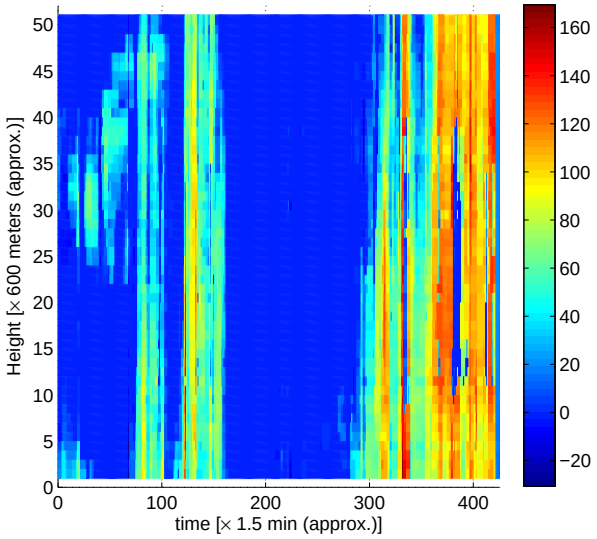

Figure 6.4: Reconstruction by SGF-LASSO

range in a cross-validation manner, by varying one of the parameters and keeping others fixed [42]. Further, since all of these parameters are sparsity promoting, and can possibly affect each other, it is expected that the search of the optimal set of parameters would be restricted to a smaller range. The parameters c_u and c_z are positive numbers and may affect the convergence rate. We take them as $c_u = c_z = 2$. As initial conditions, the vectors $\mathbf{x}^{[0]}$, $\mathbf{u}^{[0]}$, $\mathbf{z}^{[0]}$, $\boldsymbol{\rho}_u^{[0]}$, $\boldsymbol{\rho}_z^{[0]}$, $\tilde{\mathbf{u}}^{[0]}$ and $\boldsymbol{\rho}_{\tilde{u}}^{[0]}$, have all been considered as zero vectors, respectively. Note that, a least-squares solution of $\mathbf{x}$, can also be considered as a warm-start to speed up the convergence rate. The group size for SGF-LASSO, LGF-LASSO and G-LASSO has been taken as 20. Therefore, the number of groups in SGF-LASSO and G-LASSO are the same, i.e. 21 . For LGF-LASSO, an overlapping factor of $K = 5$ has been used, and therefore the number of overlapping groups of size 20 are $\tilde{G} = 28$. We use a maximum of 250 iterations for each algorithm. We have observed that a tolerance level of 10^{-3} between consecutive updates is reached much earlier than this limit, and therefore we stop the algorithm at this stage. Figure 6.2 shows the reconstruction performance of SGF-LASSO, LGF-LASSO and G-LASSO for a particular cloud height, when the signal was sensed with a compression ratio $\mu = 0.5$. We can see that the performance of SGF-LASSO and LGF-LASSO is very close to each other and both are able to recover the smooth transitions of the original signal. On the other hand, the performance of G-LASSO deteriorates both on the front of smoothness as well as block size. Note that in contrast to SGF-LASSO and LGF-LASSO, λ_g is the only sparsity creating parameter for G-LASSO. Therefore, we increase its value to 122.5, which is the minimum to recreate the actual zero blocks. Also in case of SGF-LASSO, we take $\lambda_g = 17.5$ in order to facilitate the parsimonious effect of λ_e. Figures 6.3-6.6 show the reconstruction performance of SGF-LASSO, LGF-LASSO and G-LASSO for the complete range of cloud heights. Again, we can see that the performance of SGF-LASSO and LGF-LASSO is better than G-LASSO and very close to the original. Table 6.1 shows the performance comparison of the proposed algorithms through the mean squared error (MSE) metric against varying compression ratios,

$$\text{MSE} \triangleq \text{E}\{\|\tilde{\mathbf{x}} - \hat{\tilde{\mathbf{x}}}\|_2^2 / N N_{CH}\}$$

where $\tilde{\mathbf{x}}$ is the concatenation of N_{CH} signals $\mathbf{x}$ (i.e., of all cloud heights), and average (E$\{.\}$) is over different noise realizations. We can see that the performance improves in general with increasing value of μ, for $0.1 \leq \mu \leq 0.7$. Nonetheless, the difference in performance follows the previously observed pattern. Note that the performance of LGF-LASSO can be improved by increasing the overlapping factor but that would cause a subsequent increase in the computational complexity.

Table 6.1: MSE comparisons w.r.t. compression ratio

μ	SGF-LASSO	LGF-LASSO	G-LASSO
0.1	0.4607	0.4523	0.4953
0.3	0.2589	0.2607	0.4122
0.5	0.1661	0.1607	0.3079
0.7	0.1250	0.1197	0.2576

6.4 Conclusions

In this paper, we have proposed two new LASSO formulations, namely, sparse group fused LASSO and latent group fused LASSO. The former uses element-wise sparsity, group sparsity (over disjoint groups) and fusion penalties, whereas the latter combines the fusion penalty with a latent group penalty. Both formulations can be used to reconstruct smooth signals from their compressed measurements. We also provide low-complexity solvers for the proposed formulations, based on the alternating direction method of multipliers. We compared the performance of our proposed algorithms with standard group LASSO over a smooth test signal. The simulation results confirm the better performance of the proposed algorithms for signal reconstruction against group LASSO. Similar results were obtained for the mean squared error metric, for varying compression ratios.

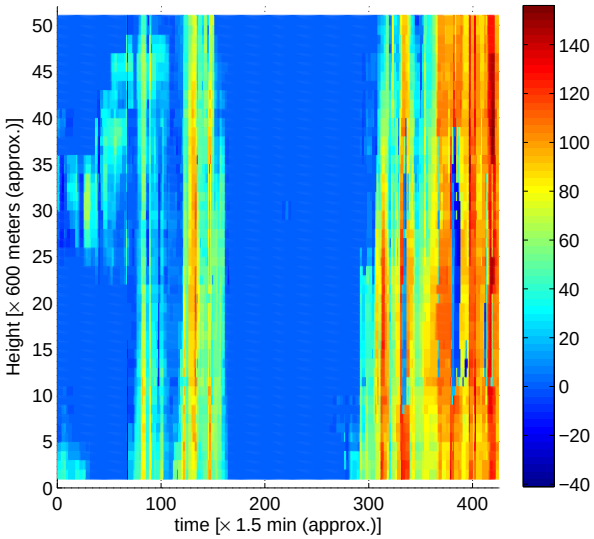

Figure 6.5: Reconstruction by LGF-LASSO

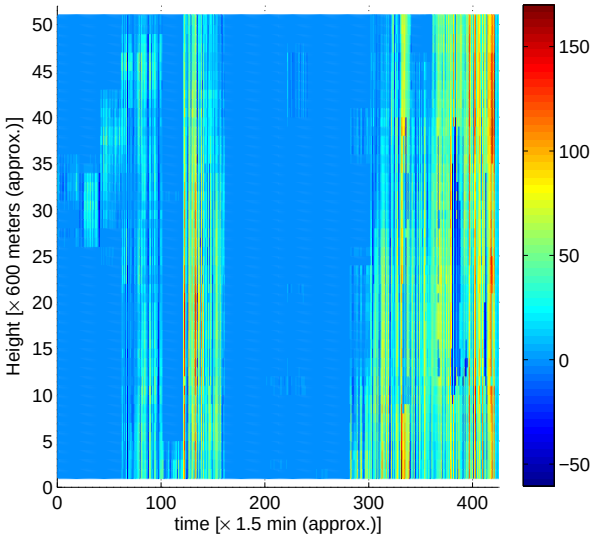

Figure 6.6: Reconstruction by G-LASSO

Chapter 7

Conclusions and Future Work

In this chapter, we provide the conclusive findings of the thesis and also enumerate some suggestions for future work.

7.1 Conclusions

In this thesis, we have shown that compressive sampling (CS) can be applied to ultra-wideband (UWB) signaling to reduce the sampling rate much below the classical Nyquist rate. We have presented practical scenarios in this regard and results have been shown through numerical experiments.

We have proposed CS-based energy detectors for UWB impulse-radio (IR) pulse position modulation (PPM) in different fading environments. We have shown that the principles of generalized maximum likelihood can be used to propose detectors which require the reconstruction of the original signal from the compressed samples and also detectors which skip the reconstruction step and carry out detection on the compressed samples directly. This can help further in reducing the complexity. We have provided exact theoretical expressions for the bit error probability (BEP) to assess the performance of our proposed detectors.

We have also proposed CS-based differential detectors for IR-UWB signals. These detectors work on consecutive symbols. We have developed detectors with separate reconstruction and detection stages as well as detectors that do these steps jointly. We have also proposed detectors which do not need reconstruction at all and can work on the compressed samples directly. However, this can put some limitations on the overall flexibility of the detector in terms of the measurement process.

To assess the performance of these detectors, we have also provided maximum a posteriori (MAP) based detectors.

We have extended the CS-based classical differential detectors to the case of multiple symbol differential detectors. To keep the implementation complexity very low, we work only with the compressed samples. We have used the principle of the generalized likelihood ratio test to eliminate the limitations on such detectors, in terms of the measurement process. Apart from proposing compressed detectors which contain full timing information, we have also proposed detectors which need such information at symbol level only. This effectively resulted in detectors which are low-cost and low-complexity.

Finally, we presented our work on the theoretical aspects of CS. We developed algorithms which exploit the varying block-size sparse structure of the signal with smooth coefficients. In this regard, we basically developed two approaches. In the first approach, we combined group sparsity with element-wise sparsity, along with sparsity in the difference of consecutive elements. This resulted in variable group sizes with smooth reconstructed signal transitions. In the second approach, we used the concept of overlapping groups along with element-wise fusion to reconstruct block sparse smooth signals of varying block sizes. For both approaches, we proposed efficient iterative solvers in the form of the alternating direction method of multipliers.

7.2 Suggestions for Future Work

CS is a very general technique and can have numerous applications. Here, we enlist some major areas for possible future research.

1. UWB signaling offers very fine timing resolution. This aspect makes UWB a favorable choice for localization. Especially in sensor networks, UWB signals can offer centimeter ranging accuracy by using time based positioning techniques, e.g., time-of-arrival and time-difference-of-arrival. Further, since power consumption and implementation complexity are critical factors for sensor nodes, CS-based UWB can be very useful in this regard. CS can be used along with UWB for this application, not only to reduce the sampling rates but also to exploit sparsity within the network. The sparsity within the network is from the perspective that not all the nodes are active at a given point in time, and therefore CS can help in optimizing the number of active sensors as well.

2. A number of publications have appeared recently which exploit higher order statistics of the signal to reduce the sampling rate by a great margin. Estimating the power spectral density of wideband signals is a case in point where signal correlations can be exploited in the compressed domain to build efficient estimators. This approach can be extended to multi-dimensional estimations as well. Such aspects can be explored in the case of UWB in terms of, for example, estimating the delay-Doppler spectrum of time varying UWB channels.

3. CS can be used in climate monitoring, e.g., to estimate the cloud density or the volume of rainfall etc. CS can be extremely helpful in this regard by optimizing the number of sensors required for monitoring and also exploit the unique structures of such signals, e.g., block sparsity and smoothness. Chapter 6 gives a first attempt to tackle such problems.

4. CS can be used for efficient field estimation. A case in point is estimating the spectral field for cognitive radios (CRs). Usual methods for spectral estimation concentrate on CRs individually. The resulting spectral estimates are quite localized and depending upon the signal propagation environment, it is possible that the CRs may not be able to detect a primary user (PU), resulting in what is known as the 'hidden-terminal' problem. Therefore, collaborative sensing mechanisms are necessary. One such technique is to develop a power spectral map over the complete space known as spectrum cartography [115]. A global overview of the spectral state results in better reutilization of the spectral holes and also helps CRs to regulate their transmit power in order to reduce interference with the PUs. However, the challenge is to estimate the field where no sensing mechanism is available. In this case, CS can be used to provide a solution by exploiting the inherent sparsity of the field.

5. CS can greatly assist in the successful implementation of new telecommunication technologies, e.g., massive MIMO. CS can be used here both for channel estimation as well as optimizing the number of active antennas.

6. Seismic exploration is a very expensive field. CS can facilitate efficient and cost effective seismic exploration to utilize sparsity of the signal as well as optimizing the number of scattered monitoring sensors. In this way, sparsity can be exploited both in the temporal and spatial domains.

7. CS can be used in radio astronomy. Normally, the received data is of very high resolution and sensing platforms, e.g., satellites, cannot offer very high

processing power and/or storage capacity, therefore sensing the astronomical information in a compressed manner can save a lot of resources.

8. CS has a great potential in the field of biomedical imaging. An interesting example is that of magnetic resonance imaging (MRI). Normally, a patient has to spend a substantial amount of time in an MRI machine in order to provide an image. Since the images are sparse, CS can greatly help in reducing the acquisition time by reconstructing the complete image with fewer frequency samples.

9. In the field of photographic imaging, advanced cameras generally have a large number of sensors and therefore become quite expensive. CS can help in reducing the number of these sensors which can result in reducing the price of such cameras.

Bibliography

[1] D. Porcino and W. Hirt, "Ultra-wideband radio technology: potential and challenges ahead," *Communications Magazine, IEEE*, vol. 41, no. 7, pp. 66–74, 2003.

[2] B. Le, T. Rondeau, J. Reed, and C. Bostian, "Analog-to-digital converters," *IEEE Signal Processing Magazine*, vol. 22, no. 6, pp. 69–77, Nov. 2005.

[3] M. Vetterli, P. Marziliano, and T. Blu, "Sampling signals with finite rate of innovation," *IEEE Transaction on Signal Processing*, vol. 50, no. 6, pp. 1417–1428, June 2002.

[4] M. Unser, "Sampling-50 years after shannon," *Proceedings of the IEEE*, vol. 88, no. 4, pp. 569–587, Apr 2000.

[5] D. L. Donoho, "Compressed sensing," *IEEE Transactions on Information Theory*, vol. 52, no. 4, April 2006.

[6] E. Candes, J. Romberg, and T. Tao, "Robust uncertainty principles: exact signal reconstruction from highly incomplete frequency information," *IEEE Transactions on Information Theory*, vol. 52, no. 2, pp. 489–509, Feb. 2006.

[7] F. ET Docket 98-153, "Revision of part 15 of the commissions rules regarding ultra-wideband transmission systems," Tech. Rep., 2002.

[8] M. Win and R. Scholtz, "Impulse radio: how it works," *IEEE Communications Letters*, vol. 2, no. 2, pp. 36–38, Feb 1998.

[9] R. Harjani, J. Harvey, and R. Sainati, "Analog/rf physical layer issues for uwb systems," in *VLSI Design, 2004. Proceedings. 17th International Conference on*, 2004, pp. 941–948.

[10] R. Walden, "Analog-to-digital converter survey and analysis," *IEEE Journal on Selected Areas in Communications*, vol. 17, no. 4, pp. 539–550, Apr 1999.

[11] P. Kenington and L. Astier, "Power consumption of a/d converters for software radio applications," *IEEE Transactions on Vehicular Technology*, vol. 49, no. 2, pp. 643–650, Mar 2000.

[12] E. Candes, "Compressive sampling," in *Proceedings of the International Congress of Mathematicians, Madrid, Spain*, 2006.

[13] E. Candes and M. Wakin, "An introduction to compressive sampling," *Signal Processing Magazine, IEEE*, vol. 25, no. 2, pp. 21–30, 2008.

[14] A. M. Bruckstein, D. L. Donoho, and M. Elad, "From sparse solutions of systems of equations to sparse modeling of signals and images," *SIAM Rev.*, vol. 51, no. 1, pp. 34–81, Feb. 2009. [Online]. Available: http://dx.doi.org/10.1137/060657704

[15] S. S. Chen, D. L. Donoho, Michael, and A. Saunders, "Atomic decomposition by basis pursuit," *SIAM Journal on Scientific Computing*, vol. 20, pp. 33–61, 1998.

[16] D. L. Donoho and M. Elad, "Optimally sparse representation in general (non-orthogonal) dictionaries via ℓ_1 minimization," in *Proc. Natl Acad. Sci. USA*, vol. 100, no. 5, 2003, pp. 2197–2202.

[17] J. Kruskal, "Three-way arrays: rank and uniqueness of trilinear decompositions, with application to arithmetic complexity and statistics," *Linear Algebra and Its Applications*, vol. 18, pp. 95–138, 1977.

[18] D. L. Donoho and X. Huo, "Uncertainty principles and ideal atomic decomposition," *IEEE Transactions on Information Theory*, vol. 47, no. 7, pp. 2845–2862, 1999.

[19] E. Candes and J. Romberg, "Sparsity and incoherence in compressive sampling," *Inverse Problems*, vol. 23, no. 3, pp. 969–985, 2007. [Online]. Available: http://stacks.iop.org/0266-5611/23/969

[20] E. Candes and T. Tao, "Decoding by linear programming," *Information Theory, IEEE Transactions on*, vol. 51, no. 12, pp. 4203–4215, 2005.

[21] D. Donoho, M. Elad, and V. Temlyakov, "Stable recovery of sparse overcomplete representations in the presence of noise," *Information Theory, IEEE Transactions on*, vol. 52, no. 1, pp. 6–18, 2006.

[22] F. Santosa and W. W. Symes, "Linear inversion of band-limited reflection seismograms," *SIAM J. Sci. Stat. Comput.*, vol. 7, no. 4, pp. 1307–1330, Oct. 1986. [Online]. Available: http://dx.doi.org/10.1137/0907087

[23] E. Candes, J. Romberg, and T. Tao, "Stable signal recovery from incomplete and inaccurate measurements," *Comm. Pure Appl. Math.*, vol. 59, no. 8, pp. 1207–1223, 2005.

[24] E. Candès and T. Tao, "Near-optimal signal recovery from random projections: Universal encoding strategies?" *Information Theory, IEEE Transactions on*, vol. 52, no. 12, pp. 5406–5425, Dec. 2006.

[25] M. Rudelson and R. Vershynin, "On sparse reconstruction from fourier and gaussian measurements," *Communications on Pure and Applied Mathematics*, vol. 61, pp. 1025–1045, August 2008.

[26] S. Mallat and Z. Zhang, "Matching pursuits with time-frequency dictionaries," *Signal Processing, IEEE Transactions on*, vol. 41, no. 12, pp. 3397–3415, Dec 1993.

[27] G. Davis and M. Avellaneda, "Adaptive greedy approximations," *Journal of Constructive Approximations*, vol. 13, pp. 57–98, 1997.

[28] S. Chen, S. A. Billings, and W. Luo, "Orthogonal least squares methods and their applications to non-linear system identification," *International Journal of Control*, vol. 50, no. 5, pp. 1873–1896, 1989.

[29] Y. C. Pati, R. Rezaiifar, Y. C. P. R. Rezaiifar, and P. S. Krishnaprasad, "Orthogonal matching pursuit: Recursive function approximation with applications to wavelet decomposition," in *Proceedings of the 27 th Annual Asilomar Conference on Signals, Systems, and Computers*, 1993, pp. 40–44.

[30] J. Tropp and A. Gilbert, "Signal recovery from random measurements via orthogonal matching pursuit," *Information Theory, IEEE Transactions on*, vol. 53, no. 12, pp. 4655–4666, Dec. 2007.

[31] G. Karabulut, L. Moura, D. Panario, and A. Yongacoglu, "Integrating flexible tree searches to orthogonal matching pursuit algorithm," *Vision, Image and Signal Processing, IEE Proceedings* -, vol. 153, no. 5, pp. 538–548, Oct. 2006.

[32] D. Needell and J. A. Tropp, "Cosamp: iterative signal recovery from incomplete and inaccurate samples," *Commun. ACM*, vol. 53, no. 12, pp. 93–100, Dec. 2010. [Online]. Available: http://doi.acm.org/10.1145/1859204.1859229

[33] I. Daubechies, M. Defrise, and C. De Mol, "An iterative thresholding algorithm for linear inverse problems with a sparsity constraint," *Communications on Pure and Applied Mathematics*, vol. 57, no. 11, pp. 1413–1457, 2004. [Online]. Available: http://dx.doi.org/10.1002/cpa.20042

[34] D. L. Donoho, A. Maleki, and A. Montanari, "Message-passing algorithms for compressed sensing," *Proceedings of the National Academy of Sciences*, vol. 106, no. 45, pp. 18 914–18 919, 2009. [Online]. Available: http://www.pnas.org/content/106/45/18914.abstract

[35] D. Donoho, A. Maleki, and A. Montanari, "Message passing algorithms for compressed sensing: I. motivation and construction," in *Information Theory Workshop (ITW), 2010 IEEE*, 2010, pp. 1–5.

[36] ——, "Message passing algorithms for compressed sensing: Ii. analysis and validation," in *Information Theory Workshop (ITW), 2010 IEEE*, 2010, pp. 1–5.

[37] R. Tibshirani, "Regression shrinkage and selection via the lasso," *Journal of the Royal Statistical Society, Series B*, vol. 58, pp. 267–288, 1994.

[38] B. Efron, T. Hastie, I. Johnstone, and R. Tibshirani, "Least angle regression," *Annals of Statistics*, vol. 32, pp. 407–499, 2004.

[39] J. Friedman, T. Hastie, H. Hfling, and R. Tibshirani, "Pathwise coordinate optimization," *Annals of Applied Statistics*, vol. 1, pp. 302–332, 2007.

[40] D. Baron, S. Sarvotham, and R. Baraniuk, "Bayesian compressive sensing via belief propagation," *Signal Processing, IEEE Transactions on*, vol. 58, no. 1, pp. 269–280, 2010.

[41] M. Yuan and Y. Lin, "Model selection and estimation in regression with grouped variables," *Journal of the Royal Statistical Society, Series B*, vol. 68, pp. 49–67, 2006.

[42] J. Friedman, T. Hastie, and R. Tibshirani, "A note on the group lasso and a sparse group lasso," Stanford University, Tech. Rep., 2010.

[43] H. Zou and T. Hastie, "Regularization and variable selection via the elastic net," *Journal of the Royal Statistical Society, Series B*, vol. 67, pp. 301–320, 2005.

[44] R. Tibshirani, M. Saunders, S. Rosset, J. Zhu, and K. Knight, "Sparsity and smoothness via the fused lasso," *Journal of the Royal Statistical Society Series B*, pp. 91–108, 2005.

[45] M. Ghavami, L. B. Michael, and R. Kohno, *Ultra Wideband signals and systems in communication engineering*, 2nd ed. West Sussex, England: John Wiley Sons, 2007.

[46] S. Kirolos, J. Laska, M. Wakin, M. Duarte, D. Baron, T. Ragheb, Y. Massoud, and R. Baraniuk, "Analog-to-information conversion via random demodulation," in *Design, Applications, Integration and Software, IEEE Dallas/CAS Workshop*, Oct. 2006, pp. 71–74.

[47] T. Blu, P.-L. Dragotti, M. Vetterli, P. Marziliano, and L. Coulot, "Sparse sampling of signal innovations," *Signal Processing Magazine, IEEE*, vol. 25, no. 2, pp. 31–40, March 2008.

[48] A. Molisch, J. Foerster, and M. Pendergrass, "Channel models for ultrawideband personal area networks," *IEEE Wireless Communications*, vol. 10, no. 6, pp. 14–21, Dec. 2003.

[49] C. Carbonelli and U. Mengali, "M-ppm noncoherent receivers for uwb applications," *Wireless Communications, IEEE Transactions*, vol. 5, no. 8, pp. 2285–2294, Aug. 2006.

[50] S. Dubouloz, B. Denis, S. De Rivaz, and L. Ouvry, "Performance analysis of ldr uwb non-coherent receivers in multipath environments," in *Ultra-Wideband, 2005. ICU 2005. 2005 IEEE International Conference on*, 2005, pp. 6 pp.–.

[51] Y. Souilmi and R. Knopp, "On the achievable rates of ultra-wideband ppm with non-coherent detection in multipath environments," in *Communications, 2003. ICC '03. IEEE International Conference on*, vol. 5, 2003, pp. 3530–3534 vol.5.

[52] Y. Vanderperren, G. Leus, and W. Dehaene, "Performance analysis of a flexible subsampling receiver for pulsed uwb signals," *Wireless Communications, IEEE Transactions on*, vol. 8, no. 8, pp. 4134–4142, 2009.

[53] J. Kusuma, A. Ridolfi, and M. Vetterli, "Sampling of communication systems with bandwidth expansion," in *Communications, 2002. ICC 2002. IEEE International Conference on*, vol. 3, 2002, pp. 1601–1605 vol.3.

[54] J. Kusuma, I. Maravic, and M. Vetterli, "Sampling with finite rate of innovation: channel and timing estimation for uwb and gps," in *Communications, 2003. ICC '03. IEEE International Conference on*, vol. 5, 2003, pp. 3540–3544 vol.5.

[55] Z. Wang, G. Arce, J. Paredes, and B. Sadler, "Compressed detection for ultra-wideband impulse radio," in *Signal Processing Advances in Wireless Communications, 2007. SPAWC 2007. IEEE 8th Workshop on*, 2007, pp. 1–5.

[56] Z. Wang, G. Arce, B. Sadler, J. Paredes, and X. Ma, "Compressed detection for pilot assisted ultra-wideband impulse radio," in *Ultra-Wideband, 2007. ICUWB 2007. IEEE International Conference on*, 2007, pp. 393–398.

[57] A. Oka and L. Lampe, "A compressed sensing receiver for uwb impulse radio in bursty applications like wireless sensor networks," *Physical Communication*, vol. 2, no. 4, pp. 248 – 264, 2009.

[58] Z. Wang, G. Arce, B. Sadler, J. Paredes, S. Hoyos, and Z. Yu, "Compressed uwb signal detection with narrowband interference mitigation," in *Ultra-Wideband, 2008. ICUWB 2008. IEEE International Conference on*, vol. 2, 2008, pp. 157–160.

[59] A. Oka and L. Lampe, "Compressed sensing reception of bursty uwb impulse radio is robust to narrow-band interference," in *Global Telecommunications Conference, 2009. GLOBECOM 2009. IEEE*, 2009, pp. 1–7.

[60] J. Paredes, G. Arce, and Z. Wang, "Ultra-wideband compressed sensing: Channel estimation," *Selected Topics in Signal Processing, IEEE Journal of*, vol. 1, no. 3, pp. 383–395, 2007.

[61] P. Zhang, Z. Hu, R. Qiu, and B. Sadler, "A compressed sensing based ultra-wideband communication system," in *Communications, 2009. ICC '09. IEEE International Conference on*, 2009, pp. 1–5.

[62] K. Gedalyahu and Y. Eldar, "Time-delay estimation from low-rate samples: A union of subspaces approach," *Signal Processing, IEEE Transactions on*, vol. 58, no. 6, pp. 3017–3031, 2010.

[63] S. Gishkori, G. Leus, and V. Lottici, "Compressive sampling based differential detection for uwb impulse radio signals," *Physical Communication*, vol. 5, no. 2, pp. 185 – 195, 2012.

[64] M. Davenport, P. Boufounos, M. Wakin, and R. Baraniuk, "Signal processing with compressive measurements," *Selected Topics in Signal Processing, IEEE Journal of*, vol. 4, no. 2, pp. 445–460, 2010.

[65] T. Ragheb, J. Laska, H. Nejati, S. Kirolos, R. Baraniuk, and Y. Massoud, "A prototype hardware for random demodulation based compressive analog-to-digital conversion," in *Circuits and Systems, 2008. MWSCAS 2008. 51st Midwest Symposium on*, 2008, pp. 37–40.

[66] Z. Yu, S. Hoyos, and B. Sadler, "Mixed-signal parallel compressed sensing and reception for cognitive radio," in *Acoustics, Speech and Signal Processing, 2008. ICASSP 2008. IEEE International Conference on*, 2008, pp. 3861–3864.

[67] A. Maleki and D. Donoho, "Optimally tuned iterative reconstruction algorithms for compressed sensing," *Selected Topics in Signal Processing, IEEE Journal of*, vol. 4, no. 2, pp. 330–341, 2010.

[68] J. Pearl, *Probabilistic reasoning in intelligent systems: networks of plausible inference*. San Francisco, CA, USA: Morgan Kaufmann Publishers Inc., 1988.

[69] F. Kschischang, B. Frey, and H.-A. Loeliger, "Factor graphs and the sum-product algorithm," *Information Theory, IEEE Transactions on*, vol. 47, no. 2, pp. 498–519, 2001.

[70] M. Bayati and A. Montanari, "The dynamics of message passing on dense graphs, with applications to compressed sensing," *Information Theory, IEEE Transactions on*, vol. 57, no. 2, pp. 764–785, 2011.

[71] S. Gishkori, G. Leus, and H. Delic, "Energy detection of wideband and ultra-wideband ppm," in *Global Telecommunications Conference (GLOBECOM 2010), 2010 IEEE*, 2010, pp. 1–5.

[72] J. Choi and W. Stark, "Performance of ultra-wideband communications with suboptimal receivers in multipath channels," *Selected Areas in Communications, IEEE Journal on*, vol. 20, no. 9, pp. 1754–1766, 2002.

[73] J. G. Proakis, *Digital Communications*, 4th ed. Avenue of Americas, NY: McGraw-Hill, 2001.

[74] I. S. Gradshteyn and I. M. Ryzhik, *Table of Integrals, Series, and Products*, 6th ed. San Diago, CA: Academic Press, 1996.

[75] S. Gishkori, G. Leus, and H. Delic, "Energy detectors for sparse signals," in *Signal Processing Advances in Wireless Communications (SPAWC), 2010 IEEE Eleventh International Workshop on*, 2010, pp. 1–5.

[76] M. Davenport, J. Laska, J. Treichler, and R. Baraniuk, "The pros and cons of compressive sensing for wideband signal acquisition: Noise folding versus dynamic range," *Signal Processing, IEEE Transactions on*, vol. 60, no. 9, pp. 4628–4642, 2012.

[77] L. Lampe and K. Witrisal, "Challenges and recent advances in ir-uwb system design," in *Circuits and Systems (ISCAS), Proceedings of 2010 IEEE International Symposium on*, 2010, pp. 3288–3291.

[78] V. Lottici, A. D'Andrea, and U. Mengali, "Channel estimation for ultra-wideband communications," *Selected Areas in Communications, IEEE Journal on*, vol. 20, no. 9, pp. 1638–1645, 2002.

[79] K. Witrisal, G. Leus, G. J. M. Janssen, M. Pausini, F. Troesch, T. Zasowski, and J. Romme, "Noncoherent ultra-wideband systems," *Signal Processing Magazine, IEEE*, vol. 26, no. 4, pp. 48–66, 2009.

[80] R. Hoctor and H. Tomlinson, "Delay-hopped transmitted-reference rf communications," in *Ultra Wideband Systems and Technologies, 2002. Digest of Papers. 2002 IEEE Conference on*, 2002, pp. 265–269.

[81] Y.-L. Chao and R. Scholtz, "Optimal and suboptimal receivers for ultra-wideband transmitted reference systems," in *Global Telecommunications Conference, 2003. GLOBECOM '03. IEEE*, vol. 2, 2003, pp. 759–763 Vol.2.

[82] M. Ho, V. Somayazulu, J. Foerster, and S. Roy, "A differential detector for an ultra-wideband communications system," in *Vehicular Technology Conference, 2002. VTC Spring 2002. IEEE 55th*, vol. 4, 2002, pp. 1896–1900 vol.4.

[83] N. Guo and R. Qiu, "Improved autocorrelation demodulation receivers based on multiple-symbol detection for uwb communications," *Wireless Communications, IEEE Transactions on*, vol. 5, no. 8, pp. 2026–2031, 2006.

[84] V. Lottici and Z. Tian, "Multiple symbol differential detection for uwb communications," *Wireless Communications, IEEE Transactions on*, vol. 7, no. 5, pp. 1656–1666, 2008.

[85] V. Lottici, Z. Tian, and G. Leus, "A novel approach to uwb data detection with symbol-level synchronization," *Physical Communication*, vol. 2, no. 4, pp. 296–305, 2009.

[86] Y. Vanderperren, W. Dehaene, and G. Leus, "Performance analysis of a flexible subsampling receiver for pulsed uwb signals," *Wireless Communications, IEEE Transactions on*, vol. 8, no. 8, pp. 4134–4142, 2009.

[87] S. Gishkori, G. Leus, and V. Lottici, "Compressive sampling based differential detection of ultra wideband signals," in *Personal Indoor and Mobile Radio Communications (PIMRC), 2010 IEEE 21st International Symposium on*, 2010, pp. 194–199.

[88] M. R. Osborne, B. Presnell, and B. A. Turlach, "On the lasso and its dual," *Journal of Computational and Graphical Statistics*, vol. 9, no. 2, pp. 319–337, 2000. [Online]. Available: http://dx.doi.org/10.2307/1390657

[89] J. Friedman, T. Hastie, and R. Tibshirani, "Regularization paths for generalized linear models via coordinate descent," 2009. [Online]. Available: http://www-stat.stanford.edu/~hastie/Papers/glmnet.pdf

[90] P. Tseng, "Convergence of a block coordinate descent method for nondifferentiable minimization," *J. Optim. Theory Appl.*, vol. 109, no. 3,

pp. 475–494, Jun. 2001. [Online]. Available: http://dx.doi.org/10.1023/A:1017501703105

[91] P. Stoica, J. Liu, J. Li, and M. A. Prasad, "The heuristic, glrt, and map detectors for double differential modulation are identical," *Information Theory, IEEE Transactions on*, vol. 51, no. 5, pp. 1860–1865, 2005.

[92] B. Efron and R. J. Tibshirani, *An Introduction to the Bootstrap*. New York: Chapman & Hall, 1993.

[93] S. Kotz, T. J. Kozubowski, and K. Podgrski, *The Laplace Distribution and Generalizations*. Boston: Birkhauser, 2001.

[94] L. Yang and G. Giannakis, "Ultra-wideband communications: an idea whose time has come," *Signal Processing Magazine, IEEE*, vol. 21, no. 6, pp. 26–54, 2004.

[95] A. Molisch, "Ultra-wide-band propagation channels," *Proceedings of the IEEE*, vol. 97, no. 2, pp. 353–371, 2009.

[96] Z. Tian and V. Lottici, "Low-complexity ml timing acquisition for uwb communications in dense multipath channels," *Wireless Communications, IEEE Transactions on*, vol. 4, no. 6, pp. 3031–3038, 2005.

[97] L. Yang and G. Giannakis, "Timing ultra-wideband signals with dirty templates," *Communications, IEEE Transactions on*, vol. 53, no. 11, pp. 1952–1963, 2005.

[98] P. Schvan, D. Pollex, S.-C. Wang, C. Falt, and N. Ben-Hamida, "A 22gs/s 5b adc in 0.13/spl mu/m sige bicmos," in *Solid-State Circuits Conference, 2006. ISSCC 2006. Digest of Technical Papers. IEEE International*, 2006, pp. 2340–2349.

[99] P.-L. Dragotti, M. Vetterli, and T. Blu, "Sampling moments and reconstructing signals of finite rate of innovation: Shannon meets Strang-Fix," *Signal Processing, IEEE Transactions on*, vol. 55, no. 5, pp. 1741–1757, 2007.

[100] S. Gishkori, G. Leus, and V. Lottici, "Compressive sampling based differential detection for uwb impulse radio signals," *Physical Communication*, vol. 5, no. 2, pp. 185 – 195, 2012.

[101] S. Gishkori and G. Leus, "Compressive sampling based energy detection of ultra-wideband pulse position modulation," *Signal Processing, IEEE Transactions on*, vol. 61, no. 15, pp. 3866–3879, 2013.

[102] A. Schenk and R. F. H. Fischer, "Compressed-sensing (decision-feedback) differential detection in impulse-radio ultra-wideband systems," in *Ultra-Wideband (ICUWB), 2011 IEEE International Conference on*, 2011, pp. 121–125.

[103] ——, "Decision-feedback differential detection in impulse-radio ultra-wideband systems," *Communications, IEEE Transactions on*, vol. 59, no. 6, pp. 1604–1611, 2011.

[104] S. Gishkori, G. Leus, and V. Lottici, "Compressive sampling based multiple symbol differential detection for uwb ir signals," in *Ultra-Wideband (ICUWB), 2012 IEEE International Conference on*, 2012, pp. 130–134.

[105] S. M. Kay, *Fundamentals of statistical signal processing: detection theory*. Upper Saddle River, NJ, USA: Prentice-Hall, Inc., 1998.

[106] U. Finkce and M. Pohst, "Improved methods for calculating vectors of short length in a lattice, including a complexity analysis," *Mathematics of Computation*, vol. 44, pp. 463–463, 1985.

[107] A. Burg, M. Borgmann, M. Wenk, M. Zellweger, W. Fichtner, and H. Bolcskei, "Vlsi implementation of mimo detection using the sphere decoding algorithm," *Solid-State Circuits, IEEE Journal of*, vol. 40, no. 7, pp. 1566–1577, 2005.

[108] B. Hassibi and H. Vikalo, "On the sphere-decoding algorithm i. expected complexity," *Signal Processing, IEEE Transactions on*, vol. 53, no. 8, pp. 2806–2818, 2005.

[109] L. Lampe, R. Schober, V. Pauli, and C. Windpassinger, "Multiple-symbol differential sphere decoding," *Communications, IEEE Transactions on*, vol. 53, no. 12, pp. 1981–1985, 2005.

[110] R. Schober, W. Gerstacker, and J. Huber, "Decision-feedback differential detection of mdpsk for flat rayleigh fading channels," *Communications, IEEE Transactions on*, vol. 47, no. 7, pp. 1025–1035, 1999.

[111] G. Obozinski, L. Jacob, and J.-P. Vert, "Group lasso with overlaps: the latent group lasso appraoch," Tech. Rep., 2011.

[112] I. Selesnick and P.-Y. Chen, "Total variation denoising with overlapping group sparsity," in *Acoustics, Speech and Signal Processing (ICASSP), 2013 IEEE International Conference on*, May 2013, pp. 5696–5700.

[113] D. P. Bertsekas and J. N. Tsitsiklis. Parallel and Distributed Computation: Numerical Methods, 1997.

[114] PSD, "Noaa/oar/esrl," Tech. Rep. [Online]. Available: http://www.esrl.noaa.gov/psd/

[115] G. Mateos, J.-A. Bazerque, and G. Giannakis, "Spline-based spectrum cartography for cognitive radios," in *Signals, Systems and Computers, 2009 Conference Record of the Forty-Third Asilomar Conference on*, Nov 2009, pp. 1025–1029.

Samenvatting

Draadloze communicatie ondergaat een enorme ontwikkeling op alle vlakken. Op het vlak van communicatie over korte afstanden, beloven technologieën zoals *ultra-wideband* (UWB) zeer hoge datasnelheden, een goede tijdsresolutie en coëxistentie met andere standaarden voor de fysische laag. Samen met deze voordelen, zorgt de belofte van apparaten met een lage kost en een lage complexiteit er voor dat UWB systemen een zeer gewilde optie zijn. De belangrijkste reden voor deze voordelen is het gebruik van een zeer grote bandbreedte. Deze voordelen komen echter tegen een prijs, zoals de hoge bemonsteringssnelheid die nodig is om dergelijke signalen te ontvangen. Volgens het Nyquist-theorema kan een signaal volledig bepaald worden als het wordt bemonsterd met een snelheid die gelijk is aan twee maal de maximale frequentie. Dit betekent dat de UWB signalen een bemonsteringssnelheid vereisen in de orde van grootte van Gigasamples per seconde. Aan de ontvanger wordt de bemonstering uitgevoerd door een *analog-to-digital converter* (ADC). Het stroomverbruik van een ADC is evenredig aan de bemonsteringssnelheid. Een zeer hoge bemonsteringssnelheid betekent dat de ADC tegen de limiet van zijn energieverbruik moet werken. Dit kan het hele idee van UWB systemen met een lage kost en een lage complexiteit in gevaar brengen. Daarom is de hulp van onderbemonsteringstechnieken onontbeerlijk. In dit verband stellen wij het gebruik van *compressive sampling* (CS) voor UWB systemen voor. CS belooft een redelijke reconstructie van het volledige signaal met behulp van slechts een beperkt aantal gecomprimeerde monsters, op voorwaarde dat het signaal spaars is. In dit proefschrift concentreren we ons op impuls-radio (IR) UWB systemen. IR-UWB signalen staan bekend voor hun spaars karakter, wat wil zeggen dat een groot deel van het ontvangen signaal nul of te verwaarlozen is. We benutten deze ijlheid in het tijdsdomein en verlagen de bemonsteringssnelheid tot beneden de Nyquist-

frequentie, maar ontwikkelen op basis hiervan toch effectieve detectoren.

Wij ontwikkelen CS-gebaseerde energiedetectoren voor IR-UWB pulspositiemodulatie (PPM) systemen in reflectieve omgevingen. We gebruiken de principes van de *general maximum likelihood* theorie om enerzijds detectoren te bestuderen voor een signaal dat gereconstrueerd wordt op basis van de comprimeerde monsters en anderzijds detectoren te ontwikkelen die deze reconstructiestap overslaan en de detectie direct op de gecomprimeerde monsters uitvoeren, waardoor de complexiteit verder verlaagt. Wij geven exacte theoretische uitdrukkingen voor de *bit error probability* (BEP) om de prestaties van onze voorgestelde detectoren te evalueren. Deze uitdrukkingen worden verder getoetst aan numerieke simulaties.

Wij poneren ook CS-gebaseerde differentiële detectoren voor IR-UWB signalen. Deze detectoren werken met opeenvolgende symbolen. Wij ontwikkelen detectoren met een aparte reconstructie- en detectiefase evenals detectoren die deze stappen gezamenlijk uitvoeren. We stellen verder detectoren voor die geen reconstructiefase nodig hebben en enkel werken met de gecomprimeerde monsters. Dit brengt echter een aantal beperkingen met zich mee met betrekking tot de flexibiliteit van het meetproces. Om de prestaties van al deze detectoren af te wegen, bieden wij ook *maximum a posteriori* (MAP) detectoren aan. Wij voeren numerieke simulaties uit om de detectieresultaten weer te geven.

We breiden de klassieke CS-gebaseerde differentiële detectoren uit naar differentiële detectoren gebaseerd op meerdere opeenvolgende symbolen. Om de complexiteit van de implementatie laag te houden, werken we alleen rechtstreeks met de gecomprimeerde monsters. Dit brengt weer beperkingen met zich mee wat betreft het meetproces, maar om die zo klein mogelijk te houden gebruiken we de principes van de *general likelihood ratio test* (GLRT). Naast de detectoren die gebaseerd zijn op de volledige tijdsinformatie, stellen we ook detectoren voor die dergelijke informatie slechts op symboolniveau nodig hebben. Dit resulteert effectief in detectoren met een lage kost en een lage complexiteit.

Tot slot presenteren we een aantal theoretische aspecten van CS. Wij ontwikkelen algoritmes die de blokspaarse structuur van het signaal uitbuiten. Deze blokspaarse eigenschap wordt gecombineerd met verschillende blokafmetingen en signaalcoëfficiënten met vloeiende overgangen. Dergelijke signalen worden vaak aangetroffen in een breed scala aan technische en biologische onderzoeksgebieden.

Propositions

1. Compressive sampling (CS) is a viable option to decrease the sampling rate much below the Nyquist rate in impulse-radio (IR) ultra-wideband (UWB) systems.
2. Noncoherent IR-UWB detectors can be realized from the reconstructed samples and their performance is independent of the spreading factor.
3. Signal detection is possible from the compressed samples directly without the need for a reconstruction stage but its performance depends upon the choice of measurement matrices.
4. The reconstruction performance of IR-UWB modulated data can be improved by exploiting the sparsity structure of the received signal.
5. Faith, perseverance and patience are essential ingredients for a PhD.
6. Life of a PhD student is like that of a bull in a china shop: mistreating every delicate theory, before settling down for a proper solution.
7. People are the same everywhere, irrespective of race or color. Therefore, their Creator must be the same.
8. There should be no restriction on opinions as long as they are not abusive and do not incite breaking the law.
9. Every human is born with an inherent right to life, justice and dignity. A policy of denying it in the name of collateral damage is despicable.
10. Governments should focus on fortifying their own borders instead of ravening weaker countries on one pretext or the other.

These propositions are considered opposable and defendable, and as such have been approved by the supervisor prof.dr.ir. G.J.T. Leus.

Stellingen

1. *Compressive sampling* (CS) is een nuttige manier om de bemonsteringssnelheid ver onder de Nyquist-frequentie te verlagen in impuls-radio (IR) *ultra-wideband* (UWB) systemen.

2. Niet-coherente IR-UWB detectoren kunnen worden gerealiseerd met behulp van de gereconstrueerde monsters en hun prestatie is onafhankelijk van de spreidingsfactor.

3. Signaaldetectie is mogelijk op basis van enkel de gecomprimeerde monsters, zonder dat er een reconstructiestap nodig is, maar de prestatie hiervan hangt af van de keuze van de meetmatrices.

4. De reconstructieprestatie van data gemoduleerd met IR-UWB kan worden verbeterd door de spaarsheid van het ontvangen signaal uit te buiten.

5. Geloof, doorzettingsvermogen en geduld zijn essentiële ingrediënten voor een PhD.

6. Het leven van een promovendus is als die van een olifant in een porseleinkast: elke delicate theorie misbruiken, om vervolgens tot een goede oplossing te komen.

7. Mensen zijn overal hetzelfde, ongeacht ras of kleur. Daarom moet hun Schepper hetzelfde zijn.

8. Er mag geen beperking zijn op meningen, zolang ze geen misbruik opleveren en niet aanzetten tot het breken van de wet.

9. Ieder mens wordt geboren met een inherent recht op leven, rechtvaardigheid en waardigheid. Een beleid dat dit ontkent in de naam van *collateral damage* is verachtelijk.

10. Overheden moeten zich richten op het versterken van hun eigen grenzen, in plaats van het leegroven van zwakkere landen op basis van een of ander voorwendsel.

Deze stellingen worden opponeerbaar en verdedigbaar geacht en zijn als zodanig goedgekeurd door de promotor prof.dr.ir. G.J.T. Leus.

Acknowledgments

All praise is due to Almighty God, The Most Gracious and The Most Merciful. Despite my many shortcomings, He has always bestowed His blessings upon me. I hope and pray that His mercy continues upon me unabatedly and that I remain only His servant till the end of my life. Verily, He is the source of all strength.

I would like to thank my supervisor, Prof. Geert Leus, for guiding me throughout my PhD. He gave me the freedom to explore different research directions as well as prevented me from getting detracted from the desired goals. His prompt help has always saved a lot of my time and perhaps is a key factor in my completing the major share of my research within four years. Apart from academics, I also admire him as a person. He has the knack of quickly perceiving social sensitivities and is always willing to respond to personal problems in a positive way. I think I was fortunate to work with a person of his capabilities and intellect. I would also like to thank him for doing Dutch translation of the summary and the propositions.

I would like to thank Prof. Alle-Jan van der Veen. His presence in the group has always been very inspiring. Joining him at lunch almost everyday has been a pleasant experience.

I would like to thank Prof. Vincenzo Lottici. We worked together on a number of papers. I have learnt many things from him. His detailed comments and precise suggestions have always been very helpful. I would like to thank him for being part of my defence committee as well. I would like to thank all other members of my defence committee, Prof. R. Fischer, Prof. F. Le Chevalier, Prof. K. Bertels, Dr. Y. Vanderperren and Dr. Y. Zhang. I would like to thank them for reading my thesis and giving me extremely useful suggestions.

From the secretariat office, I would like to thank Laura Bruns, Minaksie Ramsoekh and the project support Rosario Salazar for their prompt help in many of the

official matters.

I would like to thank my past colleagues and friends, Nauman Kyani, Umar Rizvi, Vijay Venkateswaran, Yiyin Wang, Yu Bi and Sina Maleki. I had a quality time when they were around and got help from them in many ways.

I would like to thank my present colleagues and friends, Adib Sarijari, Andrea Simonetto, Chockalingam Veerappan, Dony Ariananda, Georg Kail, Hadi Jamali-Rad, Hamid Ramezani, Jorge Martinez, Millad Sardarabadi, Nihan Cicek, Raj Rajan, Rocio Arroyo, Seyran Khademi, Sharil Abdullah, Sumeet Kumar, Sundeep Chepuri, Venkat Roy, Yan Xie, and Yonchang Hu. I had a personal connection with almost each one of them. I am sure I will miss them. I wish them all the best. I would especially like to thank my old friend Dony, who has always been ready to discuss any thing with me.

I would also like to thank my Pakistani friends, Zubair Nawaz, Muhammad Nadeem, Laiq Hassan, Hisham bin Zubair, Sajid Aqeel, Mottaqillah (your are almost a Pakistani), Waqas Syed, Abrar Hakeem, Imran Ashraf, Ashfaq Ahmed, Faisal Nadeem, Fakhar Anjum, Seyab, Ibrahim Daud, Hamayun Khan, Iftikhar Faraz, Tariq Abdullah, Aqeel Wahla, Samee ur Rehman, Akram Chaudhary, Atiq ur Rehman, Bilal Ahmed, Hamid Mushtaq, Atif Bulelzai, Abdul Hannan, Fahim Raees, Shah Muhammad, Umar Altaf, Muhammd Zubair, Rajab Ali, Younis, Osama, Adeel Javed, AN Tabish, Nauman Ahmed and all those whose names I have missed. I had a memorable time with most of them. I would also like to thank my friends Maxim Volkov and Andre Abi Khaled for giving me company at weekends, and Ismail Yatim at sports.

There are many more of my friends back in Pakistan and in different parts of the world, who have always wished good of me and I know, pray for my success. I thank them all for being a part of my life.

I would like to thank my father and my elder sister for their support and encouragement throughout my masters and PhD. I would especially like to thank my younger siblings, Javad, Gull, Shahab, Dilshad and Junaid, who perhaps suffered the most because of my absence. Special thanks to Gull for designing the thesis cover as well. I would also like to thank my nephews, Abdullah and Absar, for their giggles and demands for chocolates, cookies, candies and toys.

Last but not the least, I would like to thank my mother. She was my first teacher both in religious as well as mundane education. Her passing away was the biggest loss of my life. I dedicate this small work to her kind memories. May her soul rest in peace, Ameen.

Curriculum Vitae

Shahzad Gishkori was born in 1979 in D.G. Khan, Pakistan. He received the B.Sc. degree in electrical engineering, with specialization in computer engineering, in 2002 from the University of Engineering and Technology Lahore, Pakistan. Later on, he worked in the industry for almost five years, of which two years were spent in the energy sector and three years in the telecommunications sector. In August 2009, he received the M.Sc. degree (cum Laude) in electrical engineering from the Delft University of Technology, The Netherlands. In November 2009, he joined the circuits and systems group at the Faculty of Electrical Engineering, Mathematics and Computer Science of the Delft University of Technology, The Netherlands, in pursuance of the Ph.D. degree. His research interests include compressive sampling (compressed sensing), signal processing for communications and wireless communications.

Publications

Journals

- S. Gishkori, V. Lottici and G. Leus, “Compressive Sampling Based Multiple Symbol Differential Detection for UWB Communications”, *IEEE Transactions on Wireless Communications - To appear*

- S. Gishkori and G. Leus, “Compressive Sampling Based Energy Detection of Ultra-Wideband Pulse Position Modulation”, *IEEE Transactions on Signal Processing*, vol. 61, no. 15, pp. 3866–3879, Aug. 2013

- S. Gishkori, G. Leus and V. Lottici, “Compressive Sampling Based Differential Detection of UWB Impulse Radio Signals”, *Elsevier Physical Communication*, vol. 5, no. 2, pp. 185–195, Jun. 2012

Conferences

- S. Gishkori and G. Leus, “Compressed Sensing for Block-Sparse Smooth Signals”, *IEEE ICASSP*, Florence, Italy, May 2014

- S. Gishkori, G. Leus and V. Lottici, “Compressive sampling based multiple symbol differential detection for UWB IR signals”, *IEEE ICUWB 2012*, Syracuse, USA, Sep. 2012

- S. Gishkori, G. Leus and V. Lottici, “MAP based differential detectors for compressed UWB impulse radio signals”, *IEEE ICASSP*, Kyoto, Japan, Mar. 2012

- S. Gishkori, G. Leus and and V. Lottici, “Energy Detection of Wideband and Ultra-Wideband PPM”, *IEEE Globecom 2010*, Miami, USA, Dec. 2010
- S. Gishkori, G. Leus and and H. Delic, “Compressive Sampling Based Differential Detection of Ultra Wideband Signals”, *IEEE PIMRC 2010*, Istanbul, Turkey, Sep. 2010
- S. Gishkori, G. Leus and and H. Delic, “Energy Detectors for Sparse Signals”, *IEEE SPAWC 2010*, Marakesh, Morocco, Jun. 2010
- S. Gishkori, G. Leus and and H. Delic, “Energy Detection of (Ultra-)Wideband PPM”, *WIC SITB 2010*, Rotterdam, The Netherlands, May 2010

Glossary

Acronyms

ADC	Analog to Digital Converter
AIC	Analog to Information Converter
AMP	Approximate Message Passing
BEP	Bit Error Probability
BP	Basis Pursuit
CS	Compressive Sampling
CoSaMP	Compressive Sampling Matching Pursuit
DD	Differential Detection
DEN	Differential Elastic Net
DMM	Different Measurement Matrix
ED	Energy Detector
EVD	Eigenvalue Decomposition
FCC	Federal Communications Commission
GML	Generalized Maximum Likelihood
GLRT	Generalized Likelihood Ratio Test

IR	Impulse Radio
ITH	Iterative Thresholding
LASSO	Least Absolute Shrinkage and Selection Operator
LOS	Line of Sight
LP	Linear Program
MAP	Maximum A Posteriori
MSE	Mean Squared Error
MSDD	Multiple Symbol Differential Detection
NR	Nyquist Rate
NLOS	Non Line of Sight
OLS	Ordinary Least Squares
OMP	Orthogonal Matching Pursuit
PDF	Probability Density Function
PPM	Pulse Position Modulation
RIP	Restricted Isometry Property
SD	Sphere Decoder
SE	State Evolution
SLS	Symbol Level Synchronization
SMM	Same Measurement Matrix
SNR	Signal to Noise Ratio
USLE	Underdetermined System of Linear Equations
UWB	Ultra-Wideband

Notations

x	Scalar x
$\mathbf{x}$	Vector $\mathbf{x}$
$\hat{\mathbf{x}}$	Estimate of vector $\mathbf{x}$
$\mathbf{x}^T$	Transpose of vector $\mathbf{x}$
$[\mathbf{x}]_i$	ith entry of the vector $\mathbf{x}$
$\mathbf{X}$	Matrix $\mathbf{X}$
$\mathbf{X}^{-1}$	Inverse of matrix $\mathbf{X}$
$[\mathbf{X}]_{i,j}$	(i,j)th element of the matrix $\mathbf{X}$
$\mathbf{I}_N$	Identity matrix of size $N \times N$
$\mathbf{1}_{M\times N}$	$M \times N$ matrix with all components one
$\mathbf{0}_{M\times N}$	$M \times N$ matrix with all components zero
$\otimes$	Kronecker product
$\star$	Convolution
diag$\{\cdot\}$	Block diagonal matrix
$\lfloor \mathbf{x} \rfloor$	Largest integer smaller or equal to $\mathbf{x}$
$\triangleq$	Defines an entity
$\|\|\mathbf{x}\|\|_p$	ℓ_p-norm of $\mathbf{x}$, i.e., $(\sum_{i=0}^{N-1} \|[\mathbf{x}]_i\|^p)^{1/p}$
$p(x)$	Probability density function of x
E$\{x\}$	Statistical expectation of x
$p(x)$	Polarity of x
$(x)_+$	$(x)_+ = x$ iff $x > 0$ otherwise $(x)_+ = 0$
$Q(x)$	Gaussian tail probability, i.e., $1/\sqrt{2\pi}\int_x^\infty e^{-u^2/2}du$